Title
The Regulation of CD8+ T Cell Fate During Chronic Toxoplasma gondii Infection

Author
Bangs, Derek Jordan

Publication Date
2021

Peer reviewed|Thesis/dissertation

The Regulation of CD8+ T Cell Fate During Chronic *Toxoplasma gondii* Infection

By

Derek Jordan Bangs

A dissertation submitted in the partial satisfaction of the

requirements for the degree of

Doctor of Philosophy

in

Infectious Disease and Immunity

in the

Graduate Division

of the

University of California, Berkeley

Committee in charge:

Professor Ellen Robey, Chair
Professor Laurent Coscoy
Professor David Raulet
Assistant Professor Michel DuPage

Summer 2021

Abstract

The Regulation of CD8+ T Cell Fate During Chronic *Toxoplasma gondii* Infection

By

Derek J. Bangs

Doctor of Philosophy in Infectious Disease and Immunity

University of California, Berkeley

Professor Ellen Robey, Chair

Production of armed effector CD8+ T cells during persistent infection requires a stable pool of stem-like cells that can give rise to short-lived effector T cells via a proliferative intermediate population. In chronic infection models marked by T cell exhaustion, this process can be transiently induced by check-point blockade, but it occurs spontaneously and continuously in the spleens of mice chronically infected with the protozoan intracellular parasite, *Toxoplasma gondii,* providing a unique opportunity to examine the steps in the differentiation process. Using this model, we observed distinct locations and gene expression patterns for stem-like memory cells, proliferative intermediate cells, and terminally differentiated effector cells, implying a link between differentiation and discrete anatomical niches in the spleen. Loss of the chemokine receptor CXCR3 on parasite-specific T cells did not impair their white pulp to red pulp migration but reduced their interactions with CXCR3 ligand-producing type 2 conventional DCs in the bridging channels and impaired their transition from memory to intermediate states, leading to a build up of memory T cells localized to the red pulp. These results demonstrate a critical role for CXCR3 during chronic infection by increasing T cell exposure to differentiation-inducing signals during red pulp migration, providing a dynamic and flexible mechanism for modulating effector differentiation in response to environmental signals.

While mice chronically infected with *T. gondii* are able to effectively establish long-term control of the pathogen, they do not establish sterilizing immunity. Although the parasite is primarily restricted to the brain during the chronic phase of infection, CD8+ T cells in the periphery experience continuous antigenic stimulation, resulting in ongoing proliferation and effector differentiation. We investigated the role of IFNγ in regulating CD8+ T cell fate during chronic *T. gondii* infection. We observed that neutralization of IFNγ during chronic infection led to dramatic changes in CD8+ T cell fate, promoting robust proliferation at the expense of terminal effector differentiation. These changes in CD8+ T cell fate were dependent on CXCR3 and linked to increases in antigen presentation in the spleen, which occurred in the absence of widespread parasite reactivation.

Finally, IFNγ neutralization resulted in the emergence of clusters of CD11c+ cells in the red pulp of the spleen that were robust producers of CXCR3 ligands and supported a proliferation rich-environment. These results highlight an ongoing role for IFNγ in mediating the clearance of *T. gondii* antigens during chronic infection and contribute to our understanding of the factors regulating CD8+ T cell fate.

Table of Contents

List of Tables and Figures

Chapter 1

Chapter 2

Chapter 3

Acknowledgements

First of all, I want to thank other members of the Robey Lab for all of their help and support through my six years at UC Berkeley. I want to especially thank my fellow graduate students Alexandra, Lydia, and Michael for helping make our lab environment so fun and relaxing (even when research was incredibly stressful). I would also like to thank Laura and Rachel for their perspective and guidance during the last few months as I finished graduate school and began preparing for my postdoc. I want to thank Shiao Chan for all her help with experiments and for being the best lab manager possible. I would have been lost without her! And finally I want to thank Kathya, who has done an incredible job as Shiao's replacement: a job many of us thought would be impossible!

I want to thank my mentor Ellen Robey for all of the guidance, support, and wisdom she has offered me during my time in graduate school. I especially want to thank her for always keeping a positive attitude about my project, even when I was certain everything had failed. Her mantra of "always follow the science" helped keep me going when things seemed impossible, and I will take that philosophy with me wherever I go. I also want to thank her for supporting my ideas and letting me do all of the crazy experiments that I proposed (see below).

I want to thank the other graduate students, both past and present, in the Infectious Disease and Immunity program for their support and for making my time at Berkeley so amazing. Being surrounded by such intelligent and passionate people pushed me to always do my best, and I will never forget some of the great memories we've shared. I want to give a special thanks for Gina and Kristi for being amazing cohort members, I never would have been able to get through this without both of you! I also want to thank the MCB and PMB graduate students who have always been so welcoming and friendly and have helped me every step of the way.

I want to thank the members of my thesis committee, Laurent Coscoy, Michel DuPage, and David Raulet, for their insightful feedback that was really critical in helping me structure my project and paper. I especially want to thank Laurent for being the chair of my qualifying exam and for his support during that process as well. I also want to thank Sarah Stanley for giving me the opportunity to work with the CEND workshop in Uganda, which was an amazing experience I will never forget and was one of the highlights of my time at Berkeley.

Finally, I want to thank all my family and friends outside of the UC Berkeley community for their support and for giving me an escape from the stressful world of grad school. I would not have been able to do this without you!

Chapter 1: Introduction

1.1: CD8+ T cell responses to *Toxoplasma gondii*: lessons from a successful parasite

T. gondii infection in mice provides an excellent model for the study of CD8+ T cell responses. Natural and engineered *T. gondii* antigens have led the way to understanding the factors regulating antigen presentation from vacuolar pathogens. *T. gondii* infection of resistant and sensitive mouse strains provides unique models to study both effective CD8+ T cell function and protection in a well controlled infection attributed to a novel T cell population, and T cell exhaustion in a progressing chronic infection. Additionally, the long-term persistence of the parasite in the brain provides a unique model of neurotropic infection used to study CD8+ T cell entry, retention and function in the brain.

CD8+ T cell responses to *T. gondii*

The protozoan intracellular parasite, *Toxoplasma gondii (T. gondii)*, is a highly successful pathogen. It is found world-wide in a variety of birds and mammals, including an estimated 20-50% of humans. Its success is largely achieved by the parasite's ability to establish a stable balance with the host immune response, thus allowing the parasite to rapidly spread through the body and establish persistent infection, while also maintaining the viability of the host. A key part of this balance involves CD8+ T cells, the primary cell type that controls the parasite in the mammalian adaptive immune response.

Experimental *T. gondii* infection of mice (a natural host) provides an outstanding model for understanding CD8+ T cell responses. Propagating the parasite in the lab is relatively safe and easy, and a large variety of genetically engineered parasite strains are available. The parasite spreads systemically, allowing for the study of CD8+ T cell responses in a variety of lymphoid and nonlymphoid tissues, including the brain, the primary site of long-term persistence. Finally, the CD8+ T cell response differs dramatically in different inbred mouse strains, leading to differential control of the parasite during chronic infection, and providing an opportunity to explore the factors that determine CD8+ T cell efficacy.

How CD8+ T cells detect vacuolar pathogens

In many viral and intracellular bacterial infections, pathogen-derived antigens are present in the host cell cytosol and can be processed and presented to CD8+ T cells via the classical Major Histocompatibility Complex Class I (MHC-I) presentation pathway. However, vacuolar pathogens such as *T. gondii* pose particular challenges for MHC-I presentation, since their antigens do not have access to the host cytosol. Nevertheless, *T. gondii* infection elicits a robust and protective CD8+ T cell response. That fact, together with a collection of several natural antigens that have been identified (Table 1), and the ability to generate

parasites expressing engineered antigens (Table 2), makes *T. gondii* a valuable model for the study of CD8+ T cell responses to vacuolar pathogens.

Although in some settings inert, phagocytosed antigens can be cross-presented by certain antigen presenting cells (APC) (*Joffre et al.* 2012), presentation of *T. gondii* antigens requires interactions of live parasites with APC (*Gubbels et al.* 2005, *Dupont et al.* 2014). Moreover, presentation of *T. gondii* antigens is strongly affected by their mode of secretion from the parasite into host cells, and their location and membrane topology within the host cell (Table 1). For example, constitutive secretion via organelles termed dense granules favors antigen presentation, whereas retention of the antigen within the parasite prevents presentation (*Gubbets et al.,* 2005, *Kwok et al.*, 2003, *Gregg et al.,* 2011). In addition, soluble antigens that are secreted into the parasitophorous vacuole (PV) lumen appear to enter the MHC-I presentation pathway via a Sec22b-dependent ER to Golgi intermediate compartment (ERGIC) pathway (*Joffre et al.,* 2012, *Goldszmid et al.,* 2009, *Cebrian et al.,* 2011), and are processed in a proteasome/TAP dependent manner (*Gubbels et al.,* 2005, *Bertholet et al.,* 2006) **(Figure 1)**. In contrast, the immunodominant GRA6 antigen, which is also secreted via dense granules, does not require Sec22b (*Buaillon et al.,* 2017). After secretion, the GRA6 protein associates with the PV membrane (PVM) with its C-terminal epitope protruding into the host cytosol, and this orientation favors efficient presentation (*Buaillon et al.,* 2017, *Feliu et al.,* 2013, *Lopez et al.,* 2015) **(Figure 1)**. Presentation of the HF10-GRA6 epitope has been shown to require components of the classical MHC-I pathway such as the proteasome, TAP, and ERAAP (*Blanchard et al.,* 2008), however it is unknown how the epitope is released from the PVM to access this pathway. It has been hypothesized that an unidentified protease may cleave the C-terminal epitope which protrudes into the host cell cytosol. Interestingly, some host proteins involved in cross-presentation, such as Rab22a and Sec61, associate directly with the PV (*Goldszmid et al.,* 2009, *Cebrian et al.,* 2016), suggesting there may be direct access of parasite antigens to the cross-presentation pathway. On the other hand, for some antigens, access to the cytosol may be accomplished through damage to the PVM by host defense mechanisms such as immunity-related GTPases (IRGs) (*Dzierszinski et al.,* 2007, *Lee et al.,* 2015).

In addition to constitutive secretion via dense granules, *T. gondii* also possesses a distinct secretory pathway via organelles termed rhoptries. Rhoptries directly discharge their contents into host cells during the invasion process, and during abortive invasion events (*Boothroyd et al.,* 2008, *Koshy et al.,* 2012). This model of secretion might be expected to favor MHC-I presentation, since the antigens have direct access to the host cytosol and the classic MHC-I presentation machinery **(Figure 1)**. However, rhoptry targeted antigens are relatively weak antigens (*Frickel et al.,* 2008), and antigenicity can be improved by retargeting a rhoptry epitope for dense granule secretion (*Grover et al.,* 2014) (Table 2). This may reflect the transient nature of rhoptry secretion, and failure to accumulate sufficient parasite antigen in the cytosol.

A model for effector CD8+ T cell responses

Most of our knowledge about CD8+ T cell responses to persistent infections comes from studies with Lymphocytic choriomeningitis virus (LCMV), in which chronic infection and persistently high antigen load leads to functional impairment of T cells, or T cell exhaustion (*Barber et al.,* 2006, *Virgin et al.,* 2009, *Wherry et al.,* 2011). HIV, one of the most medically important chronic viral infections, also results in T cell exhaustion (*Goepfert et al.,* 2000, *Shankar et al.,* 2000, *Day et al.,* 2006) but is difficult to study due to lack of an appropriate mouse model. Well-controlled viral infections can be complicated by factors such as periods of viral latency or the phenomena of epitope switching and "memory inflation" observed in Murine Cytomegalovirus (MCMV) infection (*Karrer et al.,* 2003, *Snyder et al.,* 2008). Therefore, our understanding of the mechanisms that maintain effective control during infection with persistent pathogens is limited and could benefit from additional mouse models. Studies focusing on T cell responses during *T. gondii* infection have provided insights into T cell function and differentiation.

Features of the CD8+ response to T. gondii

CD8+ T cells are critical for effective control of many intracellular pathogens, including *T. gondii* (*Gigley et al.,* 2011). Early work utilizing depletion or knockout studies demonstrated that CD8+ T cells are the most protective adaptive immune cell type during infection (*Suzuki et al.,* 1990, *Parker et al.,* 1991, *Schaeffer et al.,* 2009). IFNγ has been identified as a key mediator of protection (*Suzuki et al.,* 1990, Suzuki *et al.,* 1988, *Norose et al.,* 2001), and CD8+ T cells, in addition to CD4+ T cells, serve as important cytokine producers. CD8+ T cells can also mediate lysis of infected cells, and recently direct lysis of parasites through granulysin secretion in the acute stage has been demonstrated as well (*Dotiwala et al.,* 2016).

The observation that BALB/c (H-2^d) mice are better at controlling *T. gondii* infection compared to C57BL/6 mice (H-2^b) led to this trait being mapped to the MHC-I L^d gene in BALB/c mice (*Brown et al.,* 1995). We and our colleagues have shown that this is due to the induction of an immunodominant and protective CD8+ T cell response directed against a peptide from the parasite protein GRA6 (*Blanchard et al.,* 2008). BALB/c mice are able to establish effective long-term control of the parasite, while C57BL/6 mice, which lack L^d and therefore cannot present the GRA6 peptide, develop progressing disease. These two contrasting settings provide a unique opportunity to study the differentiation, exhaustion, and maintenance of CD8+ T cell responses to infection in the context of a well-controlled infection versus a poorly-controlled progressing infection.

CD8+ T cell differentiation during acute infection

During an immune response, naive pathogen-specific CD8+ T cells differentiate into functionally heterogeneous populations characterized by distinct

memory potential and effector functions (*Williams et al.,* 2007). This differentiation is regulated by various signals, including T cell receptor signaling, co-stimulatory signals, and cytokine signals received from APC or other bystander cells. In particular, inflammatory cytokines such as IL-12 and type-I interferons have been shown to function as a "signal 3", directly signaling activated CD8+ T cells to promote proliferation and effector functions *in vitro* and *in vivo* (*Curtsinger et al.,* 1999, *Curtsinger et al.,* 2005, *Kolumam et al.,* 2005).

The specific cytokines that drive early effector differentiation can vary between models, and studies examining CD8+ T cell fate during acute *T. gondii* infection in C57BL/6 mice have identified a critical role for IL-12 in this system. IL-12 knockout mice fail to generate large numbers of effector CD8+ T cells and show reduced expression of KLRG1 (*Wilson et al.,* 2008, *Wilson et al.,* 2010), a widely used marker of effector differentiation. Co-infection of mice with *T. gondii* and an intestinal helminth can promote the type-II cytokine IL-4, which together with IL-10 suppresses IL-12 responses and dampens effector CD8+ differentiation (*Marple et al.,* 2017). IL-12 impacts the different stages of effector T cell differentiation both by signaling directly to the T cell or through activating other cell types to make IFNγ (*Shah et al.,*2015) **(Figure 2)**.

As CD8+ T cells differentiate during acute infection, their localization within lymphoid tissues changes. *Shah et al*. tracked the location of T cell populations in the spleen as they progressed through various stages of differentiation after vaccination with an attenuated parasite strain (*Sha et al.,* 2015). As cells matured from naïve to terminally differentiated effectors, they moved from the white pulp through the marginal zone into the red pulp. This migration into the red pulp appears to be regulated by the chemokine receptor CXCR3 and its ligands CXCL9 and CXCL10, similar to the role of CXCR3 on CD8+ T cells in other models (*Hu et al.,* 2011, *Kurachi et al.,* 2011). This relationship between fate and location suggests there may be environmental signals promoting distinct fates in these different regions.

CD8+ T cells in progressing chronic infection

Although C57BL/6 mice are able to mount effective CD8+ T cell responses during acute infection, they are ultimately unable to control the parasite in chronic stages of infection, resulting in mouse mortality due to toxoplasmic encephalitis (TE). In this setting, CD8+ T cells upregulate the inhibitory receptor PD-1, a marker of T cell exhaustion typically upregulated in chronic viral infections (*Bhadra et al.,* 2011). These CD8+ T cells also lose effector functions, and become more susceptible to apoptosis (*Bhadra et al.,* 2012)**.** *In vivo* blockade of the receptor for PD-1, PD-L1, referred to as checkpoint blockade, rescues PD-1+ CD8+ T cells, leading to improved CD8+ T cell responses and prevention of TE-associated mortality (*Bhadra et al.,* 2018). However, the infection model may impact the efficacy of this treatment, as neutralization of inhibitory receptors failed to reverse CD8+ T cell exhaustion and rescue infected mice after challenge with hyper-virulent strains (*Splitt et al.,* 2018).

Recently, a progenitor-like CD8+ T cell population that responds to checkpoint blockade in certain models of chronic infection and tumors has been identified and characterized (*Im et al.,* 2016, *Utzschneider et al.,* 2016, *Kurtulus et al.,* 2019). These cells share some common features across models, the most prominent being expression of *Tcf7*/TCF1, a transcription factor associated with self-renewal capacity. It will be interesting to determine whether a similar progenitor-like CD8+ T cell population is present in mice chronically infected by *T. gondii,* and whether its presence or absence correlates with the response of mice to checkpoint blockade.

CD4+ T cell help plays a role in preventing or reversing CD8+ T cell exhaustion during infection with *T. gondii* and other chronic viral pathogens. Expression of the transcription factor Blimp-1 in CD4+ T cells correlates with CD4+ T cell exhaustion during *T. gondii* infection **(Figure 2)**, and deletion of Blimp-1 restores function of these CD4+ T cells (*Hwang et al.,* 2016). Boosting CD4+ T cell function by deletion of Blimp-1 or adoptive transfer of functional CD4+ T cells into chronically infected mice can also restore CD8+ T cell function after exhaustion (*Hwang et al.,* 2016). IL-21 is a key cytokine produced by follicular helper CD4+ T cells (Tfh) that has an important role in proper B cell activation. Interestingly, IL-21 also appears to be critical in maintaining CD8+ T cell functionality during chronic *T. gondii* infection. Exhausted CD4+ T cells lose IL-21 production but re-gain production after Blimp-1 ablation (*Hwang et al.,* 2016, *Moretto et al.,* 2017). In addition, IL-21 knockout mice have impaired CD8+ responses and reduced ability to control the parasite compared to wild-type mice (*Moretto et al.,* 2017).

CD8+ T cells in a well controlled chronic infection

Utilizing the unique model of parasite control in H-2^d-expressing mice allows for investigations of the factors regulating CD8+ T cells in a well-controlled chronic infection and provides an interesting contrast to the H-2^b model of susceptibility. H-2^d-linked protection is mediated by an immunodominant CD8+ T cell response against the parasite protein GRA6 (*Blanchard et al.,* 2008). Investigations into the processing and presentation of the GRA6 epitope have advanced our understanding of MHC-I presentation (see above), and this unique response has begun to provide key insights into novel features of CD8+ T cell function as well. Unlike T cells in most chronic infections, GRA6-specific CD8+ T cells do not upregulate PD-1 or other inhibitory receptors and retain cytotoxic capacity and cytokine production throughout chronic infection (*Chu et al.,* 2016). Investigating the exact mechanisms behind this may provide novel therapeutic targets to prevent or reverse T cell exhaustion.

The protective capacity of CD8+ T cell responses against GRA6 have also been demonstrated by other groups. Sanecka et al. showed that GRA6-specific transnuclear CD8+ T cells significantly reduced parasite burden during the acute phase of infection (*Sanecka et al.,* 2016), while Sa et al. provided evidence that GRA6-specific CD8+ T cells play a role in cyst removal during chronic infection (*Sa et al.,* 2017).

The GRA6 response also develops a unique differentiation profile. GRA6-specific T cells maintain a balance between three functionally distinct populations defined by surface expression of CXCR3 and KLRG1 (*Chu et al.,* 2016). A long-lived memory population (T_{MEM}) gives rise to a highly proliferative intermediate population (T_{INT}) that allows the generation of a large number of terminally differentiated effectors (T_{EFF}). Modeling studies demonstrated the importance of this novel T_{INT} population in rapidly producing new T_{EFF} cells without depleting the T_{MEM} population, and subdominant responses lacking this T_{INT} population were not maintained well throughout the chronic stages of infection.

Certain similarities exist between the wave of effector T cell differentiation that occurs following *T. gondii* vaccination and the continuous production of effector T cells that occurs during well-controlled *T. gondii* infection **(Figure 2)**. In both settings, CXCR3 is expressed early but is subsequently lost as cells progress to terminal differentiation. KLRG1 expression is regulated inversely, with initial upregulation being observed during the intermediate stages of differentiation and high expression continuing through terminal differentiation. Both models also feature proliferation specifically within a CXCR3+ KLRG1+ population (*Shah et al.,* 2015, *Chu et al.,* 2016). In light of these similarities it is important to investigate the location of each GRA6-specific population within the spleen during chronic infection and the role of inflammatory cytokines like IL-12 and IFNγ.

CD8+ T Cell Responses in the Brain

During infection, *T. gondii* crosses the blood-brain barrier and establishes brain cysts that allow the parasite to persist into the chronic phase. Control of the parasite necessitates an ongoing immune response in the brain, providing a unique opportunity to study CD8+ T cell entry, retention, and function in the brain.

T cell entry into the brain

T cell entry into the brain is a multi-step process mediated by interactions with endothelial cells and dependent on an array of adhesion molecules and chemokine receptors (*Landrith et al.,* 2015). *T. gondii* infection induces endothelial cells to express increased amounts of integrins and selectins like PECAM-1, ICAM-1 and VCAM-1. These integrins appear to be critical for T cell entry, as antibody blocking of VLA-4, the ligand for VCAM-1, prevents entry (*Wilson et al.,* 2009). Infection also increases the expression of the inflammatory chemokines CXCL9 and CXCL10 in the brain (*Harris et al.,* 2012), which function as ligands for the chemokine receptor CXCR3. CXCR3 plays a critical role in T cell entry in the brain in other viral and parasitic infection models (*Klein et al.,* 2005, *Campanella et al.,* 2008, Zhang *et al.,* 2008). Antibody blockade of CXCL9 (*Ochiai et al.,* 2015) or CXCL10 (*Harris et al.,* 2012) during infection dramatically reduces the numbers of brain-infiltrating CD8+ T cells, supporting a vital role of this axis during *T. gondii* infection as well. Together, these studies indicate that inflammation appears to be a key element regulating T cell infiltration into the

brain. Anti-PDL1 treatment also results in increases in CD3+ and CD8+ cells in the brains of *T. gondii* infected mice (*Xiao et al.,* 2018). While the exact mechanisms remain unclear, it is possible that increased inflammation following checkpoint blockade mediates this increase in T cell infiltration in the brain.

T cell retention in the brain

While inflammatory signals are sufficient to mediate the initial entry of antigen-experienced T cells into the brain, only T cells with the appropriate antigen specificity are efficiently retained in the brain. OVA-specific CD8+ T cells activated *in vitro* and then transferred into mice infected with *T. gondii* were observed in the brain, despite the absence of the OVA epitope in this model (*Schaeffer et al.,* 2009). While these OVA-specific T cells were capable of entering the brain, their numbers rapidly declined in this setting. T cells' affinity for their antigen may also regulate their retention. Two T cell clones with different affinities for the same epitope were shown to enter the brain in similar numbers, but the lower affinity clone exhibited more rapid contraction in the brain five weeks post-infection (*Sanecka et al.,* 2018).

T cell-mediated protection in the brain

While antigen recognition appears to promote T cell retention and effector function in the brain, the nature of the brain cells that present parasite antigens to T cells remains incompletely understood. Static imaging of brain sections revealed that parasite-specific T cells interacted with granuloma-like aggregates of CD11b+ cells harboring parasite material (*Schaeffer et al.,* 2009). In contrast, no interaction was observed between T cells and intact cysts (*Schaeffer et al.,* 2009), which were likely contained within neurons (*Ferguson et al.,* 1994). However, recent evidence suggests that neurons can present antigen directly to T cells, and that this presentation is critical for parasite control in the brain (*Salvioni et al.,* 2019). L^d-expressing mice with a neuron-specific L^d knockout had dramatically increased numbers of brain cysts and increased amounts of parasite DNA despite high numbers of antigen-specific CD8+ T cells. Restricting the expression of the immunodominant antigen specifically to the tachyzoite stage did not significantly reduce the CD8+ T cell response, nor reduce their ability to protect from encephalitis (Table 2). Together with the previous imaging data, this suggests that tachyzoite recognition within neurons may result in critical T cell:neuron interactions, while bradyzoites within cysts remain relatively invisible to T cells.

Resident memory T cells

Resident memory T cells (T_{RM}) are a distinct lineage of cells that confer protection directly in the relevant tissues rather than within the lymphatic system. Traditionally, tissue residence has been defined by an inability of these cells to recirculate in the mouse as shown by parabiosis experiments. CD8+ T cells that

remain in the brain during *T. gondii* infection appear to adopt a T_{RM} phenotype, evidenced by surface expression of CD69 and CD103 (*Chu et al.,* 2016, *Sanecka et al.,* 2018). Supporting their status as bona-fide T_{RM} cells, CD8+ T cells in the brains of *T. gondii* infected mice also have a transcriptional profile resembling a T_{RM} signature (*Landrith et al.,* 2017), though parabiosis experiments have not demonstrated their tissue residence status using the classic definition. *T. gondii* infection may provide a unique opportunity to study these cells, and future work investigating the development and protective capacity of these cells will be of great interest.

Concluding Remarks and Future Perspectives

Studies of *T. gondii* infection in mice have made seminal contributions to the field of CD8+ T cell biology and our understanding of how CD8+ T cells detect and respond to intracellular pathogens. The *T. gondii*-mouse infection model will be instrumental in addressing additional questions in the field. The *T. gondii* parasite provides us with a unique model to investigate the requirements for presentation of vacuolar antigens, which cannot be studied with a viral model in which antigens are translated in the cytosol. As we learn more about how *T. gondii* antigens are processed and presented to CD8+ T cells, it is becoming clear that different antigens use distinct pathways based on their location and trafficking within host cells. Future studies to address the detailed mechanisms of these pathways will provide additional insight into the general problem of how exogenous and vacuolar antigens are cross-presented via MHC-I. Moreover, *T. gondii* shows considerable promise as a vaccine vector (*Fox et al.,* 2017), and understanding the factors that lead to efficient processing and presentation of parasite antigens may also help to realize the full potential of this approach.

Much of our understanding of how CD8+ T cells respond to chronic infections is based on a limited number of mouse infection models, particularly the widely studied LCMV clone 13 model of chronic infection. The addition of the *T. gondii* infection model has broadened our perspective on this topic. *T. gondii* infection has contributed to our understanding of CD8+ T cell responses to infection in the central nervous system (CNS), as neurotropic viral mouse models are limited. Additionally, the difference in control of *T. gondii* infection between two strains of inbred mice provides the unique opportunity to compare CD8+ T cell function in a progressing disease setting *versus* a well-controlled chronic infection. Studies have identified a novel T cell population fundamental for control in the resistant setting, as well as cellular mechanisms leading to disease in susceptible mice.

One example demonstrating the potential of this system can be found in Salvioni et al. (2019), where the authors engineered a parasite strain expressing the OVA epitope in a manner similar to the immunodominant GRA6 epitope (*Salvioni et al.,* 2019) (see Table 2). This system allowed the authors to recapitulate H-2^d-mediated protection in the typically susceptible H-2^b setting, highlighting the critical importance of antigen processing in generating parasite control. Similar efforts to take lessons from the H-2^d-restricted protective setting

and manipulate the H-2^b-restricted susceptible setting to improve protective capacity may lead to exciting advancements in our understanding of CD8+ T cell function.

1.2: Memory and Proliferative CD8+ T cell Populations During Chronic Infections

Effective CD8+ T cell-mediated control of chronic pathogens requires the maintenance of a long-lived stem-like population of CD8+ T cells that continuously supply a pool of effector cells. Recent studies have identified stem-like memory CD8+ T cells across various mouse models of chronic infection, including LCMV, MCMV, and *T. gondii*. In addition to the identification of memory and effector subsets, these three models have also identified proliferative intermediate cells that link the two, providing a proliferative burst that allows the relatively quiescent stem population to produce a large number of effectors without depleting itself. Despite the many differences between infection with these pathogens, the stem, intermediate, and effector CD8+ T cells that exist during chronic infection retain many similarities between them that provide insight into how distinct cell fates may be regulated.

CD8+ T cell fate during chronic LCMV infection

Mouse infection with LCMV is one of the most widely studied experimental infection models. Certain strains of LCMV establish a chronic infection that is characterized by high viral burden and widespread inflammation, resulting in CD8+ T cells becoming highly exhausted. Exhausted T cells lose effector capabilities and the ability to proliferate due to elevated expression of inhibitory receptors like PD-1, Tim-3, and Lag-3 *(Wherry*, 2011). Treating mice with anti-PD-1 checkpoint blockade therapy reverses some of the effects of exhaustion, resulting in a burst of proliferation (*Barber et al.,* 2006). Studies investigating the cells responding to checkpoint blockade determined that the responding subset is a putative stem-like population of CD8+ T cells (*Im et al.,* 2016). The initial identification of these cells used CXCR5 expression (*Im et al.*, 2016; *Leong et al.*, 2016), but eventually expression of the master transcription factor *Tcf7* (encoding TCF1) became the defining marker (*Utzschneider et al.*, 2016). After treatment with anti-PD1 therapy, TCF1+ stem-like CD8+ T cells became reinvigorated and were able to give rise to a large number of proliferative intermediate cells, termed Transitory cells (*Hudson et al.*, 2019). Transitory cells have an effector-like phenotype, low levels of exhaustion markers, and are identified as Tim3+ CD101- CX3CR1+ cells. *Hudson et al.* observed that Transitory cells are specifically produced after anti-PD-L1 treatment, and using a CX3CR1-DTR mouse strain they demonstrated a critical role of these cells in mediating pathogen control. The paradigm that emerges from these studies suggests three distinct lineages of CD8+ T cells that persist during chronic LCMV infection: Stem cells with a TCF1+ Tim3- CD101- phenotype, proliferative Transitory intermediate

cells with a TCF1- Tim3+ CX3CR1+ CD101- phenotype, and terminally-differentiated Exhausted effector cells with a TCF1- Tim3+ CD101+ phenotype.

CD8+ T cell fate during chronic MCMV infection

In contrast to LCMV, MCMV establishes a relatively well-controlled chronic infection characterized by viral latency and the virus being sequestered primarily to the salivary glands. CD8+ T cells responding to MCMV infection experience a phenomenon termed memory inflation, whereby some populations of antigen-specific T cells continuously expand during chronic infection (*Klenerman*, 2018). Studies focusing on memory inflation utilized adoptive transfers to determine that a stem-like memory population was retained within the inflation memory pool (*Quinn et al.*, 2015), and subsequently a TCF1+ population with a memory phenotype was identified (*Welten et al.*, 2020). Upon antigen encounter MCMV-specific TCF1+ cells proliferate and feed into the robust TCF1- KLRG1+ population of effector cells. Despite this critical role for TCF1+ cells in maintaining the memory inflation population, it was determined that the major proliferative population *in vivo* during infection is a KLRG1+ subset (*Smith, Turula and Snyder, 2014)*, suggesting a population with an effector phenotype analogous to Transitory cells exists. These proliferating KLRG1+ cells were found primarily in the spleen (*Smith, Turula and Snyder*, 2014) and led to the production of short-lived, highly functional effector T cells (*Snyder et al.*, 2008). Subsequently, *Gordon et al*. used the marker CX3CR1 to identify three functionally distinct populations present during memory inflation: CX3CR1- memory-like precursor cells, $CX3CR1^{int}$ cells that are highly proliferative intermediate cells, and $CX3CR1^{hi}$ terminally differentiated effector cells (Gordon *et al.*, 2018). The authors observed these subsets during both humans mouse CMV infection, indicating these populations are likely critical for responses to human chronic infections as well.

CD8+ T cell fate during chronic T. gondii infection

Similar to MCMV, chronic *T. gondii* infection in $H\text{-}2^{d}$ mice establishes a well-controlled chronic infection characterized by the absence of detectable parasites in the periphery but an ongoing infection in the brain enabled by neuronal cysts. While both LCMV and MCMV infection induce an array of potent antigen-specific CD8+ T cell responses, *T. gondii* infection induces a single immunodominant population of CD8+ T cells specific against a peptide within the parasite protein GRA6. Despite the lack of detectable parasites outside the brain, GRA6-specific CD8+ T cells in the spleen experience continuous antigen exposure and continue to proliferate throughout chronic infection. Our work investigating GRA6-specific CD8+ T cell fate during chronic infection led to the discovery of three antigen-specific populations that can be identified using the surface markers CXCR3 and KLRG1 (*Chu et al.,* 2016). CXCR3+ KLRG1- memory cells (T_{MEM}) are relatively quiescent cells with stem-like capacity. T_{MEM} cells give rise to CXCR3+ KLRG1+ intermediate cells (T_{INT}) that are highly

proliferative and capable of producing a large population of CXCR3- KLRG1+ terminally-differentiated effector cells (T_{EFF}). Phenotypic analysis of these subsets revealed that T_{INT} cells are highly metabolically active and possess both memory and effector qualities, and mathematical modeling demonstrated that T_{INT} cells are critical for the ability of the immune response to produce sufficient numbers of T_{EFF} cells without depleting the T_{MEM} pool.

Common and unique features of Stem and Proliferative CD8+ T cell Populations

While the stem, proliferative, and terminally differentiated CD8+ T cell populations described above have all been identified using various surface markers in different infection contexts, many common features have emerged. The most prominent similarity between the different models is the shared expression of *Tcf7*/TCF1, which has previously been demonstrated to mark stem cells in LCMV and MCMV infection and which we demonstrate herein marks the T_{MEM} cells in *T. gondii* infection. Stem populations in all three infection models possess common memory markers including a CD127^{hi} KLRG1^{lo} GzmB- CX3CR1- phenotype. While the stem-like cells in *T. gondii* and MCMV infection are marked by reduced effector functions, during LCMV infection TCF1+ cells are the most capable of producing cytokines, perhaps due to the widespread exhaustion of the more terminally differentiated subsets. The proliferative intermediate populations in each infection model share several phenotypic similarities as well. Most notable is the common expression of KLRG1 in all three infection models. All three populations also show a loss of CCR7 and CD62L expression. In contrast, CD127 expression is mixed during *T. gondii* and MCMV infection, while Transitory cells express little *Il7r* mRNA. CX3CR1 is also intermediately expressed in *T. gondii* and MCMV but is uniquely expressed by Transitory cells. These features suggest that T_{INT} cells and MCMV-specific CX3CR1^{int} cells are closely related, while the Transitory cells appear the most divergent.

The transcriptional profile of stem cells during LCMV has been investigated, and herein we describe the transcriptional profile of T_{MEM} cells during *T. gondii* infection. In both infections, stem cells express transcription factors typical of classic memory, including increased expression of *Tcf7* and *Id3* and low expression of *Id2* and *Prdm1* (encoding Blimp-1). Both stem subsets also display elevated expression of costimulatory proteins and expression of a small subset of toll-like receptors, suggesting they may be highly poised to respond to environmental cues. While several transcription factors are shared between the subsets, the expression of Tbet and Eomes, two transcription factors critical for CD8+ T cell fate and function, differs between the three models. Stem cells in LCMV and *T. gondii* appear to express Tbet, while during MCMV infection they are Tbet^{lo}. In contrast, Eomes is expressed by stem cells in LCMV and MCMV infection, while during *T. gondii* infection the T_{MEM} cells show only minor Eomes expression compared to T_{INT}. Finally, FOXO1 is critical for sustaining stem cells in both LCMV and MCMV, while its role during *T. gondii* infection has not been addressed. Despite these parallels between the stem

populations, LCMV-specific stem cells have a unique expression of a follicular CD4 T_{FH} phenotype, including high expression of *Bcl6* and CXCR5. The absence of this phenotype on cells during *T. gondii* infection may be due, in part, to differences in pathogen tropism, as LCMV readily infects B cells.

The expression of CXCR5 by TCF1+ cells during LCMV infection led to the hypothesis that the B cell zone may be a critical niche for these cells. Indeed, images taken from chronically infected mice showed that many TCF1+ cells localized to the B cell follicle, though the T cell zone contained a greater fraction of the cells. Our studies herein describe the localization of T_{MEM}, T_{INT}, and T_{EFF} cells and demonstrate that T_{MEM} cells reside primarily within the splenic white pulp. In line with the lack of robust CXCR5 expression, few T_{MEM} cells localized to the B cell follicle. We also observed that proliferating T_{INT} cells are localized to the red pulp, which parallels results showing that proliferating KLRG1+ cells in the MCMV-specific inflation memory pool occupy the highly blood-exposed region of the spleen. While the exact localization of Transitory cells has not been identified, it seems likely they will be found in the red pulp as well due to their lack of *Ccr7* and high expression of *S1pr5*.

Perhaps the most critical difference observed in the intermediate populations is the degree to which they are sustained during infection. Continuous proliferation and effector differentiation are both observed during *T. gondii* and MCMV infection, while Transitory cells are rare during LCMV infection and require checkpoint blockade to emerge. This difference is likely caused by the exhaustion of the stem-like precursor cells. During the well-controlled *T. gondii* and MCMV infections, TCF1+ cells retain functionality and continue to feed into the effector pool, reflecting the environment of LCMV infection after checkpoint blockade. Thus, studying the dynamics of CD8+ T cell differentiation both in the context of widespread exhaustion and efficient control are critical for developing efficient ways of targeting these cells to improve vaccine design and produce novel immunotherapies.

1.3: References

Joffre, O. et al. (2012) Cross-presentation by dendritic cells. Nat. Rev. Immunol. 12, 557-569

Gubbels, M.J. et al. (2005) Class I major histocompatibility complex presentation of antigens that escape from the parasitophorous vacuole of *Toxoplasma gondii*. Infect. Immun. *73*, 703-711

Dupont, C.D. et al. (2014) Parasite Fate and Involvement of Infected Cells in the Induction of CD4+ and CD8+ T Cell Responses to *Toxoplasma gondii*. PLoS Pathog. 10(4), DOI: 10.1371/journal/ppat.1004047

Kwok, L.Y. et al. (2003). The induction and kinetics of antigen-specific CD8 T cells are defined by the stage specificity and compartmentalization of the antigen in murine toxoplasmosis. J. Immunol. 170, 1949-1957

Gregg, B. et al. (2011) Subcellular Antigen Location Influences T-Cell Activation during Acute Infection with *Toxoplasma gondii*. PLoS One 6(7), DOI: 10.1371/journal.pone.0022936

Goldszmid, R.S. et al. (2009) Host ER-parasitophorous vacuole interaction provides a route of entry for antigen cross-presentation in *Toxoplasma gondii*-infected dendritic cells. J. Exp. Med. 206, 399-410

Cebrian, I. et al. (2011) Sec22b regulates phagosomal maturation and antigen cross-presentation by dendritic cells. Cell 147(6), 1355-1368

Bertholet, S. et al. (2006) *Leishmania* antigens are presented to CD8+ T cells by a transporter associated with antigen processing-independent pathway *in vitro* and *in vivo*. J Immunol. 177(6), 3525-3533.

Buaillon, C. et al. (2017) MHC I presentation of *Toxoplasma gondii* immunodominant antigen does not require Sec22b and is regulated by antigen orientation at the vacuole membrane. Eur. J. Immunol. 47, 1160-1170

Feliu, V. et al. (2013) Location of the CD8 T Cell Epitope within the Antigenic Precursor Determines Immunogenicity and Protection against the *Toxoplasma gondii* Parasite. PLoS Pathog. 9, DOI: 10.1371/journal.ppat.1003449

Lopez, J. et al. (2015) Intravacuolar membranes regulate CD8 T cell recognition of membrane-bound *Toxoplasma gondii* protective antigen. Cell Rep. 13(10), 2273-2286

Blanchard, N. et al. (2008) Immunodominant, protective response to the parasite *Toxoplasma gondii* requires antigen processing in the endoplasmic reticulum. Nat. Immunol. *9*, 937-944

Cebrian, I. et al. (2016) Rab22a controls MHC-I intracellular trafficking and antigen cross-presentation by dendritic cells. EMBO Rep. 17, 1753-1765

Dzierszinski, F. et al. (2007) Presentation of *Toxoplasma gondii* antigens via the endogenous major histocompatibility complex class I pathway in nonprofessional and professional antigen-presenting cells. Infect. Immun. 75, 5200-5209

Lee, Y. et al. (2015) p62 plays a specific role in Interferon-g-induced presentation of a *Toxoplasma* vacuolar antigen. Cell Rep. 13(2), 223-233

Boothroyd, J.C. and Dubremetz J.F. (2008) Kiss and split: the dual roles of *Toxoplasma* rhoptries. Nat. Rev. Microbiol. 6(1), 79-88

Koshy, A. et al. (2012) *Toxoplasma* co-opts host cells it does not invade. PLoS Pathog. 8(7), DOI: 10.1371/journal.ppat.1002825

Frickel, E.M. et al. (2008) Parasite stage-specific recognition of endogenous *Toxoplasma gondii*-derived CD8+ T cell epitopes. J. Inf. Dis. 198, 1625-1633

Grover, H.S. et al. (2014) Impact of regulated secretion on antiparasitic CD8 T cell responses. Cell Rep. 7, 1716-1728

Barber, D.L. et al. (2006) Restoring function in exhausted CD8 T cells during chronic viral infection. Nature 439(7077), 682-687

Virgin, H.W., et al. (2009) Redefining chronic viral infection. Cell 138, 30-50

Wherry, E.J. (2011) T cell exhaustion. Nat. Immunol. 12, 492-499

Goepfert, P.A. et al. (2000) A significant number of human immunodeficiency virus epitope-specific cytotoxic T lymphocytes detected by tetramer binding do not produce gamma interferon. J. Virol. 74(21), 10249-10255

Shankar, P. et al. (2000) Impaired function of circulating HIV-specific CD8+ T cells in chronic human immunodeficiency virus infection. Blood 96, 3094-3101

Day, C.L. et al. (2006) PD-1 expression on HIV-specific T cells is associated with T-cell exhaustion and disease progression. Nature 443(7109), 350-354

Karrer, U. et al. (2003) Memory inflation: continuous accumulation of antiviral CD8+ T cells over time. J. Immunol. 170, 2022-2029

Snyder, C.M. et al. (2008) Memory inflation during chronic viral infection is maintained by continuous production of short-lived, functional T cells. Immunity 29, 650-659

Gigley, J. P. et al. (2011) CD8 T cells and *Toxoplasma gondii*: a new paradigm. J. Parasitol. Res. 2011, DOI: 10.1155/2011/243796

Suzuki, Y. and Remington, J.S. (1990) The effect of anti-IFN-gamma antibody on the protective effect of Lyt-2+ immune T cells against toxoplasmosis in mice. J. Immunol. 144(5), 1954-1956

Parker, S.J. et al. (1991) CD8+ T cells are the major lymphocyte subpopulation involved in the protective immune response to *Toxoplasma gondii* in mice. Clin. Exp. Immunol. 84, 207-212

Schaeffer, M. et al. (2009) Dynamic imaging of T cell-parasite interactions in the brains of mice chronically infected with *Toxoplasma gondii*. J. Immunol. 182, 6379-6393

Suzuki, Y. et al. (1988) Interferon-gamma: the major mediator of resistance against *Toxoplasma gondii*. Science 240(4851), 516-518

Norose, K. et al. (2001) Organ infectivity of *Toxoplasma gondii* in interferon-gamma knockout mice. J. Parasitol. 87(2):447-452

Dotiwala, F. et al. (2016) Killer lymphocytes use granulysin, perforin and granzymes to kill intracellular parasites. Nat. Med. 22, 210-216

Brown, C.R. et al. (1995) Definitive identification of a gene that confers resistance against *Toxoplasma* cyst burden and encephalitis. Immunology 85, 419-428

Williams, M.A. and Bevan, B.J. (2007) Effector and Memory CTL Differentiation. Annu. Rev. Immunol. 25:171-92

Curtsinger, J.M. et al. (1999) Inflammatory cytokines provide a third signal for activation of naïve CD4+ and CD8+ T cells. J. Immunol. 162(6), 3256-62

Curtsinger, J.M. et al. (2005) Type I IFNs provide a third signal to CD8 T cells to stimulate clonal expansion and differentiation. J. Immunol. 174, 4465–4469

Kolumam, G.A. et al. (2005) Type I interferons act directly on CD8 T cells to allow clonal expansion and memory formation in response to viral infection. J. Exp. Med. 202, 637–50

Wilson, D. et al. (2008) IL-12 signaling drives CD8+ T cell IFNg production and differentiation of KLRG1+ effector subpopulations during *Toxoplasma gondii* infection. J. Immunol. 180(9), 5935-5945

Wilson, D.C. et al. (2010) Differential regulation of effector- and central-memory responses to *Toxoplasma gondii* Infection by IL-12 revealed by tracking of Tgd057-specific CD8+ T cells. PLoS Pathog. 6, DOI: 10.1371/journal.ppat.1000815

Marple et al. (2017) Cutting Edge: Helminth Coinfection Blocks Effector Differentiation of CD8 T Cells through Alternate Host Th2- and IL-10-Mediated Responses. J. Immunol. 198(2), 634-639

Shah et al. (2015) An extrafollicular pathway for the generation of effector CD8+ T cells driven by the proinflammatory cytokine, IL-12. eLife 4, DOI: 10.7554/eLife.09017

Hu et al. (2011) Expression of chemokine receptor CXCR3 on T cells affects the balance between effector and memory CD8 T-cell generation. PNAS. 108(21) , E118-27

Kurachi, et al. (2011) Chemokine receptor CXCR3 facilitates CD8+ T cell differentiation into short-lived effector cells leading to memory degeneration. J. Exp. Med. 208(8), 1605-20

Bhadra, R. et al. (2011) Control of *Toxoplasma* reactivation by rescue of dysfunctional CD8+ T-cell response via PD-1-PDL-1 blockade. PNAS 108, 9196-9201

Bhadra, R. et al. (2012) PD-1-mediated attrition of polyfunctional memory CD8+ T cells in chronic *toxoplasma* infection. J. Inf. Dis. 206, 125-134

Splitt, S.D. et al. (2018) PD-L1, TIM-3, and CTLA-4 Blockade Fails To Promote Resistance to Secondary Infection with Virulent Strains of *Toxoplasma gondii*. Infect. Immun. 86, DOI: 10.1128/IAI.00459-18

Im, S.J. et al. (2016) Defining CD8+ T cells that provide the proliferative burst after PD-1 therapy. Nature 537(7620), 417-421

Utzschneider, D.T. et al. (2016) T cell factor 1-expressing memory-like CD8(+) T cells sustain the immune response to chronic viral infections. Immunity 45(2), 415-427

Kurtulus, S. et al. (2019) Checkpoint blockade immunotherapy induces dynamic changes in PD-1-CD8+ tumor-infiltrating T cells. Immunity 50(1), 181-194

Hwang, S. et al. (2016) Blimp-1-mediated CD4 T cell exhaustion causes CD8 T cell dysfunction during chronic toxoplasmosis. J. Exp. Med. 213(9), 1799-1818

Moretto, M.M. et al. (2017) Downregulated IL-21 Response and T Follicular Helper Cell Exhaustion Correlate with Compromised CD8 T Cell Immunity during Chronic Toxoplasmosis. Front. Immunol. 8, 1436

Chu et al. (2016) Continuous Effector CD8+ T cell Production in a Controlled Persistent Infection is Sustained by a Proliferative Intermediate Population. Immunity. 45(1), 159-171

Sanecka, A. et al. (2016) Transnuclear CD8 T cells specific for the immunodominant epitope Gra6 lower acute-phase *Toxoplasma gondii* burden. Immunology 149(3), 270-279

Sa, Q. et al. (2017) Determination of a key antigen for immunolgical intervention to target the latent stage of *Toxoplasma gondii*. J. Immunol. 198(11), 4425-4434

Landrith T.A. et al. (2015) Characteristics and critical function of CD8+ T cells in the *Toxoplasma*-infected brain. Semin. Immunopathol. 37(3), 261-70

Wilson et al. (2009) Behavior of parasite-specific effector CD8+ T cells in the brain and visualization of a kinesis-associated system of reticular fibers. Immunity. 30(2), 300-311

Harris, T. et al. (2012) Generalized Levy walks and the role of chemokines in migration of effector CD8+ T cells. Nature 486, 545-548

Klein et al. (2005) Neuronal CXCL10 directs CD8+ T-cell recruitment and control of West Nile virus encephalitis. J. Virol. 79(17), 11457-66

Campanella et al. (2008) Chemokine receptor CXCR3 and its ligands CXCL9 and CXCL10 are required for the development of murine cerebral malaria. PNAS, 105(12):4814-9

Zhang et al. (2008) CXCR3 mediates region-specific antiviral T cell trafficking within the central nervous system during West Nile virus encephalitis. J. Immunol. 180(4), 2541-9

Ochiai et al. (2015) CXCL9 is Important for Recruiting Immune T Cells into the Brain and Inducing an Accumulation of the T Cells to the Areas of Tachyzoite Proliferation to Prevent Reactivation of Chronic Cerebral Infection with *Toxoplasma gondii*. Am. J. Pathol. 185(2), 314-24

Xiao et al. (2018) PD-1 immune checkpoint blockade promotes brain leukocyte infiltration and diminishes cyst burden in a mouse model of *Toxoplasma* infection. J. Neuroimmunol. 319, 55-62

Sanecka, A. et al. (2018) T Cell Receptor-Major Histocompatibility Complex Interaction Strength Defines Trafficking and CD103(+) Memory Status of CD8 T Cells in the Brain. Front. Immunol. 9, 1290

Ferguson, D.J. et al. (1994) A morphological study of chronic cerebral toxoplasmosis in mice: comparison of four different strains of *Toxoplasma gondii*. Parasitol. Res. 80(6), 493-501

Cabral, C.M. et al. (2016) Neurons are the primary target cell for the brain-tropic intracellular parasite *Toxoplasma gondii*. PLoS Pathog. 12(2), DOI: 10.1371/journal.ppat.1005447

Salvioni, A. et al. (2019) Robust control of a brain-persisting parasite through MHC I presentation by infected neurons. Cell Rep. 27(11), 3254-3268

Landrith, T.A. et al. (2017) CD103+ CD8 T cells in the *Toxoplasma*-infected brain exhibit a tissue-resident memory transcriptional profile. Font. Immunol. 8, 335

Fox, B. et al. (2017) Cancer therapy in a microbial bottle: Uncorking the novel biology of the protozoan *Toxoplasma gondii.* PLoS Pathog. 13(9); DOI: 10.1371/journal.ppat.1006523

Gordon, C. L. *et al.* (2018) 'Induction and Maintenance of CX3CR1-Intermediate Peripheral Memory CD8+ T Cells by Persistent Viruses and Vaccines', *Cell Reports*. ElsevierCompany., 23(3), pp. 768–782. doi: 10.1016/j.celrep.2018.03.074.

Hudson, W. H. *et al.* (2019) 'Proliferating Transitory T Cells with an Effector-like Transcriptional Signature Emerge from PD-1 + Stem- Article Proliferating Transitory T Cells with an Effector-like Transcriptional Signature Emerge from PD-1 + Stem-like CD8 + T Cells during Chronic In', *Immunity*. Elsevier Inc., pp. 1–16. doi: 10.1016/j.immuni.2019.11.002.

Klenerman, P. (2018) 'The (gradual) rise of memory inflation', pp. 99–112. doi: 10.1111/imr.12653.

Leong, Y. A. *et al.* (2016) 'CXCR5 + follicular cytotoxic T cells control viral infection in B cell follicles', 17(August). doi: 10.1038/ni.3543.NATURE.

Quinn, M. *et al.* (2015) 'Memory T Cells Specific for Murine Cytomegalovirus Re-Emerge after Multiple Challenges and Recapitulate Immunity in Various Adoptive Transfer Scenarios', *The Journal of Immunology*, 194(4), pp. 1726–1736. doi: 10.4049/jimmunol.1402757.

Smith, C. J., Turula, H. and Snyder, C. M. (2014) 'Systemic Hematogenous Maintenance of Memory Inflation by MCMV Infection', 10(7). doi: 10.1371/journal.ppat.1004233.

Welten, S. P. M. *et al.* (2020) 'Tcf1+ cells are required to maintain the inflationary T cell pool upon MCMV infection', *Nature Communications*. Springer US, 11(1), pp. 1–14. doi: 10.1038/s41467-020-16219-3.

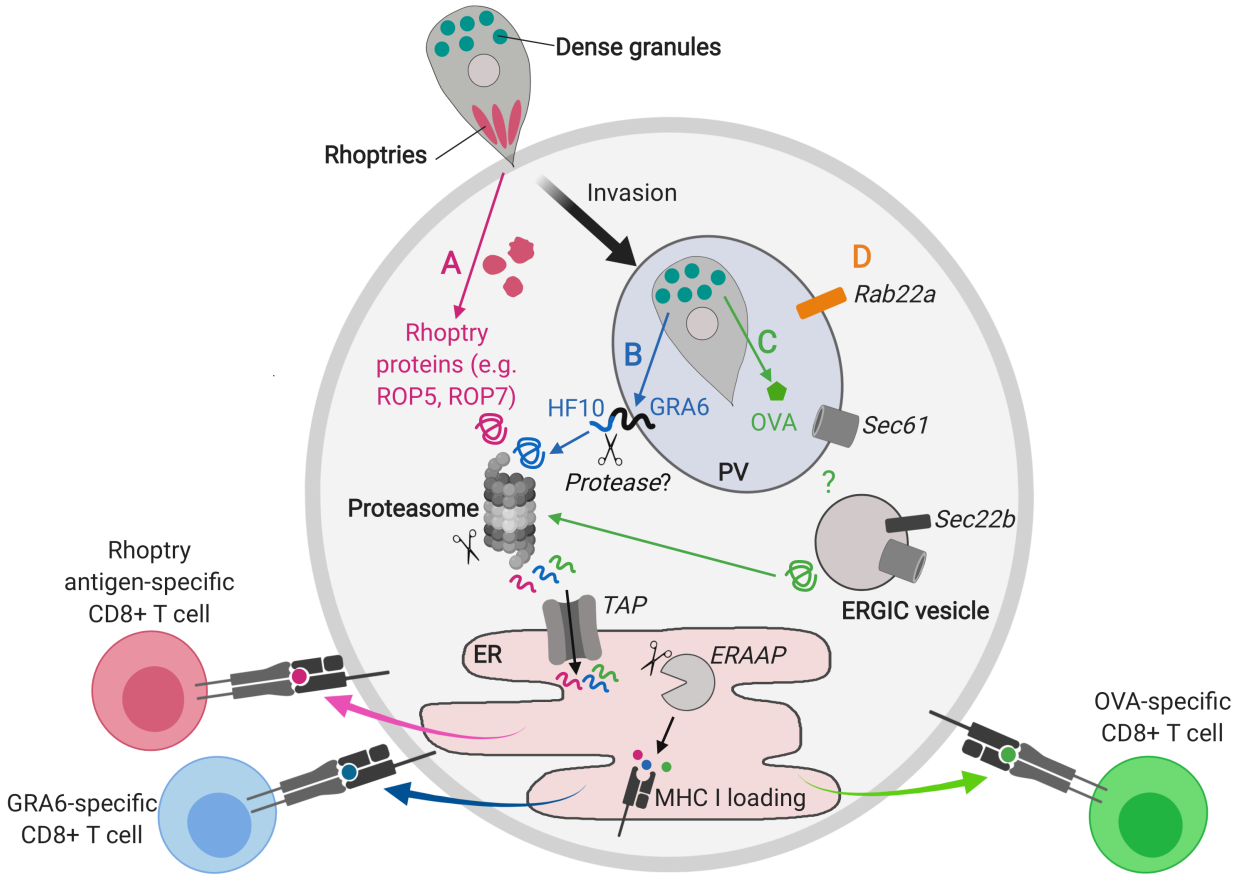

Figure 1: Modes of MHC-I presentation of vacuolar antigens. Distinct pathways of MHC-I antigen processing and presentation are shown for different *T. gondii* antigens. (a) During host cell invasion or abortive invasion events, parasites secrete the contents of their rhoptries into the host cell cytosol, allowing rhoptry proteins to access the classical MHC-I presentation pathway. In the classical MHC-I pathway, antigens are cleaved by the proteasome and transported to the ER for further processing and loading onto MHC-I. MHC-I-peptide complexes are transported to the surface of the antigen-presenting cells (APC) to be presented to CD8+ T cells. (b,c) After invasion of the host cell, the parasite generates a parasitophorous vacuole (PV) and dense granules are constitutively secreted into the PV lumen. The dense granule antigen GRA6 (b) associates with the parasitophorous vacuole membrane (PVM) with the C-terminal antigenic peptide protruding into the host cell cytosol. Processing of this peptide requires components of the classical MHC I pathway. It has been hypothesized that a protease may cleave the C-terminal epitope. Soluble dense granule proteins such as the model antigen OVA (c) secreted from transgenic parasites localize within the PV lumen. The antigen may be trafficked to the host cytosol following fusion of ER-Golgi intermediate compartment (ERGIC) vesicles with the PV, mediated by the Sec22b SNARE protein, however this part of the pathway is not fully understood. d) Additional proteins involved in cross-presentation like the Rab22a GTPase, which may play a role in recycling MHC-I molecules, accumulate on the PV in infected DCs. (Figure created with BioRender)

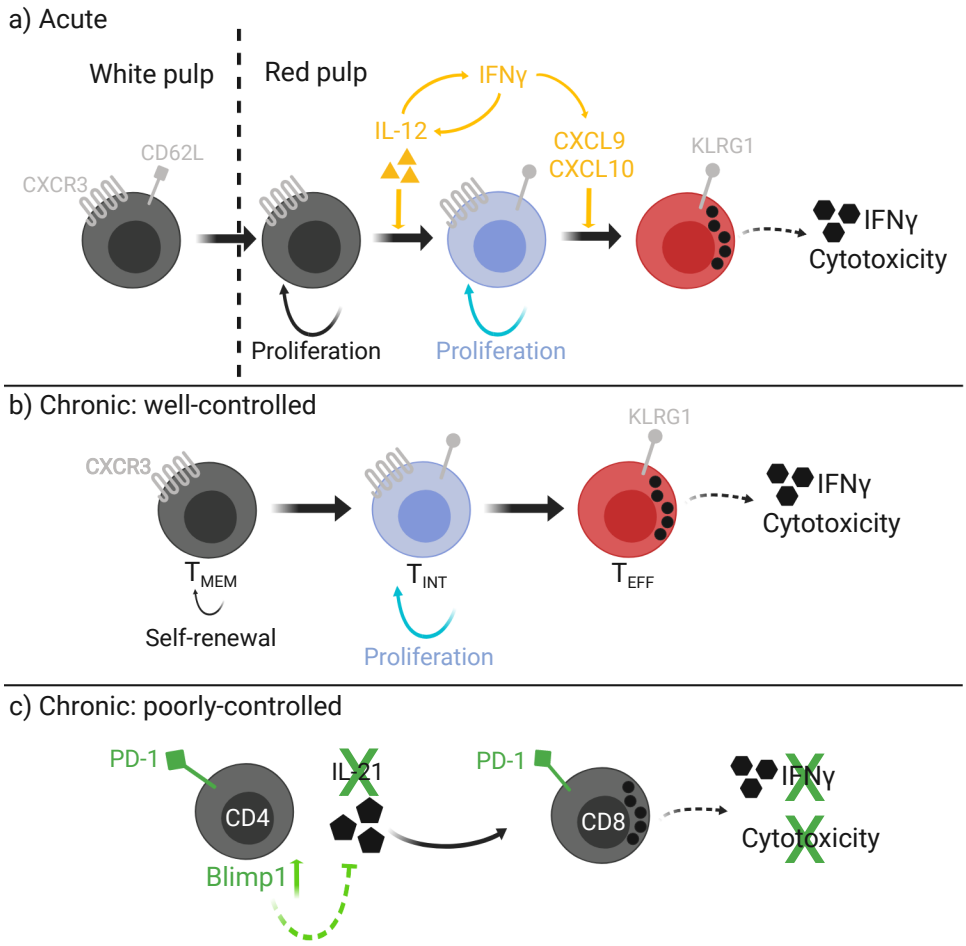

Figure 2: CD8+ T cell fate during *T. gondii* infection. Features of CD8+ T cell differentiation and function are shown for the different settings of *T. gondii* responses in mice. a) During an acute response or after vaccination, CD8+ T cell differentiation is linked to their migration and exposure to environmental signals. As naive cells are activated and differentiate into effector cells, they migrate from the white pulp of the spleen to the red pulp in a CXCR3:CXCL9/10-dependent manner. This migration results in exposure to a network of key cytokines like IL-12 and IFNγ (yellow) that drive changes in CXCR3 and KLRG1 expression (grey) and promote effector differentiation b) CD8+ T cells during well-controlled chronic infection give rise to three functionally distinct subsets of antigen-specific T cells. The differentiation of these populations shares many similarities to acute infection, including the expression pattern of surface receptors CXCR3 and KLRG1 on different subsets (grey) and a proliferative intermediate population (blue) that generates terminally differentiated effectors (red). However, unlike the vaccine setting, in which a single wave of T cell effector differentiation occurs, during well-controlled chronic infection, effector T cells are continuously replenished from memory and intermediate precursor populations. c) During infection, CD4+ T cells provide help to CD8+ T cells in the form of key cytokines like IL-21. In the setting of poorly-controlled progressing infection (green), CD4+ T cells become exhausted and lose their ability to produce these cytokines, resulting in subsequent CD8+ T cell exhaustion. (Figure created with BioRender)

Table 1: Natural CD8+ T cell epitopes in *Toxoplasma gondii*

Antigenic peptide	Source protein	MHC restriction	Subcellular location	T cell response	Refs
HPGSVNEFDF (HF10)	GRA6	H-2L^{d}	Constitutively secreted by dense granules in PV; localizes to PV membrane; C terminal epitope may extend into cytosol	Immunodominant response; responsible for protection in BALB/c mice	[9,11,12,54]
SPMNGGYYM (SM9)	GRA4	H-2L^{d}	Constitutively secreted by dense granules into PV lumen; localizes to **intravacuolar network (IVN)**	Subdominant response; not protective	[10,18]
YAVANYFFL (YAL9)	ROP5	H-2D^{b}	Secreted by rhoptries into host cell during invasion	Subdominant response; not protective	[19]
IPAAAGRFF (IF9)	ROP7	H-2L^{d}	Secreted by rhoptries into host cell during invasion	Subdominant response; not protective	[10,18]
SVLAFRRL (SVL8)	Tgd057	H-2K^{b}	Secreted by dense granules in PV lumen	High frequency of Tgd057-specific T cells post vaccination; adoptive transfer of CTLs protective against lethal parasite challenge	[11,41,71]

Table 2:Engineered CD8+ T cell antigens

Antigen	Description	Effect on antigen presentation and T cell response	Refs	Conclusion
SAG1ΔGPI-OVA	Model antigen OVA secreted by dense granules	OVA secreted into the PV results in efficient presentation; low $CD8^+$ T cell activation with nonsecreted OVA	[2,5]	Secreted antigen > nonsecreted antigen
Cytoplasmic β-galactosid-ase	Cytoplasmic expression of β-galactosidase under the tachyzoite-specific promoter, SAG1	No β-gal-specific $CD8^+$ T cell response	[4]	
Secreted β-galactosid-ase	β-galactosidase secreted into the PV lumen	Production of long-lasting dominant response against L^d restricted β-gal epitope	[4]	
GRA6-YAL9	YAL9 peptide targeted to dense granules instead of rhoptries	Increased presentation, higher $CD8^+$ T cell response	[19]	Dense granule targeting > rhoptry targeting
GRA6-ROP5	ROP5 protein targeted to dense granules instead of rhoptries	Increased presentation, 10- to 20-fold higher $CD8^+$ T cell response (more than GRA6-YAL9); better parasite control	[19]	
ROP5-HF10	HF10 peptide targeted to rhoptries instead of dense granules	Decreased presentation, 3- to 4-fold lower $CD8^+$ T cell response	[19]	
GRA6II-L, GRA6II-HA	GRA6 protein extended by a leucine or HA tag	HF10 presentation is lost; no T cell response; weaker protection	[10]	C terminal epitope position is important
GRA6II-SM9Cter	SM9 peptide at C terminus of GRA6 protein	Enhanced presentation; stronger $CD8^+$ T cell response; stronger parasite control	[10]	
TgRH GRA5-HF10	HF10 epitope at C terminus of GRA5 protein: HF10 inverted to face the PV lumen	Reduced presentation *in vitro*	[9]	Host cell cytosolic epitope > PV lumenal epitope
SAG1-GRA6-HF10	SAG1 N terminal domain with GRA6-HF10: converts to soluble protein	Reduced presentation	[11]	PV membrane localization > soluble within PV lumen
TgRH GRA6-HF10 gra2KO	GRA2 KO eliminates the IVN; GRA6 preferentially localizes to PV membrane	Enhanced presentation and $CD8^+$ T cell response	[11]	

Tg.pGRA6/ GRA6-OVA	OVA-derived SIINFEKL epitope at the C terminus of the GRA6 protein, under the GRA6 promoter	Antigen processed more efficiently than vacuolar SIINFEKL epitope from parental strain; lower parasite load in the brain; reduced brain inflammation	[68]	Dense granule targeting > soluble vacuolar localization
SAG1/GRA6-OVA	Same protein construct as above, but restricted to tachyzoites by SAG1 promoter	OVA-specific $CD8^+$ T cell response not significantly affected; effective parasite control in the CNS	[68]	Tachyzoite restricted antigen presentation is sufficient to confer protection

Chapter 2: CXCR3 regulates stem and proliferative CD8+ T cells during chronic infection by promoting interactions with DCs in splenic bridging channels

Abstract

Production of armed effector CD8+ T cells during persistent infection requires a stable pool of stem-like cells that can give rise to short-lived effector T cells via a proliferative intermediate population. In chronic infection models marked by T cell exhaustion, this process can be transiently induced by check-point blockade, but it occurs spontaneously and continuously in the spleens of mice chronically infected with the protozoan intracellular parasite, *Toxoplasma gondii,* providing a unique opportunity to examine the steps in the differentiation process. Using this model, we observed distinct locations and gene expression patterns for stem-like memory cells, proliferative intermediate cells, and terminally differentiated effector cells, implying a link between differentiation and discrete anatomical niches in the spleen. Loss of the chemokine receptor CXCR3 on parasite-specific T cells did not impair their white pulp to red pulp migration but reduced their interactions with CXCR3 ligand-producing type 2 conventional DCs in the bridging channels and impaired their transition from memory to intermediate states, leading to a build up of memory T cells localized to the red pulp. These results demonstrate a critical role for CXCR3 during chronic infection by increasing T cell exposure to differentiation-inducing signals during red pulp migration, providing a dynamic and flexible mechanism for modulating effector differentiation in response to environmental signals.

2.1: Introduction

Upon infection, naïve pathogen-specific CD8+ T cells rapidly expand and differentiate to give rise to functionally heterogeneous populations of effector and memory T cells (Williams and Bevan, 2007). Effector cells directly control infection by efficiently killing invaded target cells and producing protective cytokines, while memory cells demonstrate less effector capacity but confer long-term immunological protection. The fate determination of CD8+ T cells towards effector or memory differentiation is regulated by cell-intrinsic processes including asymmetric cell division (Chang *et al.*, 2007; Lin *et al.*, 2015), but can also be influenced by environmental signals, including the strength of T cell receptor signaling, costimulatory signals, and cytokines (Chang, Wherry and Goldrath, 2014). The signals a T cell receives *in vivo* are largely dependent on their local environment and their interaction with specific populations of antigen presenting cells (APCs). While some of the signals directing effector and memory differentiation have been identified, our understanding of the anatomical niches that control T cell fate remains limited. An important component of these niches are dendritic cells (DCs), specialized APCs that are critical for T cell priming and activation. DCs are heterogenous in phenotype and function, and recent evidence suggests that T cell fate is influenced by interactions with distinct

lineages of DCs (Li *et al.*, 2016; Brown *et al.*, 2019; Eisenbarth, 2019; Kotov *et al.*, 2019; Shin *et al.*, 2019; Opejin *et al.*, 2020).

The chemokine receptor CXCR3 is expressed by populations of antigen-experienced CD8+ T cells and plays a critical role in determining how T cells migrate and interact with APC within tissues. CXCR3 ligands, CXCL9 and CXCL10 (CXCL11, the third ligand, is not expressed in C57BL/6J mice), are expressed by a variety of cells upon exposure to inflammatory cytokines and can help guide T cells into inflamed tissues. In the spleen, both CD4+ and CD8+ T cells utilize CXCR3 to migrate to and interact with APCs during T cell priming and recall responses (Sung *et al.*, 2012; Goldberg *et al.*, 2018; Maurice *et al.*, 2019; Duckworth *et al.*, 2021). In particular, the marginal zone and red pulp of the spleen are important sites of antigen presentation during infection due to their high exposure to circulation, and CXCR3 mediates the migration of activated CD8+ T cells into these compartments during infection, promoting the generation of short-lived effector cells at the expense of the long-lived memory precursor pool (Hu *et al.*, 2011; Kurachi *et al.*, 2011).

While the role of CXCR3 in directing T cell differentiation during acute infection is well established, much less is known about its role during chronic infection. After the establishment of chronic infection, armed effector T cells (T_{EFF}) can be generated from a stem-like memory population (T_{MEM}) via a proliferative intermediate state (T_{INT}), a process that was first characterized in a well-controlled model of infection of mice with the intracellular protozoan parasite *Toxoplasma gondii* (Chu *et al.*, 2016). Similar stem-like and proliferative intermediate populations have been defined in other chronic infection models, including CMV in both mice and humans (Gordon, Lee, Swadling, Folgori, *et al.*, 2018; Welten *et al.*, 2020) and LCMV in mice (Im *et al.*, 2016; Utzschneider *et al.*, 2016; Hudson *et al.*, 2019). However, unlike the LCMV chronic infection model, in which T cells express the inhibitor receptor PD1 and exhibit functional exhaustion, T cells in the *T. gondii* infection model retain potent effector function and lack expression of inhibitory receptors. As a result, proliferative intermediate cells are only produced transiently following PD-1 blockade in the LCMV infection model, whereas T_{MEM} (CXCR3+KLRG1-), T_{INT} (CXCR3+KLRG1+), and T_{EFF} (CXCR3-KLRG1+) populations are produced spontaneously and continuously in *T. gondii* infected mice (Chu *et al.*, 2016; Tsitsiklis *et al.*, 2020). These features make *T. gondii* infection a valuable model to investigate the differentiation of memory, intermediate, and effector T cells in the setting of chronic infection., and advancing our understanding of this model may lead to improved strategies to manipulate CD8+ T cell responses during chronic infection and cancer.

Here we showed that T_{MEM}, T_{INT}, and T_{EFF} cells expressed unique gene expression programs, correlating with their location within distinct regions of the spleen. We also identified a critical role for the chemokine receptor CXCR3 in promoting the conversion of T_{MEM} cells into T_{INT} cells. Interestingly, while CXCR3 was critical for T cell differentiation, it was not required for the migration from white pulp to red pulp that normally accompanies effector differentiation. Instead, CXCR3 mediates interactions between T cells and populations of CXCR3 ligand-producing type 2 conventional DCs (cDC-2s) located within the bridging channel

of the spleen. Our data support a model in which CXCR3 promotes transient interactions between T_{MEM} cells and cDC-2s during their migration from the white pulp to the red pulp, resulting in a balanced differentiation signal that allows for T_{INT} development and further clonal expansion prior to terminal effector differentiation.

2.2: Results

T_{MEM} and T_{INT} cells are transcriptionally distinct precursors to effector cells

We have previously described a highly protective, immunodominant CD8+ T cell response mounted against a peptide derived from the parasite protein GRA6 presented by the MHC Class I molecule H-2L^d (Blanchard *et al.*, 2008; Feliu *et al.*, 2013; Chu *et al.*, 2016; Salvioni *et al.*, 2019; Tsitsiklis *et al.*, 2020). During chronic infection in H-2L^d expressing mice, GRA6-specific CD8+ T cells experience continuous antigen stimulation in the spleen and reach a steady state marked by ongoing proliferation and differentiation. To understand the factors regulating CD8+ T cell differentiation in this infection model, we infected B6xB6.c H-2$^{b/d}$ mice with *T. gondii*, and six weeks post-infection we isolated GRA6-tetramer+ T_{MEM}, T_{INT}, and T_{EFF} cells from the spleen based on CXCR3 and KLRG1 expression and performed RNA sequencing (RNA-seq) **(Fig 1A)**. Principal components analysis (PCA) of the transcriptional data showed that the populations segregated into separate clusters, confirming that they represent transcriptionally distinct subsets **(Fig 1B)**. Examination of differentially expressed transcripts revealed a large set of genes that increased with effector differentiation (**Fig 1C**, clusters 1, 2), including canonical genes related to CTL activity (e.g. *GzmB*, *Prf1,* and *Fasl)* **(Supp. Fig 1)**. Other groups of genes were selectively upregulated in the T_{MEM} (gene cluster 5) or T_{INT} (gene cluster 7) populations, indicative of two distinct differentiation states amongst antigen-experienced progenitors to T_{EFF} cells. To gain a broad understanding of the pathways defining each population, we performed Gene Set Enrichment Analysis (GSEA) **(Fig 1D, Supp. Fig 1)**. T_{MEM} cells were enriched for pathways related to cytokine signaling and inflammation, including receptors for cytokines with known roles in regulating T cell fate, such as *Il21r*, *Il2rb*, and *Il7r* **(Fig 1D, Supp. Fig 1)**. In contrast, T_{INT} cells were enriched for cell cycle associated genes, consistent with their proliferative nature **(Fig 1D)**. T_{INT} cells also showed enrichment for several metabolic pathways, with oxidative phosphorylation showing the strongest enrichment relative to both the T_{MEM} and T_{EFF} populations **(Fig 1D)**. Interestingly, T_{INT} cells had reduced expression of genes associated with TGFβ and wnt/β-catenin signaling and were enriched in complement pathway genes relative to T_{MEM} and T_{EFF} populations **(Fig 1D)**. Finally, T_{MEM}, T_{INT}, and T_{EFF} cells showed differential expression of several transcription factors known to be critical for driving T cell fate **(Fig 1E)**. T_{INT} cells showed elevated expression of *Eomes* mRNA, consistent with previous measurements at the protein level (Chu *et al.*, 2016). T_{MEM} cells expressed elevated *Tcf7* (encoding TCF1) and *Id3*, but lacked *Id2* and *Prdm1* (encoding Blimp-1), similar to stem-like TCF1+ CD8+ T cells that arise during chronic viral infection **(Supp. Fig 1).**

To further compare the T_{MEM} and T_{INT} populations in the *Toxoplasma* infection model to the progenitors of exhausted effector T cells described in other settings, we performed GSEA analyses using gene signatures derived from published transcriptional data on stem-like and transitory proliferative CD8+ T cells during LCMV infection (Utzschneider *et al.*, 2016; Hudson *et al.*, 2019). We observed that T_{MEM} cells showed an enrichment for stem-like signatures **(Supp. Fig 1)**, and both populations exhibited elevated expression of key co-stimulatory molecules (including *Cd28* and *Icos*) and *Tlr* genes **(Supp. Fig 1)**. In addition, most of the genes that were specifically upregulated in T_{INT} cells **(Fig 1C**, cluster 7**)** were also selectively expressed in the transitory T population from LMCV, relative to stem-like and exhausted effector cells **(Supp. Fig 1)**. This included genes involved in oxidative phosphorylation, fatty acid, and cholesterol metabolism (including *Ndufs4, Tmem97, Cd5l*, and *Fabp5*), as well as set of transcriptional regulators and genes involved in binding divalent metal cations **(Fig 1G).** Thus, T_{MEM} cells resemble the stem-like TCF1+ cells described in other models of infection and cancer, and the T_{INT} population represents a distinct proliferative and metabolically active transitional population that parallels the transitory intermediate cells that arise during LCMV infection.

T_{MEM} to T_{EFF} cell differentiation in spleen coincides with white pulp to red pulp migration

In line with their divergent gene expression patterns, the three different GRA6-specific T cell populations also expressed distinct levels of many genes important for localization within the spleen, including *Ccr7*, *Cd69*, *Xcl1, S1pr1*, and *S1pr5* **(Fig 1E,F)**. We hypothesized that this may result in differences in the location of these cells in the spleen, which in turn may control which signals these cells are exposed to *in vivo*. To investigate this, we generated partial hematopoietic chimeras in which a small percentage of T cells expressed rearranged T cell receptor (TCR) α and β transgenes specific for the GRA6 peptide/H2-L^d complex, referred to as TG6 (Chu *et al.*, 2016), along with a GFP transgene **(Supp. Fig 2)**. We infected adult TG6-GFP chimeric mice with *T. gondii*, and six weeks post-infection the spleens of these mice were analyzed by confocal microscopy **(Fig 2)**. The majority (80%) of TG6-GFP cells were found in the red pulp of the spleen, while a smaller fraction (20%) resided in the white pulp **(Fig 2A-D)**. To identify T_{MEM} cells, we stained section with antibodies specific for TCF1, a transcription factor associated with stem-like T cells in other chronic infections (Im *et al.*, 2016; Utzschneider *et al.*, 2016; Welten *et al.*, 2020), and whose expression at the RNA and protein level correlated well with T_{MEM} cells as defined by CXCR3 and KLRG1 expression **(Fig 1E,F)**. We observed that the majority of TCF1+ T_{MEM} cells (72%) were localized to the white pulp of the spleen, specifically in the T cell zone **(Fig 2A, D)**. Proliferating Ki67+ cells (enriched for T_{INT}) were located primarily in the red pulp (81%) **(Fig 2B, D)**, and KLRG1+ cells (marking both T_{INT}, T_{EFF}) were localized almost entirely (99%) in the red pulp **(Fig 2C, D)**. To confirm these results and extend our conclusions to a polyclonal T cell population, we utilized intravenous (i.v.) anti-CD8 antibody labeling to measure the blood exposure of each GRA6 tetramer-positive

population in the spleens of wild-type infected mice (Anderson *et al.*, 2014). Cells in the marginal zone and red pulp are more blood-exposed than cells in the white pulp, allowing us to infer the localization of these cells based on the relative amount of antibody labeling. T_{MEM} cells showed the lowest proportion of i.v. antibody labeling, with T_{INT} and T_{EFF} cells showing significantly higher labeling **(Fig 2E)**. This suggests that similar to the TCR transgenic cells, polyclonal T_{MEM} cells reside in the white pulp while T_{INT} and T_{EFF} reside in the red pulp. The transcriptional profiles of polyclonal T_{INT} and T_{EFF} cells showed a specific enrichment for heme metabolism **(Fig 1D)**, further supporting the notion that these cells reside within the blood-exposed compartments of the spleen.

As an alternative approach to determine the localization of GRA6-specific subsets we utilized an adoptive transfer method **(Fig 2F)**. T_{MEM}, T_{INT}, and T_{EFF} cells from chronically infected TG6-GFP neonatal chimeric mice were sorted based on CXCR3 and KLRG1 expression, adoptively transferred into separate infection-matched WT recipients, and analyzed 48 hours later. Flow cytometry analysis confirmed that the transferred cells retained their CXCR3 and KLRG1 phenotype at this time point, consistent with previous findings (Chu *et al.*, 2016). We observed that a large fraction of T_{MEM} cells were found within the T cell zone **(Fig 2F and Supp. Fig 3)**. In contrast, only a small fraction of T_{INT} cells and almost no T_{EFF} cells were found in the white pulp, instead residing in the red pulp similar to their observed localization *in situ*. Together, this data indicates that T_{MEM} cells have specific access and residency in a niche within the splenic white pulp, and that migration into the red pulp coincides with differentiation into T_{INT} and T_{EFF} subsets.

CXCR3 deficient CD8+ T cells exhibit an inflated T_{MEM} pool and an impaired T_{MEM} to T_{INT} transition

Having observed clear differences in the subsets' localization in the spleen, we sought to investigate specific factors that may regulate this migration and impact T cell fate. CXCR3 is a chemokine receptor expressed by populations of antigen-experienced CD8+ T cells, including T_{MEM} and T_{INT} cells, and has been implicated in driving T cells into the splenic red pulp and towards an effector fate in settings of early acute infection and vaccination (Hu *et al.*, 2011; Kohlmeier *et al.*, 2011; Kurachi *et al.*, 2011; Shah *et al.*, 2015). To interrogate the role of CXCR3 during chronic *T. gondii* infection, we co-transferred equal numbers of WT and CXCR3 KO naive TG6 CD8+ T cells into mice one day prior to infection, and tracked the two populations at different time-points after infection **(Fig 3A)**. By the peak of the acute phase of infection (2 weeks post-infection), both populations had robustly expanded, consistent with previous reports that loss of CXCR3 does not impair T cell priming (Kurachi *et al.*, 2011) **(Fig 3B)**. However, CXCR3 KO T cells outnumbered WT cells in the spleen at three weeks post-infection, and by six weeks post-infection the CXCR3 KO cells were completely dominant, with many mice showing no detectable WT populations **(Fig 3B-D)**. To understand the competitive advantage of the KO population, we investigated the phenotype of the WT and KO cells. Due to the absence of CXCR3 as a surface marker on these cells, we utilized Ki67 and KLRG1 staining to identify T_{MEM}, T_{INT},

and T_{EFF} cells. Compared to the WT cells, CXCR3 KO cells showed a significant increase in the proportion and number of T_{MEM} cells at both three weeks and six weeks post-infection **(Fig 3E-G)**. In addition, the ratio of T_{MEM} to T_{INT} cells was increased in the CXCR3 KO population, raising the possibility that CXCR3 KO T_{MEM} cells were less efficient at differentiating into the T_{INT} stage. Despite this, CXCR3 KO cells generated similar or greater absolute numbers of total T_{INT} and T_{EFF} cells compared to WT, likely due to the inflated precursor pool of T_{MEM} cells **(Fig 3G)**.

To test if the loss of CXCR3 leads to a block in T_{MEM} to T_{INT} differentiation, we performed adoptive transfer experiments. We sorted WT and CXCR3 KO T_{MEM} cells from infected mice and co-transferred both populations into infection-matched recipients at 3 or 6 weeks post infection. We analyzed the donor population by flow cytometry five days after transfer **(Fig 3H),** a time point at which transferred T_{MEM} cells give rise to T_{INT} cells but do not yet produce a large pool of T_{EFF} cells (Chu *et al.*, 2016). We measured the conversion of T_{MEM} cells into T_{INT} using KLRG1 expression and proliferation (measured by dye dilution), two hallmarks of T_{INT} fate. After adoptive transfer, the WT T_{MEM} population produced a larger KLRG1+ population and divided significantly more than the KO population, demonstrating they were more efficient at producing T_{INT} cells **(Fig 3I,J)**. Taken together, these results indicate that loss of CXCR3 impairs the differentiation of T_{MEM} cells into T_{INT}, leading to an expanded T_{MEM} population.

CXCR3 KO cells migrate to the red pulp while retaining a TCF1+ T_{MEM} phenotype

Given the role of CXCR3 in driving T_{MEM} cell differentiation, and given our observation that the differentiation of T_{MEM} into T_{INT} correlates with their migration from the white pulp into the red pulp, we predicted that cells lacking CXCR3 would be "trapped" in the white pulp niche, similar to the observed localization of CXCR3 deficient CD8+ T cells during the early stages of acute infection (Kurachi *et al.*, 2011). To test this, we performed confocal imaging on spleen sections from chronically infected TG6-GFP CXCR3 KO chimeric mice. Surprisingly, we observed no global defect in red pulp migration in the CXCR3 KO cells **(Fig 4A-D)**. Compared to the WT chimeras, the KO cells had a similar distribution in the spleen, with approximately 80% of the total GFP population found in the red pulp and 20% in the white pulp.

Next, we investigated the impact of CXCR3 deletion on the location of CD8+ subsets defined by expression of TCF1, Ki67, and KLRG1 as in Figure 2. Similar to the WT mice, we observed that GFP+ cells in the white pulp retained a uniformly TCF1+ T_{MEM} phenotype **(Fig 4A)**. However, contrary to our initial expectations, we observed a large increase in the proportion of TCF1+ cells in the red pulp. This indicated that T_{MEM} cells lacking CXCR3 were able to efficiently migrate into the red pulp, but no longer uniformly converted into T_{INT} cells during that transition. The presence of a large population of red pulp T_{MEM} cells was also indicated by the KLRG1 staining; a large fraction of red pulp resident TG6-GFP CXCR3 KO T cells were KLRG1 negative **(Fig 4C)**. Ki67+ cells remained primarily localized to the red pulp and did not show a significant change between

the WT and KO populations **(Fig 4B,D)**. Together these data indicate that in the absence of CXCR3, T_{MEM} cells still migrate normally into the red pulp. However, while the migration of CXCR3 sufficient T cells to the red pulp is accompanied by their transition into a TCF1- KLRG1+ population, CXCR3 KO T cells retain a TCF1+ KLRG1- phenotype after migrating to the red pulp.

Bridging channels are a splenic structure that connects the T cell zone to the red pulp and represent an important migratory pathway for T cells in the spleen (Khanna, McNamara and Lefrançois, 2007; Chauveau *et al.*, 2020). We analyzed the phenotype of GFP+ cells occupying bridging channels and observed that the proportion of cells expressing TCF1 and KLRG1 was intermediate compared to the white pulp and red pulp, suggesting that migration along bridging channels to the red pulp coincided with conversion of the T_{MEM} cells into a T_{INT} phenotype **(Fig 4D, Supp. Fig 4)**. CXCR3 KO cells in the bridging channels also had a mixed phenotype, but with a higher % of TCF1+ and lower % of KLRG1+ cells compared to WT cells **(Fig 4D)**, though these differences were not as pronounced as in the red pulp. Together, these data suggest that bridging channels may be a critical site for the CXCR3-dependent transition of T_{MEM} cells into T_{INT}.

Conventional dendritic cells are an important source of CXCR3 ligands

The observation that CXCR3 plays a critical role in the differentiation of CD8+ T cells but has no obvious role in their migration within the spleen suggests that CXCR3 may regulate localized interactions between T cells and other cell types. To characterize expression of the CXCR3 ligands, CXCL9 and CXCL10, we utilized the REX3 strain of dual reporter mice, which contains a transgenic construct with a CXCL9-RFP and CXCL10-BFP insert (Groom *et al.*, 2012). Uninfected REX3 mice displayed a small amount of basal CXCL9 and CXCL10 production in the spleen, but the proportion and numbers of chemokine-producing cells substantially increased during acute infection and remained elevated during chronic infection **(Fig 5A-C)**. To identify the cell types producing CXCL9 and CXCL10 during infection, we stained splenocytes isolated from chronically infected REX3 mice with surface markers to delineate myeloid and lymphoid immune cell types **(Fig 5D, E)**. While CD11c+ cells comprised only a small fraction of the total splenocyte population, they made up a majority of the cells within the CXCL9+ and CXCL10+ subsets. Both CXCL9+ CXCL10- cells and CXCL9+ CXCL10+ cells were almost entirely CD11c+. The CXCL9-CXCL10+ fraction were predominantly lymphoid cells, including CD4+ T cells, and also contained a substantial portion of CD11c+ cells. CD11c is a marker expressed primarily by dendritic cells, which can be divided into populations of conventional dendritic cells (cDC-1s and cDC-2s), monocyte-derived dendritic cells (mDCs), and plasmacytoid dendritic cells (pDCs). We stained for markers to identify these different DC subsets in splenocytes from chronically infected REX3 mice **(Supp. Fig 5)**. We found that cDC-1s produced high levels of CXCL9 and moderate levels of CXCL10, with very little change in the proportion or mean fluorescence of CXCL9 or CXCL10 after infection **(Fig 5F)**. mDCs expressed some CXCL9 and CXCL10 after infection, while pDCs expressed very little of

either chemokine. Interestingly, cDC-2s made no CXCL9 or CXCL10 in uninfected mice but became prominent producers of both chemokines during infection. In addition, cDC-2s upregulated FcεR1 (MAR-1) upon infection, indicative of an inflammatory phenotype (Bosteels *et al.*, 2020), and expressed high levels of CD80 (B7-1) and PDL1 both before and after infection **(Supp. Fig 5)**. Together, these results indicate that conventional dendritic cells are an important source of CXCR3 ligands in the spleen, and that cDC-2s with an inflammatory phenotype show the greatest infection-induced increase in CXCR3 ligand expression.

GRA6-specific CD8+ T cells form CXCR3-dependent interactions with cDC-2s in the bridging channels of the spleen

T cell:dendritic cell interactions are critical for regulating the activation and differentiation of CD8+ T cells, and CXCR3 can promote more frequent and long lasting interactions between these two cell types (Groom *et al.*, 2012). Because we observed that conventional dendritic cells are significant producers of CXCR3 ligands *in vivo* during chronic infection, we sought to characterize interactions between T_{MEM} cells and chemokine-producing dendritic cells in the spleen. We imaged spleen sections of chronically infected REX3 mice to determine the location of chemokine-producing cells during chronic infection **(Fig 6A)**. CXCL9 expression was observed throughout the spleen, with slightly higher signal localized to the marginal zone and red pulp **(Fig 6A,B)**. Much of the observed CXCL9 expression was co-localized with CXCL10, though a population of CXCL9 single-positive cells was evident primarily in the T cell zone. CXCL10 was not evident in the white pulp, but was highly expressed in the red pulp with a maximum signal in the marginal zone **(Fig 6B)**. Marginal zone CXCL10 appeared to primarily come from clusters of CXCL9+ CXCL10+ double positive cells.

The distinct pattern of chemokine expression observed by flow cytometry **(Fig 5F)** combined with the localization pattern of chemokines suggested that cDC-1s and cDC-2s occupy distinct splenic niches during chronic *T. gondii* infection. To more specifically localize each population of dendritic cells, we stained chronically infected mice with antibodies against XCR1 **(Fig 6B)** and DCIR2 (clone 33D1**, Fig 6C**) together with CD11c to identify the location of cDC-1s and cDC-2s, respectively. XCR1+ CD11c+ cells (cDC-1) were found scattered throughout the spleen, with maximal XCR1 signal coming from the white pulp but considerable fluorescence in the marginal zone and red pulp as well **(Fig 6B)**. This is consistent with previous reports suggesting splenic cDC-1s patrol the marginal zone and red pulp before migrating into the T cell zone to present blood-derived antigens (Backer, Diener and Clausen, 2019; Eisenbarth, 2019). In contrast, 33D1+ CD11c+ cells (cDC-2) were enriched in dense clusters found in the bridging channels and marginal zones connecting the white and red pulp **(Fig 6C)**. Flow cytometric analysis of REX3 reporter mice shows that most XCR1+CD11c+ cDC-1 in chronically infected mice express CXCL9, whereas most 33D1+CD11c+ cDC-2 express CXCL10 and a substantial fraction express CXCL9 **(Supp. Fig 5).** Together, these results suggest that T_{MEM} cells encounter primarily CXCL9-expressing cDC-1s in the white pulp but encounter CXCL9 and

CXCL10-expressing cDC-2 networks during their migration through bridging channels.

The localization of CXCL10-expressing cDC-2 clusters at the bridging channels made them a particularly interesting population, since they co-localized with the CXCR3-dependent conversion of T_{MEM} cells into T_{INT}. To investigate if CD8+ T cells formed CXCR3-dependent interactions with cDC-2s, we quantified the occupancy of TG6-GFP cells in 33D1+ clusters in the spleens of chronically infected mice. We measured the density of WT and CXCR3 KO TG6-GFP cells in 33D1+ clusters and normalized to the density of cells in the total slice to account for the overall increase in the numbers of CXCR3 KO TG6-GFP cells. We observed that WT TG6-GFP cells were enriched in 33D1+ clusters while CXCR3 KO cells showed no enrichment **(Fig 6D,E)**, demonstrating that CD8+ T cells experience CXCR3-dependent interactions with cDC-2 in the bridging channels.

cDC-2s confer a CD25^{hi} phenotype on T_{MEM} cells *in vitro*

Evidence that CXCR3 both mediates the interaction of CD8+ T cells with cDC-2s and also impacts their differentiation raises the possibility that CXCR3-dependent interactions with cDC-2s may directly modulate effector differentiation. To explore this possibility, we devised an *ex vivo* co-culture system to investigate how different DC populations from infected mice affect T_{MEM} differentiation, and the contribution of CXCR3 to this effect. WT or CXCR3 KO T_{MEM} cells were sorted from chronically infected mice. In parallel, dendritic cell subsets (cDC-1, cDC-2, or mDC) were isolated from infection-matched mice and loaded with the GRA6 peptide **(Supp. Fig 6)**. T_{MEM} cells and peptide-loaded DCs were co-cultured *in vitro* for 3 days, and the activation of the T_{MEM} cells was measured by dilution of a proliferation dye (CFSE) and expression of surface markers. As expected, all three subsets of dendritic cells were capable of inducing robust proliferation of the WT T_{MEM} cells, however cDC-2s induced slightly less division compared to cDC-1s and mDCs **(Fig 7B,C)**. While we did not observe KLRG1 expression in any of the conditions tested (data not shown), we observed significant differences in the ability of the dendritic cells to induce expression of CD25 on activated T_{MEM} cells. cDC-1s and mDCs produced modest CD25 expression among the CFSE^{lo} population **(Fig 7B)**. In contrast, the cells stimulated by cDC-2s were almost uniformly CD25+ and had higher CD25 gMFI. Increased CD25 expression and IL-2 signaling can bias CD8+ T cells towards terminal differentiation (Kalia *et al.*, 2010; Pipkin *et al.*, 2010), suggesting that cDC-2s may be more effective at stimulating effector differentiation compared to other DC subsets from infected mice.

CXCR3 KO T_{MEM} cells showed similar trends after activation with all three dendritic cell subsets, with cDC-2s inducing the highest levels of CD25 within the population of divided cells **(Fig 7D,E)**. Interestingly, we observed that CXCR3 KO T_{MEM} cells had reduced expression of CD25 compared to the WT T_{MEM} cells after stimulation with all three of the dendritic cell subsets **(Fig 7F,G)**. This suggests CXCR3 KO cells experience altered dendritic cell interaction and are thus less capable of adopting a CD25^{hi} effector phenotype. Additionally, we observed that

WT T_{MEM} cells treated with either anti-CXCL9 or anti-CXCR3 (clone CXCR3-173, which specifically blocks the activity of CXCL10 binding) showed reduced activation by cDC-2s, both in their ability to divide and express CD25 **(Supp. Fig 6)**. These results indicate that loss of CXCR3 results in altered stimulation of T_{MEM} cells by dendritic cells *in vitro*, resulting in a bias towards a $CD25^{lo}$ phenotype.

2.3: Discussion

Maintaining a protective CD8+ T cell response during chronic infection requires a balance between preserving a pool of stem-like memory cells while providing for continuous production of short-lived effector T cells, as exemplified by a protective CD8+ T cell response in mice chronically infected with *T.gondii*. Here we show that most T_{MEM} cells in this model reside in the white pulp of the spleen, whereas T_{INT} and T_{EFF} populations are predominantly found in red pulp, implying a link between T cell differentiation and white pulp to red pulp migration. Loss of CXCR3 impairs T_{MEM} differentiation but does not impair their migration, leading to an inflated memory population with many T_{MEM} cells mislocalized in the splenic red pulp. We also provide evidence that infection induces expression of the CXCR3 ligands CXCL9 and CXCL10 in a population of cDC-2s residing in the bridging channels, promoting their interactions with T_{MEM} cells during white pulp to red pulp migration. While CXCR3-dependent cDC-2 interactions in bridging channels promote T_{MEM} differentiation, they do not directly drive terminal T_{EFF} differentiation. Instead they lead to a transcriptionally distinct, proliferative T_{INT} population, which expands before eventually giving rise to armed T_{EFF} cells. Our data reveal how transient interactions with cDC-2 populations during migration between T_{MEM} and T_{EFF} niches in the spleen can deliver balanced differentiation signals that allow for both efficient T_{EFF} production and robust memory preservation.

While early studies of the CXCR3:CXCL9/10 axis focused on its role in driving the entry of activated T cells into inflamed tissues, more recent studies have highlighted its role in T cell positioning and effector differentiation within lymph nodes and spleen (Kohlmeier *et al.*, 2011; Kurachi *et al.*, 2011; Sung *et al.*, 2012; Shah *et al.*, 2015; Maurice *et al.*, 2019). CXCR3 ligands are induced by inflammatory signals such as IL-12 and type-I IFNs (Groom and Luster, 2011), leading to accumulation and effector differentiation of antigen experienced CD8+ T cells near sources of CXCR3 ligand induction in the splenic red pulp and marginal zone (Kurachi *et al.*, 2011; Shah *et al.*, 2015). However in mice chronically infected with *T. gondii*, CXCR3 does not mediate CD8+ T cell migration to the red pulp, nor does it lead directly to their terminal effector differentiation. Instead the CXCR3:CXCL9/10 axis appears to exert a transient and localized differentiation signal by promoting interactions with DCs, similar to its proposed function in lymph nodes (Groom *et al.*, 2012; Duckworth *et al.*, 2021) and tumors (Chow *et al.*, 2019). Given that CXCR3 ligands are regulated by inflammatory signals generated in response to infection, it is tempting to

speculate that this system may allow for dynamic modulation of effector cell production during chronic infection, such that transient increases in parasite load are met with transient increases in effector T cell production, ensuring a stable host-pathogen balance over time.

Given that T cell migration to red pulp still occurs in the absence of CXCR3, other signals must regulate this transition. CCR7 and S1P are known regulators of lymphocyte migration in and out of the white pulp, respectively, (Förster *et al.*, 1999; Arnon and Cyster, 2014), and our transcriptional analyses indicate these pathways likely regulate the migration of GRA6-specific CD8+ T cells. T_{MEM} cells had little expression of *S1pr1* and *S1pr5* but elevated expression of *Ccr7* as well as *Cd69,* which can oppose the action of S1P (Mackay *et al.*, 2015). Together, this expression pattern allows for entry and occupancy of the white pulp while resisting exit signals. The downregulation of *Ccr7* and *Cd69* together with the upregulation of *S1pr1* and *S1pr5* observed in the T_{INT} and T_{EFF} cells may initiate white pulp to red pulp migration. CXCR3 ligands (especially CXCL10 which has a higher binding affinity for CXCR3 than CXCL9 (Weng *et al.*, 1998)) may enhance migration as well as promote transient interactions with cDC-2s as T cells pass through the bridging channels. Interestingly, loss of CXCR3 on T cells uncouples differentiation and red pulp migration, further supporting the notion that differentiation-inducing signals come primarily from BC/marginal zones rather than the red pulp. Thus the combined action of S1P, CCR7, and CXCR3 can coordinate the migration and differentiation of CD8+ T cells in the spleen.

The retention of T_{MEM} cells in the white pulp suggests that this compartment serves as a niche for stem-like CD8+ T cells, and raises the question: what aspects of the white pulp support a T_{MEM} fate? One defining feature of the white pulp niche is elevated TGF-β expression, which promotes memory fate during acute viral infection (Seo *et al.*, 2016) and can promote stem-like cells during chronic viral infection through metabolic programming (Gabriel *et al.*, 2021). Indeed, we observed that genes associated with TGF-β signaling were specifically lost in the T_{INT} stage, supporting the notion that migration away from the white pulp niche coincides with the loss of TGF-β signals. This migration may allow T_{INT} cells to approporiately proliferate and differentiate in the absence of the metabolic constrains imposed by TGF-β. In addition to TGF-β, T_{MEM} cells in the white pulp are also exposed to cDC-1s, and stimulation by cDC-1s *in vitro* resulted in the lowest CD25 expression on T_{MEM} cells. Thus, cDC-1s may have an inherent capacity to promote memory fate and may be a critical component defining the memory niche as well. It is interesting to note that cDC-1s can bias CD4+ T cells towards the T_{REG} lineage, which can be potent sources of TGF-β, whereas cDC-2s tend to induce a T_{H1} fate (Brown *et al.*, 2019; Opejin *et al.*, 2020). Thus DCs and CD4+ T cells in the white pulp may collaborate to drive local environments supporting stem-like CD8+ T cells, in contrast to the tendency of DCs in the MZ and BC to promote effector differentiation.

In the initial delineation of conventional DCs into 2 subsets, cDC-1s and cDC-2s were identified as important for priming of CD8+ and CD4+ T cells respectively (Den Haan and Bevan, 2002; Eisenbarth, 2019). However recent

studies have demonstrated that, upon exposure to inflammation, cDC-2s can acquire the ability to cross-present antigens on MHC-I and can play an important role in CD8+ T cell activation (Calabro *et al.*, 2016; Bosteels *et al.*, 2020). In line with this data, we observed that cDC-2s during chronic *T. gondii* infection increased MAR-1 staining, a phenotype that coincides with the ability to cross-presenting antigen to CD8+ T cells (Bosteels *et al.*, 2020). This raises the possibility that cDC-2s may influence CD8+ fate through direct antigenic stimulation. cDC-2s also have a distinct costimulatory profile, with elevated CD80 (B7-1) expression. CD80 binds to CD28 with higher avidity compared to CD86 (Sansom, Manzotti and Zheng, 2003; Thomas *et al.*, 2007), suggesting that cDC-2s may provide more intense co-stimulatory signals to CD8+ T cells thereby promoting effector differentiation. This fits with the results of our *in vitro* stimulations, where cDC-2s induced the highest expression of CD25 on stimulated T_{MEM} cells. MAR-1+ cDC-2s have been reported to be potent IL-12 producers (Bosteels *et al.*, 2020), and populations of cDC-2s express high levels of transcripts for other inflammatory cytokines such as *Il1B* and *Il27* (Brown *et al.*, 2019), suggesting cDC-2s may directly contribute to a cytokine environment that favors effector differentiation in the bridging channel. Thus, the CXCR3 axis represents a tunable system whereby the immune response can tailor the generation of effector cells by favoring interactions with cDC-1s or cDC-2s depending on the inflammatory environment, analogous to what has been proposed during acute viral infection (Duckworth *et al.*, 2021).

While cDC-2s are equipped to promote T effector differentiation, they also have high levels of PD-L1, suggesting they may have differential impacts on the fate of stem and proliferative populations depending on the specific setting. We have previously shown that GRA6-specific CD8+ T cells during chronic *T. gondii* infection are resistant to exhaustion and do not express PD-1, partially due to atypical features of their restricting H-2L^d MHC-I molecule, resulting in unusually low reactivity to self-peptide-MHC complexes (Tsitsiklis *et al.*, 2020; Lutes *et al.*, 2021). Thus, GRA6-specific cells are poised to receive activating signals from cDC-2s while remaining ignorant of the inhibitory signals provided by PD-1. In contrast, chronic infections that induce widespread T cell exhaustion, such as LCMV clone-13 infection, result in a pool of stem-like cells that express high levels of PD-1 (Im *et al.*, 2016; Utzschneider *et al.*, 2016). These PD-1+ stem-like cells would likely receive inhibitory signals upon encounter with DCs, leading to impaired effector function and reduced proliferation. Targeting the PD-1/PD-L1 axis with antibody therapies may block the inhibitory signals provided by DCs and allow for the generation of proliferative intermediate cells similar to the T_{INT} subset of the GRA6 response. Indeed, PD-1 blockade during chronic LCMV infection results in a burst of intermediate proliferating cells emerging from the exhausted TCF1+ precursor pool (Im *et al.*, 2016; Hudson *et al.*, 2019). Given that CXCR3 is critical for the efficient production of T_{INT} in the GRA6-specific response, it seems likely CXCR3 will be necessary for effective checkpoint blockade treatment during chronic viral infection, similar to its role in the tumor setting (Chow *et al.*, 2019). Advancing our understanding of this system will be critical to improving therapeutic strategies for a wide range of chronic infections,

as stem-like TCF1+ cells and proliferative intermediate cells are critical for sustaining CD8+ responses to many chronic pathogens in both mice and humans (Wieland *et al.*, 2017; Gordon, Lee, Swadling, Hutchings, *et al.*, 2018; Hudson *et al.*, 2019; Kefalakes *et al.*, 2019; Welten *et al.*, 2020; Rutishauser *et al.*, 2021).

2.4: Materials and Methods

Mice and Infections

C57BL/6, B6c (B6.C-*H2d*/bByJ), Ubi-GFP, and CXCR3 KO B6 mice were originally purchased from The Jackson Laboratory. TG6 transgenic mice were generated in our lab as previously described (Chu *et al.*, 2016). REX3 transgenic mice were received from the lab of Andrew Luster. All mice were bred in the UC Berkeley animal facility and were used with the approval of the Animal Care and Use Committee (ACUC) of the University of California. All experiments were performed on B6xB6c H-$2^{b/d}$ F1 mice. For all infections, mice received 10^5 tachyzoites of the type II Prugniuad-tomato-OVA strain i.p. as previously described (Chu *et al.*, 2016). Neonatal chimeric mice were generated as previously described (Ladi, Herzmark and Robey, 2008). Briefly, donor bone marrow was isolated and RBC lysed using ACK lysis buffer (0.15M NH4CL, 1mM KHC3, 0.1mM Na2EDTA) for 5 minutes at room temperature. Bone marrow cells were resuspended in PBS, and 10^6 cells were injected into 5-7 day old recipient mice intrahepatically. Adult chimeric mice were then infected with *T. gondii*, and TG6 GFP+ populations were expanded.

Spleen tissue cryosectioning

Spleens from infected mice were removed and cut in half laterally. Spleens were fixed in 4% paraformaldehyde at room temperature in the dark for one hour, washed twice with PBS, then dehydrated in 10% sucrose, 20% sucrose, and 30% sucrose for at least 6 hours each at 4°C. Spleens were imbedded in OCT (Fisher) cut side-down and frozen in a slurry of dry ice and ethanol, then stored at -80°C until sectioning. Spleens were cut into 12-micron sections on a cryostat microtome (Leica Biosystems) and stored at -80°C until used for immunofluorescence. REX3 transgenic reporter spleens were fixed for 6 hours in 4% paraformaldehyde at room temperature instead of 1 hour.

Immunofluorescence

Spleen sections were thawed at room temperature in the dark until dry. Sections were rehydrated with PBS for 10 minutes, fixed with 4% paraformaldehyde for 3 minutes, and permeabilized in 0.5% Triton-X for 15 minutes. Samples were blocked with CAS-Block (ThermoFisher) at 4°C for 1 hour, then stained with antibodies overnight. Samples were stained with antibodies against B220 (RA3-6B2), F4/80 (BM8), GFP (polyclonal), TCF1 (C63D9), Ki67 (SolA15), KLRG1 (2F1), CD11c (N418), XCR1 (ZET), and DCIR2 (33D1). Samples were imaged using a LSM 880 NLO AxioExaminer (Zeiss). Analysis of T cell location was performed using ImageJ and Imaris software (Bitplane Scientific Software). For analysis of intracellular expression by lymphocytes (i.e. TCF1, Ki67) Imaris

software was used. In Imaris, GFP+ cells in images were identified and the mean fluorescence of TCF1 and Ki67 was reported for cells classified as localized in each splenic region. Dynamic *in situ* cytometry (DISC) was used to convert data to an FCS format (Moreau *et al.*, 2012), and FlowJo software was used to classify cells as positive or negative for protein expression. For surface staining (KLRG1, XCR1, 33D1) and REX3 CXCL9-RFP/CXCL10-BFP analysis, ImageJ was used. KLRG1 expression on GFP cells was scored by hand, and results were confirmed by an independent and blinded third party.

Flow Cytometry

Spleens were dissociated in FACS buffer (0.5% BSA in PBS) to generate single-cell suspensions. Splenocytes were passed through a 70um filter and then RBC lysed using ACK lysis buffer (0.15M NH4CL, 1mM KHC3, 0.1mM Na2EDTA) for 5 minutes at room temperature. Samples were stained with Ghost Dye Violet 510 (Tonbo) for 20 minutes at 4°C, then stained with the following antibodies: CD4 (GK1.5), B220 (RA3-6B2), CD8b (YTS156.7.7), CXCR3 (CXCR3-173), KLRG1 (2F1/KLRG1), Ki67 (B56), CD44 (1M7), CD3 (145-2C11), CD11c (N418), MHC-II (M5/114.15.2), CD11b (M1/70), XCR1 (ZET), DCIR2 (33D1), CD25 (PC61), CD45.1 (A20), CD45.2 (104), NK1.1 (PK136), Ly6G (1A8). In some experiments, cells were labeled with CFSE proliferation dye (ThermoFisher) following the manufacturer's protocol. For intracellular staining, samples were fixed and permeabilized using the eBioscience FoxP3 staining kit (ThermoFisher). Samples were processed using an LSR Fortessa Analyzer (BD) and analyzed using FlowJo software.

Adoptive Transfers

For adoptive transfer of naïve CD8+ T cells, spleens were isolated from donor mice and single-cell suspensions were generated. CD8+ T cells were isolated by negative enrichment using a magnetic column (Miltenyi Biotec.) according to manufacturer's instruction. $5x10^4$ naïve CD8+ T cells were transferred into recipient mice intravenously (i.v.) and recipient mice were infected 24 hours later. In experiments where two naïve CD8+ T cell populations were transferred, $2.5x10^4$ of each population was injected. For adoptive transfer of TG6-GFP antigen-experienced populations, CD8+ T cells were isolated from infected TG6-GFP chimeras and enriched through magnetic bead selection as described above. Cells were then sorted for GFP-expression and CXCR3xKLRG1 phenotype using a BD influx cell sorter (BD Biosciences) and adoptively transferred into separate mice through i.v. injection. For adoptive transfer of WT and CXCR3 KO T_{MEM} cells, CD8+ T cells were isolated from infected mice and enriched through magnetic bead isolation as described above. T_{MEM} cells were then sorted (CD4- B220- CD45.1+/- KLRG1-) using a BD influx cell sorter and 10^5 cells were injected i.v. into infected recipient mice.

T cell:dendritic cell co-culture

Dendritic cells were enriched prior to cell sorting using density gradient selection (Bosteels, Lambrecht and Hammad, 2018). Briefly, spleens from infected mice

were injected and flushed out with collagenase D and DNAse I, cut into small pieces, and incubated at 37°C for 1 hour. Tissues were then dissociated and filtered. Filtered splenocytes were placed over a density column (Opti-Prep) and centrifuged at 400g for 20 minutes with no brake, and the interphase was removed. Cells were stained with Live/Dead and antibodies for CD3, B220, MHC-II, CD11c, XCR1, CD11b, and 33D1. Cells were sorted using an Influx Cell Sorter (BD) through a 100-micron nozzle. Sorted cells were then pulsed with 1uM GRA6 peptide (Peptide2.0 Inc) at 37°C for 1 hour and plated in flat bottom 96-well plates at a density of 5,000 cells per well. In parallel, TG6 donor mice spleens were enriched for CD8+ T cells using a magnetic column (Miltenyi) and stained with antibodies for CD4, B220, CD45.1, CD45.2, KLRG1. T_{MEM} cells were sorted (CD4/B220-, CD45.1+/-, KLRG1-) through an 85-micron nozzle and co-cultured with dendritic cells at a density of 25,000 cells per well. Media was refreshed on day 2 of culture, and cells were harvested and stained on day 3. In some experiments, anti-CXCL9 (MIG-2F5.5, BioXCell) and anti-CXCR3 (CXCR3-173, BioXCell) were added at a concentration of 40ug/mL.

RNA Sequencing

Splenocytes were isolated from mice infected with *T. gondii* for 6 weeks. GRA6-specific T_{MEM}, T_{INT}, and T_{EFF} cells were sorted using a BD FACSAria Fusion by CD44+ GRA6 Tetramer+ and CXCR3xKLRG1 staining. RNA was harvested using a Quick-RNA Microprep Kit from Zymo Research (Cat. No. R1050) according to manufacturer's instructions. RNA integrity was confirmed via Bioanalyzer and Qbit. RNA was sent to BGI Genomics for library generation and RNA sequencing on an Illumina HiSeq2500/4000 to a depth of 20 million reads.

RNA-seq analysis

Sequencing reads were processed with Trimmomatic (Bolger, Lohse and Usadel, 2014) to remove adapter sequences and trim low-quality bases. Reads were aligned to the mm10 genome using Bowtie2 (Langmead and Salzberg, 2012) and transcripts were quantified using RSEM (Li and Dewey, 2011). PCA was performed on RNA-seq data following normalization by VST with DESeq2 (Love, Huber and Anders, 2014). Differential expression testing was performed using DESeq2, which produced adjusted p-values corrected by the Benjamini-Hochberg procedure. In each test, genes with an adjusted p-value < 0.05 and $|\log_2$ fold change$| > 1$ were considered differentially expressed. Gene set enrichment analysis (GSEA) was performed for each DESeq2 comparison using FGSEA (Korotkevich *et al.*, 2016) with gene sets downloaded from MsigDB (Liberzon *et al.*, 2011). GSEA was also performed on gene sets generated from Utzschneider et al. (2016) and Hudson et al. (2019). To generate these gene sets, published data was filtered to include significantly differentially expressed genes (adjusted p-value < 0.05 and $|\log_2$ fold change$| > 1$) in each relevant comparison. Significantly upregulated and significantly downregulated genes both contributed towards the GSEA enrichment score by accounting for the signed expression (i.e., upregulated genes in the gene set contribute towards the enrichment score when upregulated in the population of interest, while

downregulated genes contribute towards the enrichment score when downregulated in the population of interest).

2.5: References

Anderson, K. G. *et al.* (2014) 'Intravascular staining for discrimination of vascular and tissue leukocytes', *Nature Protocols*. Nature Publishing Group, 9(1), pp. 209–222. doi: 10.1038/nprot.2014.005.

Arnon, T. I. and Cyster, J. G. (2014) 'Blood, sphingosine-1-phosphate and lymphocyte migration dynamics in the spleen', *Current Topics in Microbiology and Immunology*, 378, pp. 107–128. doi: 10.1007/978-3-319-05879-5_5.

Backer, R. A., Diener, N. and Clausen, B. E. (2019) 'Langerin+CD8+ dendritic cells in the splenic marginal zone: Not so marginal after all', *Frontiers in Immunology*, 10(APR). doi: 10.3389/fimmu.2019.00741.

Blanchard, N. *et al.* (2008) 'Immunodominant, protective response to the parasite Toxoplasma gondii requires antigen processing in the endoplasmic reticulum.', *Nature immunology*, 9(8), pp. 937–44. doi: 10.1038/ni.1629.

Bolger, A. M., Lohse, M. and Usadel, B. (2014) 'Trimmomatic: A flexible trimmer for Illumina sequence data', *Bioinformatics*, 30(15), pp. 2114–2120. doi: 10.1093/bioinformatics/btu170.

Bosteels, C. *et al.* (2020) 'Inflammatory Type 2 cDCs Acquire Features of cDC1s and Macrophages to Orchestrate Immunity to Respiratory Virus Infection', *Immunity*. Elsevier Inc., pp. 1–18. doi: 10.1016/j.immuni.2020.04.005.

Bosteels, C., Lambrecht, B. N. and Hammad, H. (2018) 'Isolation of conventional murine lung dendritic cell subsets', *Current Protocols in Immunology*, 2018, pp. 3.7B.1-3.7B.16. doi: 10.1002/cpim.39.

Brown, C. C. *et al.* (2019) 'Transcriptional Basis of Mouse and Human Dendritic Cell Heterogeneity', *Cell*, 179(4), pp. 846-863.e24. doi: 10.1016/j.cell.2019.09.035.

Calabro, S. *et al.* (2016) 'Differential Intrasplenic Migration of Dendritic Cell Subsets Tailors Adaptive Immunity', *Cell Reports*. ElsevierCompany., 16(9), pp. 2472–2485. doi: 10.1016/j.celrep.2016.07.076.

Chang, J. T. *et al.* (2007) 'Asymmetric T lymphocyte division in the initiation of adaptive immune responses', *Science*, 315(5819), pp. 1687–1691. doi: 10.1126/science.1139393.

Chang, J. T., Wherry, E. J. and Goldrath, A. W. (2014) 'Molecular regulation of

effector and memory T cell differentiation', *Nature Reviews Immunology*, 15(12), pp. 1104–1115. doi: 10.1038/ni.3031.1104.

Chauveau, A. *et al.* (2020) 'Visualization of T Cell Migration in the Spleen Reveals a Network of Perivascular Pathways that Guide Entry into T Zones', *Immunity*. Elsevier Inc., 52(5), pp. 794-807.e7. doi: 10.1016/j.immuni.2020.03.010.

Chow, M. T. *et al.* (2019) 'Intratumoral Activity of the CXCR3 Chemokine System Is Required for the Efficacy of Anti-PD-1 Therapy', *Immunity*. Elsevier Inc., 50(6), pp. 1498-1512.e5. doi: 10.1016/j.immuni.2019.04.010.

Chu, H. H. *et al.* (2016) 'Continuous Effector CD8+ T Cell Production in a Controlled Persistent Infection Is Sustained by a Proliferative Intermediate Population', *Immunity*, pp. 159–171. doi: 10.1016/j.immuni.2016.06.013.

Duckworth, B. C. *et al.* (2021) 'Effector and stem-like memory cell fates are imprinted in distinct lymph node niches directed by CXCR3 ligands.', *Nature immunology*. Springer US. doi: 10.1038/s41590-021-00878-5.

Eisenbarth, S. C. (2019) 'Dendritic cell subsets in T cell programming: location dictates function', *Nature Reviews Immunology*. Springer US, 19(2), pp. 89–103. doi: 10.1038/s41577-018-0088-1.

Feliu, V. *et al.* (2013) 'Location of the CD8 T Cell Epitope within the Antigenic Precursor Determines Immunogenicity and Protection against the Toxoplasma gondii Parasite', *PLoS Pathogens*, 9(6), pp. 1–14. doi: 10.1371/journal.ppat.1003449.

Förster, R. *et al.* (1999) 'CCR7 coordinates the primary immune response by establishing functional microenvironments in secondary lymphoid organs', *Cell*, 99(1), pp. 23–33. doi: 10.1016/S0092-8674(00)80059-8.

Gabriel, S. S. *et al.* (2021) 'Article Transforming growth factor- b -regulated mTOR activity preserves cellular metabolism to maintain long-term T cell responses in chronic infection Article Transforming growth factor- b -regulated mTOR activity preserves cellular metabolism to mainta', pp. 1–17. doi: 10.1016/j.immuni.2021.06.007.

Goldberg, M. F. *et al.* (2018) 'Salmonella Persist in Activated Macrophages in T Cell-Sparse Granulomas but Are Contained by Surrounding CXCR3 Ligand-Positioned Th1 Cells', *Immunity*. Elsevier Inc., 49(6), pp. 1090-1102.e7. doi: 10.1016/j.immuni.2018.10.009.

Gordon, C. L., Lee, L. N., Swadling, L., Folgori, A., *et al.* (2018) 'Induction and Maintenance of CX3CR1-Intermediate Peripheral Memory CD8 + T Cells by

Persistent Viruses and Vaccines Article Induction and Maintenance of CX3CR1-Intermediate Peripheral Memory CD8 + T Cells by Persistent Viruses and Vaccines', *CellReports*. ElsevierCompany., 23(3), pp. 768–782. doi: 10.1016/j.celrep.2018.03.074.

Groom, J. R. *et al.* (2012) 'CXCR3 Chemokine Receptor-Ligand Interactions in the Lymph Node Optimize CD4+ T Helper 1 Cell Differentiation', *Immunity*. Elsevier Inc., 37(6), pp. 1091–1103. doi: 10.1016/j.immuni.2012.08.016.

Groom, J. R. and Luster, A. D. (2011) 'CXCR3 ligands: redundant, collaborative and antagonistic functions.', *Immunology and cell biology*. Nature Publishing Group, 89(2), pp. 207–15. doi: 10.1038/icb.2010.158.

Den Haan, J. M. M. and Bevan, M. J. (2002) 'Constitutive versus activation-dependent cross-presentation of immune complexes by CD8+ and CD8- dendritic cells in vivo', *Journal of Experimental Medicine*, 196(6), pp. 817–827. doi: 10.1084/jem.20020295.

Hu, J. K. *et al.* (2011) 'Expression of chemokine receptor CXCR3 on T cells affects the balance between effector and memory CD8 T-cell generation.', *Proceedings of the National Academy of Sciences of the United States of America*, 108(21), pp. E118–E127. doi: 10.1073/pnas.1101881108.

Hudson, W. H. *et al.* (2019) 'Proliferating Transitory T Cells with an Effector-like Transcriptional Signature Emerge from PD-1 + Stem- Article Proliferating Transitory T Cells with an Effector-like Transcriptional Signature Emerge from PD-1 + Stem-like CD8 + T Cells during Chronic In', *Immunity*. Elsevier Inc., pp. 1–16. doi: 10.1016/j.immuni.2019.11.002.

Im, S. J. *et al.* (2016) 'Defining CD8+ T cells that provide the proliferative burst after PD-1 therapy', *Nature*. Nature Publishing Group, 537(7620), pp. 417–421. doi: 10.1038/nature19330.

Kalia, V. *et al.* (2010) 'Prolonged Interleukin-2Rα Expression on Virus-Specific CD8+ T Cells Favors Terminal-Effector Differentiation In Vivo', *Immunity*. Elsevier Inc., 32(1), pp. 91–103. doi: 10.1016/j.immuni.2009.11.010.

Kefalakes, H. *et al.* (2019) 'Hepatitis D Virus-Specific CD8+ T Cells Have a Memory-Like Phenotype Associated With Viral Immune Escape in Patients With Chronic Hepatitis D Virus Infection', *Gastroenterology*. Elsevier, Inc, 156(6), pp. 1805-1819.e9. doi: 10.1053/j.gastro.2019.01.035.

Khanna, K. M., McNamara, J. T. and Lefrançois, L. (2007) 'In situ imaging of the endogenous CD8 T cell response to infection.', *Science (New York, N.Y.)*, 318(5847), pp. 116–120. doi: 10.1126/science.1146291.

Kohlmeier, J. E. *et al.* (2011) 'Inflammatory chemokine receptors regulate CD8 $^{+}$ T cell contraction and memory generation following infection', *The Journal of Experimental Medicine*, 208(8), pp. 1621–1634. doi: 10.1084/jem.20102110.

Korotkevich, G. *et al.* (2016) 'Fast gene set enrichment analysis', pp. 1–29. doi: 10.1101/060012.

Kotov, D. I. *et al.* (2019) 'TCR Affinity Biases Th Cell Differentiation by Regulating CD25, Eef1e1, and Gbp2', *The Journal of Immunology*, 202(9), pp. 2535–2545. doi: 10.4049/jimmunol.1801609.

Kurachi, M. *et al.* (2011) 'Chemokine receptor CXCR3 facilitates CD8 $^{+}$ T cell differentiation into short-lived effector cells leading to memory degeneration', *The Journal of Experimental Medicine*, 208(8), pp. 1605–1620. doi: 10.1084/jem.20102101.

Ladi, E., Herzmark, P. and Robey, E. (2008) 'In situ imaging of the mouse thymus using 2-photon microscopy', *Journal of Visualized Experiments*, 166(11), p. 2008. doi: 10.3791/652.

Langmead, B. and Salzberg, S. L. (2012) 'Fast gapped-read alignment with Bowtie 2', *Nature Methods*, 9(4), pp. 357–359. doi: 10.1038/nmeth.1923.

Li, B. and Dewey, C. N. (2011) 'RSEM: accurate transcript quantification from RNA-Seq data with or without a reference genome', *Bioinformatics*, pp. 21–40. doi: 10.1186/1471-2105-12-323.

Li, J. *et al.* (2016) 'EBI2 augments Tfh cell fate by promoting interaction with IL-2-quenching dendritic cells', *Nature*. Nature Publishing Group, 533(7601), pp. 110–114. doi: 10.1038/nature17947.

Liberzon, A. *et al.* (2011) 'Molecular signatures database (MSigDB) 3.0', *Bioinformatics*, 27(12), pp. 1739–1740. doi: 10.1093/bioinformatics/btr260.

Lin, W.-H. W. *et al.* (2015) 'CD8+ T Lymphocyte Self-renewal during Effector Cell Determination', 344(6188), pp. 1173–1178. doi: 10.1126/science.1249098.Sleep.

Love, M. I., Huber, W. and Anders, S. (2014) 'Moderated estimation of fold change and dispersion for RNA-seq data with DESeq2', *Genome Biology*, 15(12), pp. 1–21. doi: 10.1186/s13059-014-0550-8.

Lutes, L. K. *et al.* (2021) 'Title: T cell self---reactivity during thymic development dictates the timing of positive 1 selection 2 3 4', *bioRxiv*, p. 2021.01.18.427079. doi: 10.1101/2021.01.18.427079.

Mackay, L. K. *et al.* (2015) 'Cutting Edge: CD69 Interference with Sphingosine-1-

Phosphate Receptor Function Regulates Peripheral T Cell Retention', *The Journal of Immunology*, 194(5), pp. 2059–2063. doi: 10.4049/jimmunol.1402256.

Maurice, N. J. *et al.* (2019) 'CXCR3 enables recruitment and site-specific bystander activation of memory CD8+ T cells', *Nature Communications*. Springer US, 10(1), pp. 1–15. doi: 10.1038/s41467-019-12980-2.

Moreau, H. D. *et al.* (2012) 'Dynamic in situ cytometry uncovers t cell receptor signaling during immunological synapses and kinapses in vivo', *Immunity*, 37(2), pp. 351–363. doi: 10.1016/j.immuni.2012.05.014.

Opejin, A. *et al.* (2020) 'A Two-Step Process of Effector Programming Governs CD4+ T Cell Fate Determination Induced by Antigenic Activation in the Steady State', *Cell Reports*. ElsevierCompany., 33(8), p. 108424. doi: 10.1016/j.celrep.2020.108424.

Pipkin, M. E. *et al.* (2010) 'Interleukin-2 and Inflammation Induce Distinct Transcriptional Programs that Promote the Differentiation of Effector Cytolytic T Cells', *Immunity*. Elsevier Ltd, 32(1), pp. 79–90. doi: 10.1016/j.immuni.2009.11.012.

Rutishauser, R. L. *et al.* (2021) 'TCF-1 regulates HIV-specific CD8+ T cell expansion capacity', *JCI Insight*, 6(3), pp. 1–16. doi: 10.1172/jci.insight.136648.

Salvioni, A. *et al.* (2019) 'Robust Control of a Brain-Persisting Parasite through MHC I Presentation by Infected Neurons', *Cell Reports*, 27(11), pp. 3254-3268.e8. doi: 10.1016/j.celrep.2019.05.051.

Sansom, D. M., Manzotti, C. N. and Zheng, Y. (2003) 'What's the difference between CD80 and CD86?', *Trends in Immunology*, 24(6), pp. 313–318. doi: 10.1016/S1471-4906(03)00111-X.

Seo, Y. J. *et al.* (2016) 'Local Cellular and Cytokine Cues in the Spleen Regulate In Situ T Cell Receptor Affinity, Function, and Fate of CD8+ T Cells', *Immunity*. Elsevier Inc., 45(5), pp. 988–998. doi: 10.1016/j.immuni.2016.10.024.

Shah, S. *et al.* (2015) 'An extrafollicular pathway for the generation of effector CD8+T cells driven by the proinflammatory cytokine, IL-12', *eLife*, 4(AUGUST2015), pp. 1–21. doi: 10.7554/eLife.09017.

Shin, K. S. *et al.* (2019) 'Monocyte-derived dendritic cells dictate the memory differentiation of CD8+ T cells during acute infection', *Frontiers in Immunology*, 10(AUG), pp. 5–7. doi: 10.3389/fimmu.2019.01887.

Sung, J. H. *et al.* (2012) 'Chemokine guidance of central memory T cells is critical for antiviral recall responses in lymph nodes', *Cell*. Elsevier Inc., 150(6),

pp. 1249–1263. doi: 10.1016/j.cell.2012.08.015.

Thomas, I. J. *et al.* (2007) ‘CD86 Has Sustained Costimulatory Effects on CD8 T Cells’, *The Journal of Immunology*, 179(9), pp. 5936–5946. doi: 10.4049/jimmunol.179.9.5936.

Tsitsiklis, A. *et al.* (2020) ‘An Unusual MHC Molecule Generates Protective CD8+ T Cell Responses to Chronic Infection’, *Frontiers in Immunology*, 11(July), pp. 1–13. doi: 10.3389/fimmu.2020.01464.

Utzschneider, D. T. *et al.* (2016) ‘T Cell Factor 1-Expressing Memory-like CD8+ T Cells Sustain the Immune Response to Chronic Viral Infections’, *Immunity*, 45(2), pp. 415–427. doi: 10.1016/j.immuni.2016.07.021.

Welten, S. P. M. *et al.* (2020) ‘Tcf1+ cells are required to maintain the inflationary T cell pool upon MCMV infection’, *Nature Communications*. Springer US, 11(1), pp. 1–14. doi: 10.1038/s41467-020-16219-3.

Weng, Y. *et al.* (1998) ‘Binding and functional properties of recombinant and endogenous CXCR3 chemokine receptors’, *Journal of Biological Chemistry*. Â© 1998 ASBMB. Currently published by Elsevier Inc; originally published by American Society for Biochemistry and Molecular Biology., 273(29), pp. 18288–18291. doi: 10.1074/jbc.273.29.18288.

Wieland, D. *et al.* (2017) ‘TCF1+ hepatitis C virus-specific CD8+ T cells are maintained after cessation of chronic antigen stimulation’, *Nature Communications*. Nature Publishing Group, 8(May), pp. 1–13. doi: 10.1038/ncomms15050.

Williams, M. A. and Bevan, M. J. (2007) ‘Effector and memory CTL differentiation’, *Annual Review of Immunology*, 25, pp. 171–192. doi: 10.1146/annurev.immunol.25.022106.141548.

Figure 1

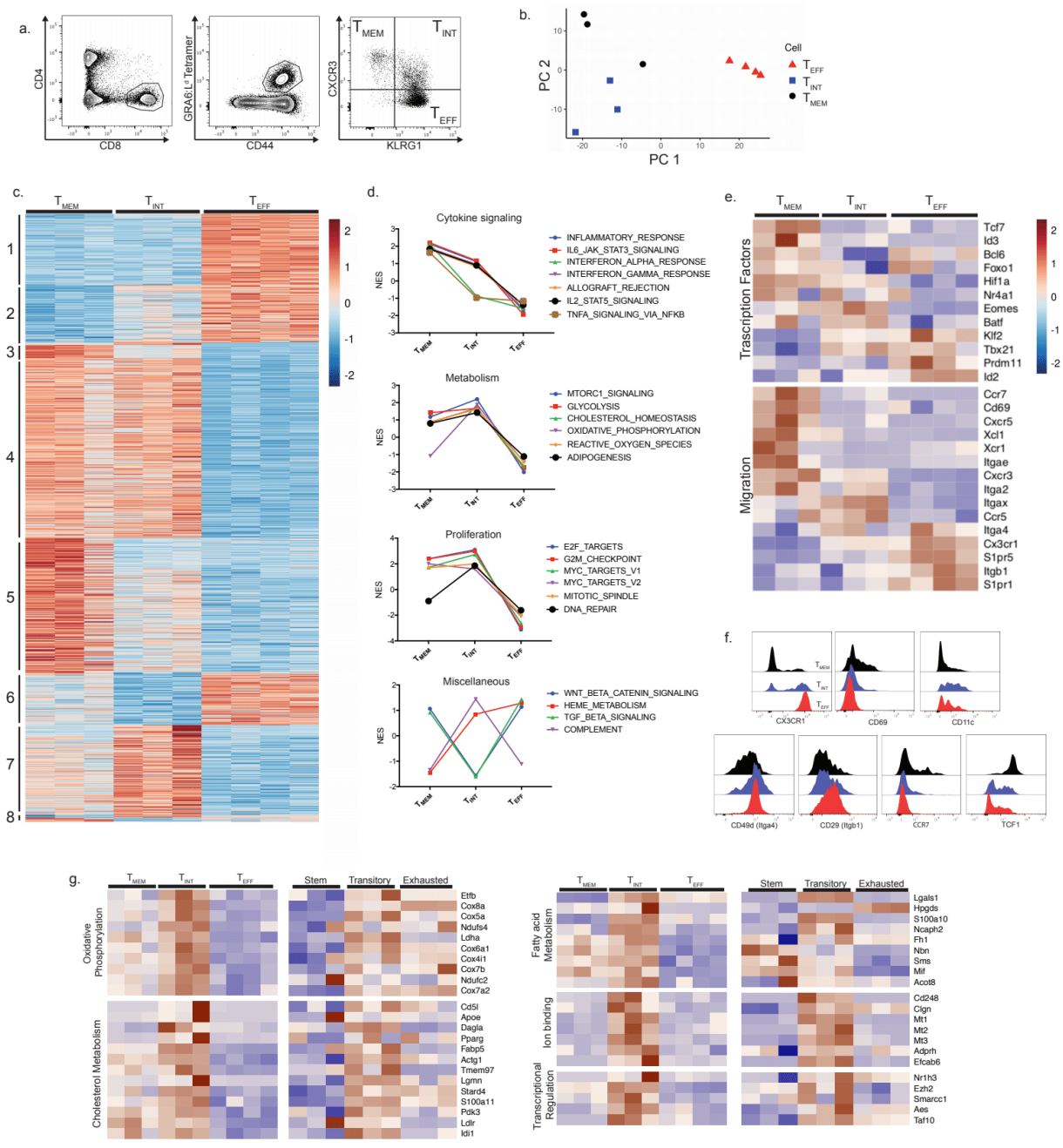
a.
CD4
CD8
GRA6:I-Ad Tetramer
CD44
CXCR3
KLRG1
T MEM
T INT
T EFF
b.
PC 2
PC 1
Cell
T EFF
T INT
T MEM
c.
T MEM
T INT
T EFF
d.
Cytokine signaling
INFLAMMATORY_RESPONSE
IL6_JAK_STAT3_SIGNALING
INTERFERON_ALPHA_RESPONSE
INTERFERON_GAMMA_RESPONSE
ALLOGRAFT_REJECTION
IL2_STAT5_SIGNALING
TNFA_SIGNALING_VIA_NFKB
Metabolism
MTORC1_SIGNALING
GLYCOLYSIS
CHOLESTEROL_HOMEOSTASIS
OXIDATIVE_PHOSPHORYLATION
REACTIVE_OXYGEN_SPECIES
ADIPOGENESIS
Proliferation
E2F_TARGETS
G2M_CHECKPOINT
MYC_TARGETS_V1
MYC_TARGETS_V2
MITOTIC_SPINDLE
DNA_REPAIR
Miscellaneous
WNT_BETA_CATENIN_SIGNALING
HEME_METABOLISM
TGF_BETA_SIGNALING
COMPLEMENT
NES
e.
Trascription Factors
Tcf7
Id3
Bcl6
Foxo1
Hif1a
Nr4a1
Eomes
Batf
Klf2
Tbx21
Prdm11
Id2
Migration
Ccr7
Cd69
Cxcr5
Xcl1
Xcr1
Itgae
Cxcr3
Itga2
Itgax
Ccr5
Itga4
Cx3cr1
S1pr5
Itgb1
S1pr1
f.
CX3CR1
CD69
CD11c
CD49d (Itga4)
CD29 (Itgb1)
CCR7
TCF1
g.
Stem
Transitory
Exhausted
Oxidative Phosphorylation
Etfb
Cox8a
Cox5a
Ndufs4
Ldha
Cox6a1
Cox4i1
Cox7b
Ndufc2
Cox7a2
Cholesterol Metabolism
Cd5l
Apoe
Dagla
Pparg
Fabp5
Actg1
Tmem97
Lgmn
Stard4
S100a11
Pdk3
Ldlr
Idi1
Fatty acid Metabolism
Lgals1
Hpgds
S100a10
Ncaph2
Fh1
Nbn
Sms
Mif
Acot8
Ion binding
Cd248
Clgn
Mt1
Mt2
Mt3
Adprh
Efcab6
Transcriptional Regulation
Nr1h3
Ezh2
Smarcc1
Aes
Taf10

Figure 1: T_{MEM}, T_{INT}, and T_{EFF} cells express distinct transcriptional profiles. A) Polyclonal T_{MEM}, T_{INT}, and T_{EFF} cells were sorted using GRA6 peptide-MHC tetramer staining in mice infected with *T. gondii* for six weeks. Cells were then processed for RNA-seq. B) The first two principal components of the sorted GRA6-specific populations. C) Heatmap displaying all genes differentially expressed in pairwise comparisons between each of the three populations. Gene expression values were normalized by the DESeq2 variance stabilizing transformation (VST) and scaled per row. Genes were ordered and grouped based on the results of differential expression tests from each pairwise comparison (T_{MEM} vs. T_{INT}, T_{INT} vs. T_{EFF}, T_{MEM} vs. T_{EFF}). Each column represents independent biological replicates (n=3 mice for T_{MEM} and T_{INT}, n=4 mice for T_{EFF}) D) Selected results of GSEA with Hallmark gene sets using one versus all comparisons (T_{MEM} vs. T_{INT} and T_{EFF}, T_{INT} vs. T_{MEM} and T_{EFF}, T_{MEM} vs. T_{EFF} and T_{INT}). Normalized enrichment scores for each T cell population are displayed for the indicated gene sets, and gene sets are grouped based on function. The full set of Hallmark gene sets that exhibited significant enrichment in at least one population (padj < 0.05) is displayed in Supplemental Figure 1. E) Heatmap displaying selected differentially-expressed genes related to the indicated function. F) Representative flow cytometry histograms showing protein staining on T_{MEM}, T_{INT}, and T_{EFF} cells to confirm differential expression of selected genes. G) Heatmap displaying the expression of selected genes from cluster 7 (specifically upregulated by GRA6-specific T_{INT} cells) grouped by the functional categories indicated. Genes that contribute to GSEA Hallmark enrichment scores are indicated with asterisks. Values displayed are from sorted GRA6-specific subsets (current study) or published transcriptional data on Stem, Transitory, and Exhausted cells during LCMV infection (Hudson *et al.,* 2019).

Figure 2

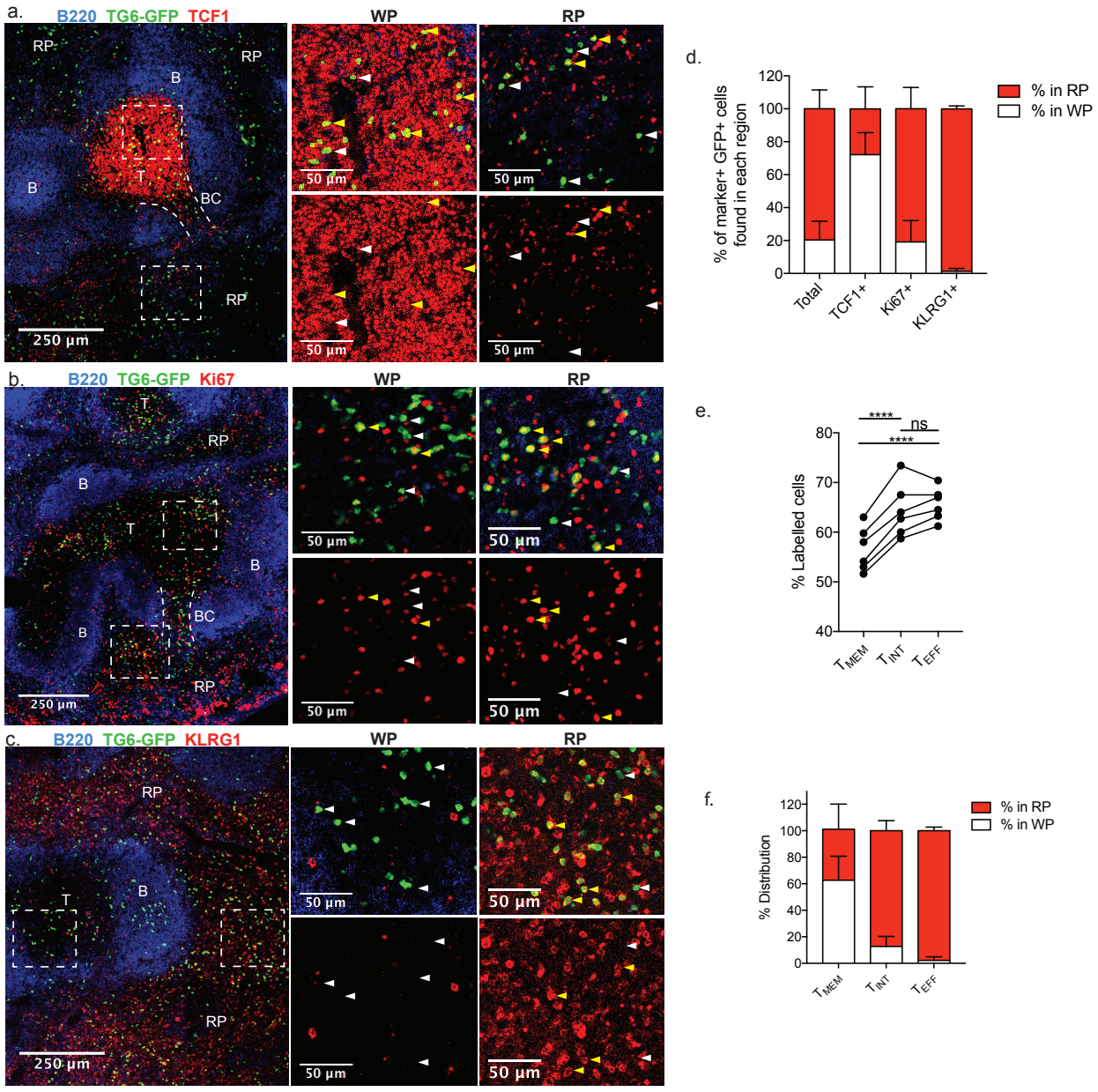
a.
B220 TG6-GFP TCF1
WP
RP
RP
RP
B
T
B
BC
RP
250 µm
50 µm
50 µm
50 µm
50 µm
b.
B220 TG6-GFP Ki67
WP
RP
T
RP
B
T
B
BC
B
RP
250 µm
50 µm
50 µm
50 µm
50 µm
c.
B220 TG6-GFP KLRG1
WP
RP
RP
T
B
RP
250 µm
50 µm
50 µm
50 µm
50 µm
d.
% of marker+ GFP+ cells found in each region
120
100
80
60
40
20
0
Total
TCF1+
Ki67+
KLRG1+
% in RP
% in WP
e.
% Labelled cells
80
70
60
50
40
****
ns
****
TMEM
TINT
TEFF
f.
% Distribution
120
100
80
60
40
20
0
TMEM
TINT
TEFF
% in RP
% in WP

Figure 2: T_{MEM}, T_{INT}, and T_{EFF} cells reside in distinct areas of the spleen during chronic infection. A-C) TG6-GFP chimeric mice infected with *T. gondii*. Six weeks post-infection, mice were sacrificed and their spleens were analyzed by confocal microscopy. Sections were stained with antibodies against TCF1 (A), Ki67 (B), and KLRG1 (C) to identify the location of T_{MEM}, T_{INT}, and T_{INT}/T_{EFF} TG6-GFP cells, respectively. B220 staining was used to identify B cell zones (B) and T cell zones (T) to map the white pulp (WP) and red pulp (RP) regions. In some images, bridging channels (BC) are marked with dotted lines. Dashed rectangles indicate the area in the zoomed-in regions at right. Examples of cells staining positively with the indicated marker are highlighted with yellow arrows and negative examples with white arrows. D) Data summarizing the location of TG6-GFP cells that stained positively for each protein. E) Mice chronically infected with *T. gondii* were treated with a PE-conjugated anti-CD8 antibody intravenously, and then sacrificed five minutes later. Data show the proportion of each GRA6-specific population labeled with the i.v. antibody. F) T_{MEM}, T_{INT}, and T_{EFF} cells were sorted from TG6-GFP chimeric mice infected with *T. gondii* for six weeks. Sorted cells were adoptively transferred into infection-matched recipients, and recipient spleens were imaged 2 days post-transfer **(Supp. Fig 3)**. Summary data shows the location of each GFP+ population in the recipient spleens. Images in A-C and data in D are representative of images taken from three or more separate mice. Data in E are taken from two separate infections and are representative of data from three separate experiments. Data in F is summarized from multiple recipient mice across three infections (T_{MEM} n=3, T_{INT} n=3, T_{EFF} n=4). Statistical significance in (E) was determined using a paired t-test (*p<0.05, **p<0.01, ***p<0.001, ****p<0.0001).

Figure 3

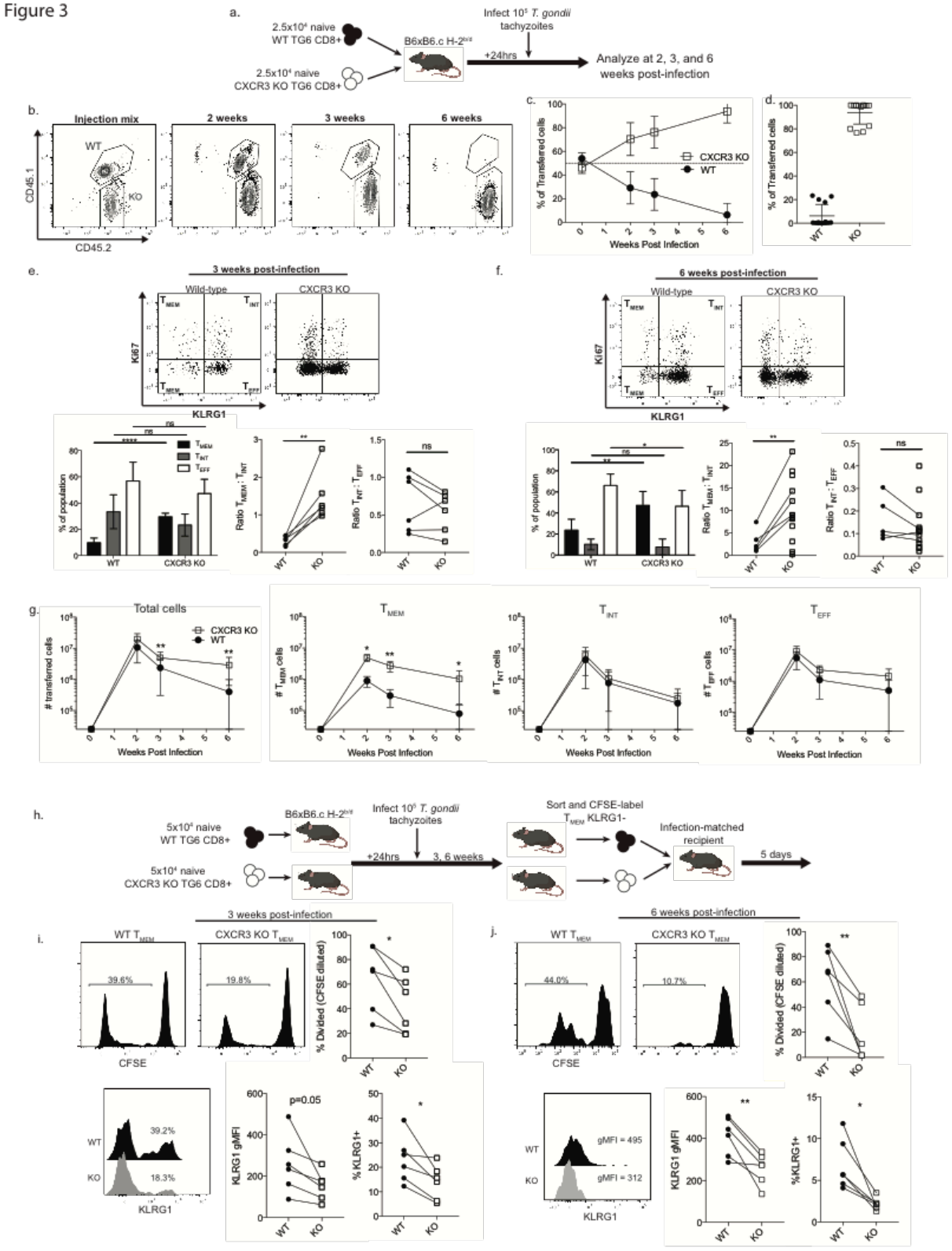
a.
2.5x10⁴ naive WT TG6 CD8+
2.5x10⁴ naive CXCR3 KO TG6 CD8+
B6xB6.c H-2^bm8
Infect 10⁵ T. gondii tachyzoites
+24hrs
Analyze at 2, 3, and 6 weeks post-infection
b.
Injection mix
2 weeks
3 weeks
6 weeks
WT
KO
CD45.1
CD45.2
c.
% of Transferred cells
CXCR3 KO
WT
Weeks Post Infection
d.
% of Transferred cells
WT
KO
e.
3 weeks post-infection
Wild-type
CXCR3 KO
Ki67
KLRG1
% of population
Ratio T_MEM : T_INT
Ratio T_INT : T_EFF
ns
f.
6 weeks post-infection
Wild-type
CXCR3 KO
Ki67
KLRG1
% of population
Ratio T_MEM : T_INT
Ratio T_INT : T_EFF
ns
g.
Total cells
T_MEM
T_INT
T_EFF
CXCR3 KO
WT
transferred cells
Weeks Post Infection
h.
5x10⁴ naive WT TG6 CD8+
5x10⁴ naive CXCR3 KO TG6 CD8+
B6xB6.c H-2^bm8
Infect 10⁵ T. gondii tachyzoites
+24hrs
3, 6 weeks
Sort and CFSE-label T_MEM KLRG1-
Infection-matched recipient
5 days
i.
3 weeks post-infection
WT T_MEM
CXCR3 KO T_MEM
39.6%
19.8%
CFSE
% Divided (CFSE dilluted)
39.2%
18.3%
KLRG1
p=0.05
KLRG1 gMFI
% KLRG1+
j.
6 weeks post-infection
WT T_MEM
CXCR3 KO T_MEM
44.0%
10.7%
CFSE
% Divided (CFSE dilluted)
gMFI = 495
gMFI = 312
KLRG1
KLRG1 gMFI
% KLRG1+

Figure 3: CXCR3-deficient CD8+ T cells develop an inflated T_{MEM} pool during chronic infection. A) Experimental design. Equal numbers of congenically distinct wild-type and CXCR3 knockout naïve TG6 CD8+ T cells were adoptively co-transferred into CD45.1/45.1 recipient mice. Recipients were infected 24 hours after transfer, and sacrificed at 2, 3, or 6 weeks post-infection. B) Representative flow cytometry plots of gated GRA6 tetramer+ CD8+ splenocytes at the indicated time points. C) Summary data showing the proportion of the transferred cells belonging to either the WT or CXCR3 KO population. D) Individual data points for the six weeks post-infection time point in (C) are shown. Of the 14 mice analyzed, only 5 had detectable WT TG6 populations. E,F) The differentiation profile of WT and CXCR3 KO TG6 cells at three weeks post-infection (E) and six weeks post-infection (F). T_{MEM}, T_{INT}, and T_{EFF} subsets were identified using Ki67 and KLRG1 staining due to the absence of CXCR3 as a functional marker. Bar graphs display the proportion of the transferred population belonging to each subset. Adjacent plots display the ratios of T_{MEM}:T_{INT} and T_{INT}:T_{EFF} cells in the WT and KO populations. Lines connect populations from the same mouse. G) Absolute numbers of cells belonging to each population. H) Experimental design. Mice received either WT or CXCR3 KO TG6 CD8+ T cells and were infected with T. gondii for 3 or 6 weeks. WT and CXCR3 KO T_{MEM} cells were then sorted from the infected recipients, labeled with CFSE, and adoptively transferred into a common recipient for five days. J,K) Representative flow plots and summary data for CFSE dilution and KLRG1 expression within the population of transferred WT and KO T_{MEM} cells at 3 weeks (I) and 6 weeks (J) post-infection. Data in A-G are combined from three independent experiments. Data in H-J are combined from two independent experiments. Statistical significance was determined using a t-test (*$p<0.05$, **$p<0.01$, ***$p<0.001$, ****$p<0.0001$).

Figure 4

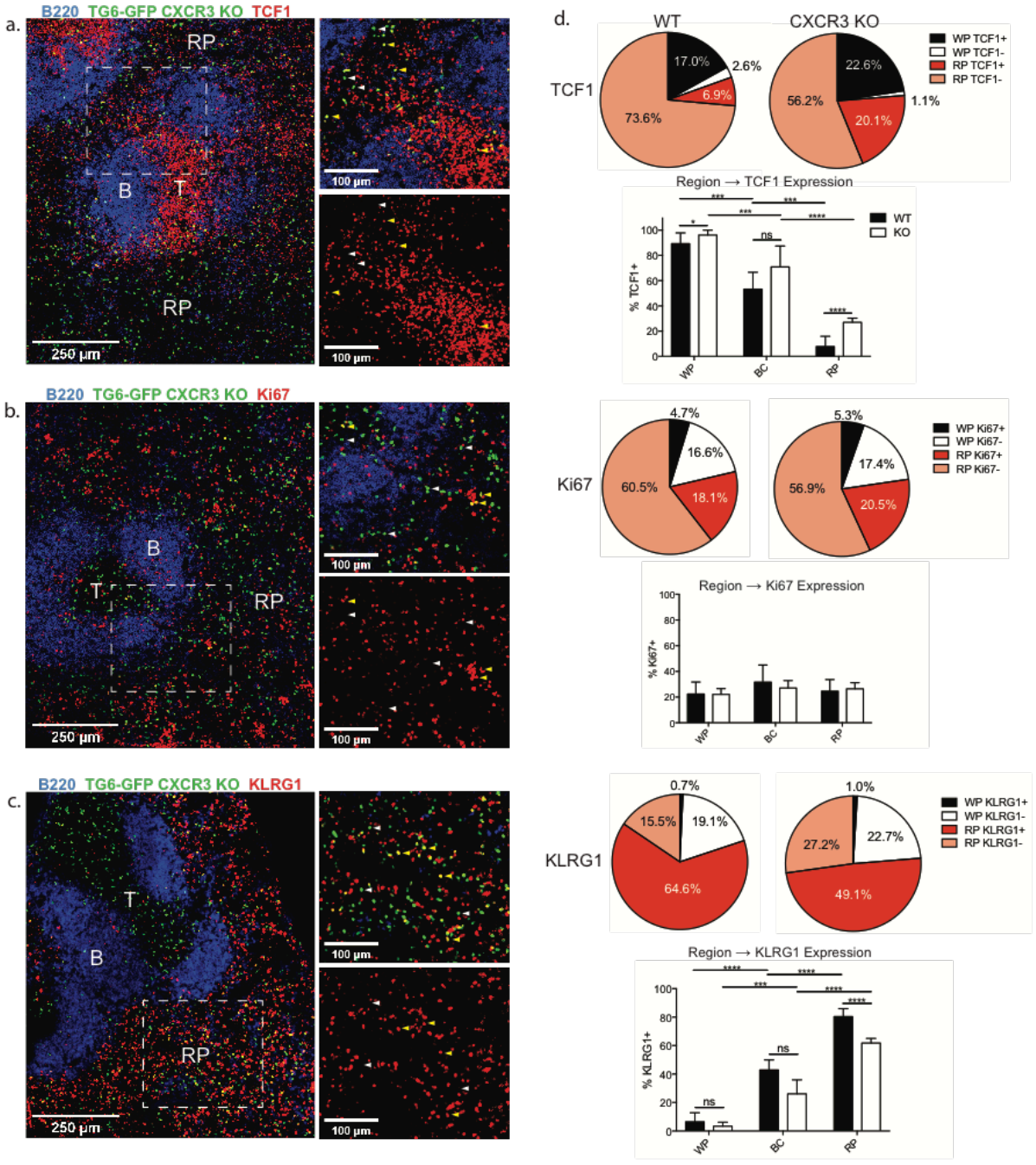
a.
B220 TG6-GFP CXCR3 KO TCF1
RP
B
T
RP
250 µm
100 µm
100 µm
b.
B220 TG6-GFP CXCR3 KO Ki67
B
T
RP
250 µm
100 µm
100 µm
c.
B220 TG6-GFP CXCR3 KO KLRG1
T
B
RP
250 µm
100 µm
100 µm
d.
WT
CXCR3 KO
TCF1
17.0%
2.6%
6.9%
73.6%
22.6%
56.2%
1.1%
20.1%
WP TCF1+
WP TCF1-
RP TCF1+
RP TCF1-
Region → TCF1 Expression
% TCF1+
WT
KO
WP
BC
RP
Ki67
4.7%
16.6%
60.5%
18.1%
5.3%
17.4%
56.9%
20.5%
WP Ki67+
WP Ki67-
RP Ki67+
RP Ki67-
Region → Ki67 Expression
% Ki67+
KLRG1
0.7%
15.5%
19.1%
64.6%
1.0%
27.2%
22.7%
49.1%
WP KLRG1+
WP KLRG1-
RP KLRG1+
RP KLRG1-
Region → KLRG1 Expression
% KLRG1+

Figure 4: CXCR3-deficient CD8+ T cells retain a memory phenotype in the red pulp. A-C) CXCR3 KO TG6-GFP neonatal chimeras were infected with *T. gondii*. Six weeks post-infection, mice were sacrificed and their spleens were analyzed by confocal microscopy. Sections were stained with antibodies against TCF1 (A), Ki67 (B), and KLRG1 (C). B220 staining was used to identify B cell zones (B) to map the T cell zone (T) and red pulp (RP) regions. Yellow arrows highlight examples of cells positively staining for the specified marker; white arrows highlight examples of negative staining. D) Summary data showing the proportion of GFP cells found in the WP or RP that are identified as either positive or negative for expression of the indicated marker. Bar graphs display the proportion of WT or CXCR3 KO GFP cells expressing the protein of interest (TCF1, Ki67, KLRG1) within the white pulp (WP), bridging channel (BC), or red pulp (RP). Statistical significance was determined using a t-test (*$p<0.05$, **$p<0.01$, ***$p<0.001$, ****$p<0.0001$).

Figure 5

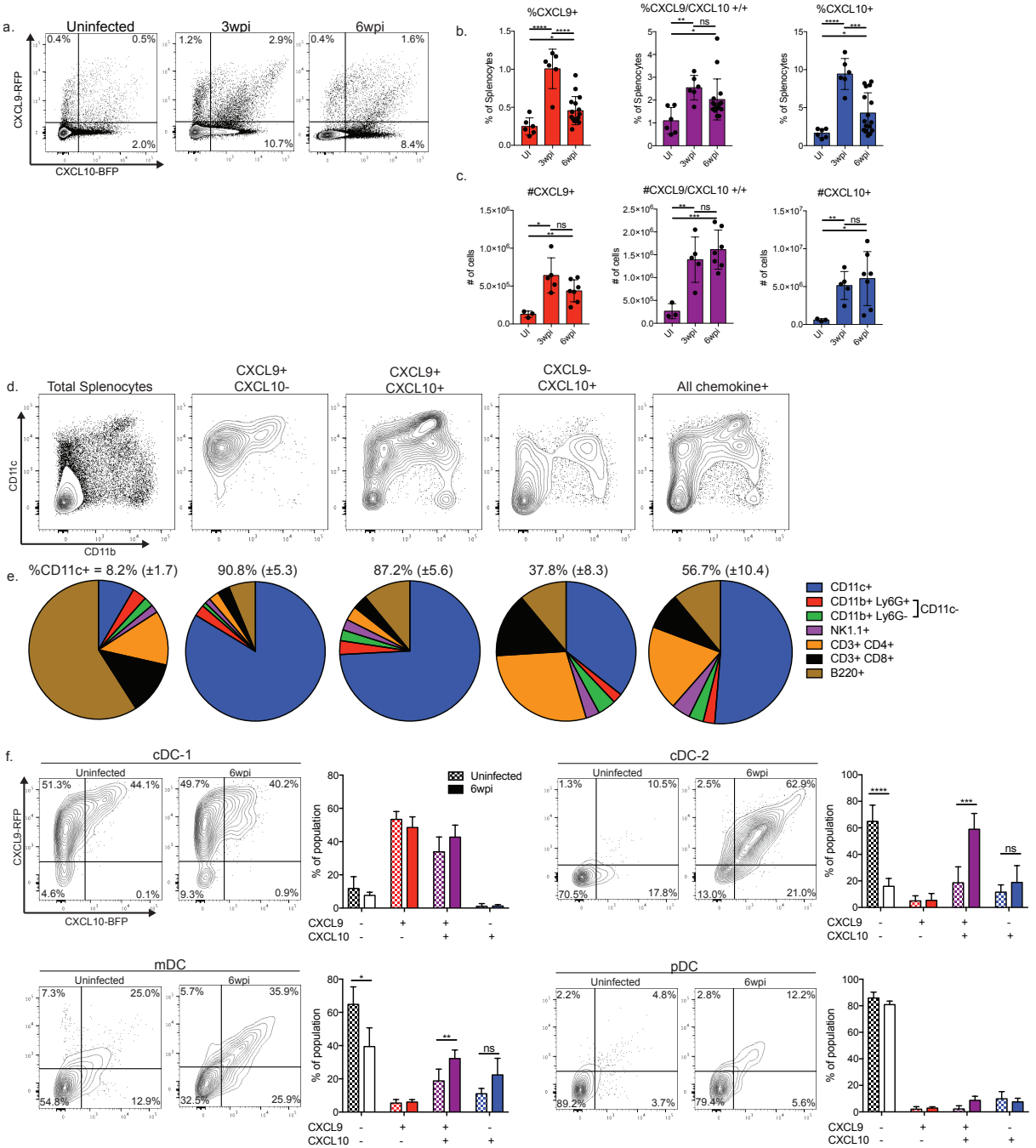
a.
Uninfected
3wpi
6wpi
CXCL9-RFP
CXCL10-BFP
b.
%CXCL9+
%CXCL9/CXCL10 +/+
%CXCL10+
% of Splenocytes
c.
#CXCL9+
#CXCL9/CXCL10 +/+
#CXCL10+
# of cells
d.
Total Splenocytes
CXCL9+ CXCL10-
CXCL9+ CXCL10+
CXCL9- CXCL10+
All chemokine+
CD11c
CD11b
e.
%CD11c+ = 8.2% (±1.7)
90.8% (±5.3)
87.2% (±5.6)
37.8% (±8.3)
56.7% (±10.4)
CD11c+
CD11b+ Ly6G+
CD11b+ Ly6G-
CD11c-
NK1.1+
CD3+ CD4+
CD3+ CD8+
B220+
f.
cDC-1
cDC-2
mDC
pDC
% of population
CXCL9
CXCL10

Figure 5: Dendritic cells are a significant source of CXCR3 ligands during chronic infection. REX3 mice expressing a dual CXCL9-RFP and CXCL10-BFP construct were infected with *T. gondii* and splenocytes were analyzed at different infection time points. A) Representative flow cytometry plots of chemokine expression before infection, at 3 weeks post-infection, and at 6 weeks post-infection. B,C) Summary data of the percent (B) and absolute numbers (C) of chemokine-producing splenocytes during infection. D,E) Splenocytes from REX3 mice were stained with the indicated surface markers to delineate various immune populations. Cells were then gated on chemokine expression and the phenotype of different chemokine-expressing subsets was measured. D) Representative plots of CD11c x CD11b staining. E) Summary data. The mean and standard deviation of the percent of CD11c+ cells in each population is displayed above each chart. F) Subsets of dendritic cells were identified (Supp Fig 6) and their chemokine expression was analyzed in uninfected mice and 6 weeks post-infection. Statistical significance was determined using a t-test (*$p<0.05$, **$p<0.01$, ***$p<0.001$, ****$p<0.0001$).

Figure 6

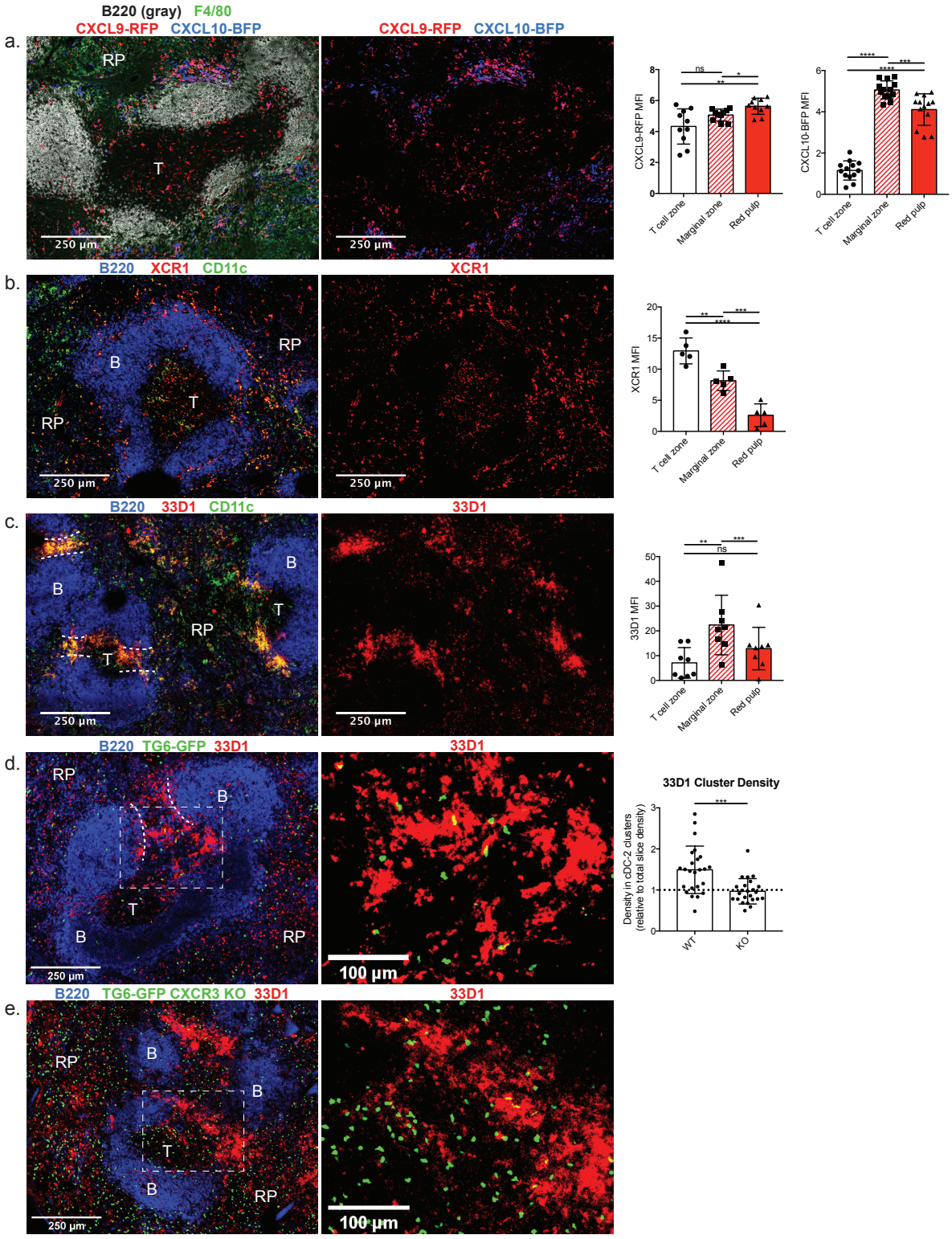
a.
B220 (gray) F4/80
CXCL9-RFP CXCL10-BFP
RP
T
250 µm
CXCL9-RFP CXCL10-BFP
250 µm
CXCL9-RFP MFI
CXCL10-BFP MFI
T cell zone
Marginal zone
Red pulp
b.
B220 XCR1 CD11c
B
RP
T
RP
250 µm
XCR1
250 µm
XCR1 MFI
c.
B220 33D1 CD11c
B
B
T
RP
T
250 µm
33D1
250 µm
33D1 MFI
d.
B220 TG6-GFP 33D1
RP
B
T
B
RP
250 µm
33D1
100 µm
33D1 Cluster Density
Density in cDC-2 clusters (relative to total slice density)
WT
KO
e.
B220 TG6-GFP CXCR3 KO 33D1
RP
B
B
T
B
RP
250 µm
33D1
100 µm

Figure 6: CXCL9/10+ dendritic cells occupy distinct regions in the spleen. A) Spleens from REX3 mice were imaged six weeks post-infection with *T. gondii*. Sections were stained with F4/80 to highlight the red pulp and B220 to highlight B cell follicles. The mean fluorescence intensity was measured for CXCL9-RFP and CXCL10-BFP in each splenic region. Data was normalized to the B cells zone to adjust for background fluorescence. B,C) Spleens from WT mice infected for six weeks were stained with XCR1 (B) or 33D1 (C) together with CD11c to identify cDC-1s and cDC-2s, respectively. Summary data shows mean fluorescence for the indicated marker in each splenic region. Data was normalized to the B cell follicle as in (A). D,E) WT (D) or CXCR3 KO (E) TG6-GFP neonatal chimeras were stained with 33D1 to identify cDC-2 clusters. The density of GFP cells within cDC-2 clusters was then measured and normalized to the total density of GFP cells in the slice. Data in (A) are representative of three mice, data in (B)-(E) are representative of two mice. Statistical significance was determined using a t-test (*$p<0.05$, **$p<0.01$, ***$p<0.001$, ****$p<0.0001$).

Figure 7

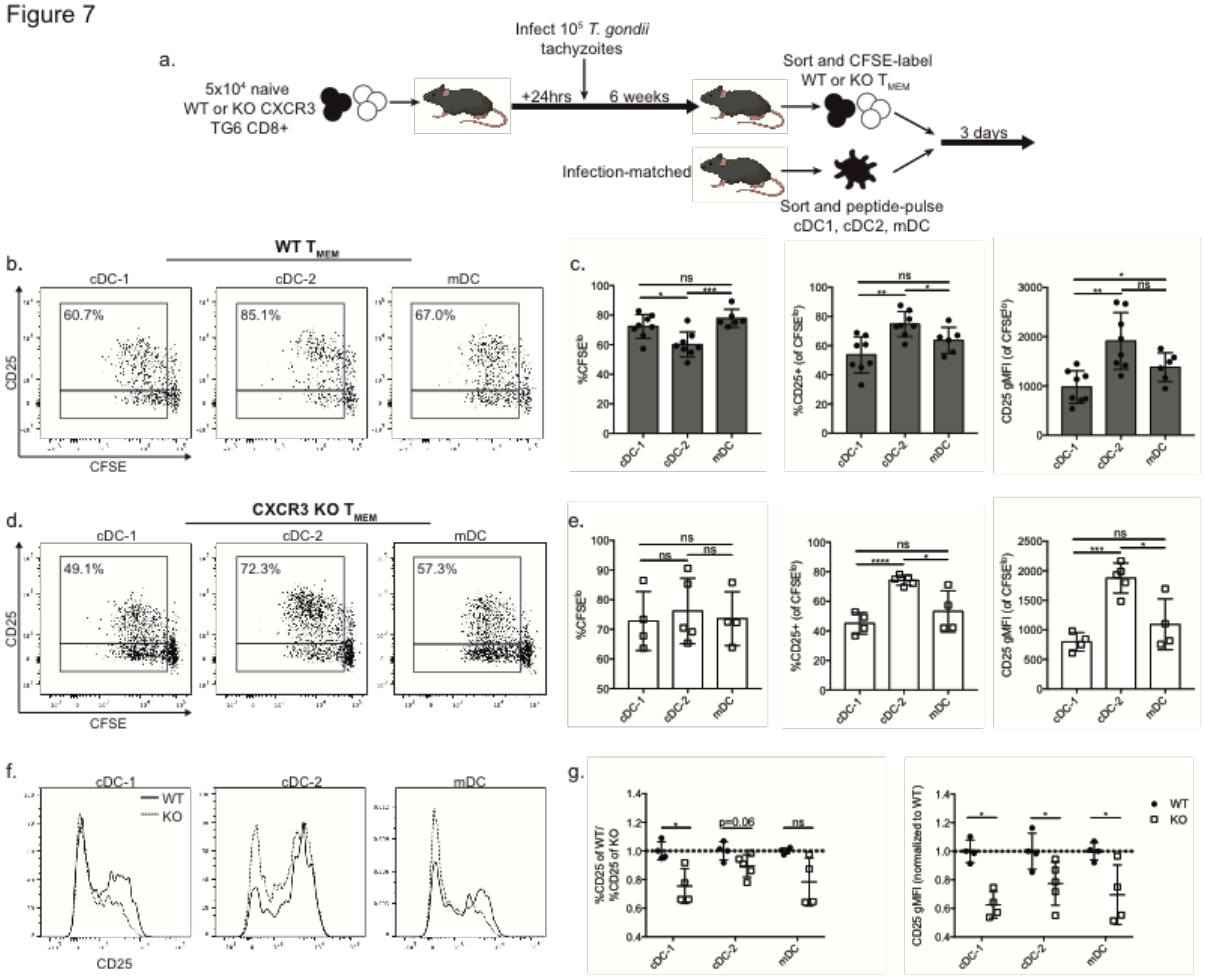
a.
Infect 10^5 T. gondii tachyzoites
5x10^4 naive WT or KO CXCR3 TG6 CD8+
+24hrs
6 weeks
Sort and CFSE-label WT or KO T_MEM
3 days
Infection-matched
Sort and peptide-pulse cDC1, cDC2, mDC
b.
WT T_MEM
cDC-1
cDC-2
mDC
60.7%
85.1%
67.0%
CD25
CFSE
c.
%CFSE^lo
%CD25+ (of CFSE^lo)
CD25 gMFI (of CFSE^lo)
d.
CXCR3 KO T_MEM
49.1%
72.3%
57.3%
e.
f.
WT
KO
g.
%CD25 of WT/ %CD25 of KO
p=0.06
CD25 gMFI (normalized to WT)

Figure 7: DC populations have distinct capacities to stimulate T_{MEM} cells *in vitro*. A) Co-culture experiment layout. WT mice received WT or CXCR3 KO naïve TG6 CD8+ T cells and were infected with *T. gondii*. WT and CXCR3 KO T_{MEM} cells were sorted at six weeks post-infection. In parallel, dendritic cells were sorted from the spleens of infection-matched mice, pulsed with GRA6 peptide, and cultured together with WT or KO T_{MEM} cells for 3 days. B) Representative flow plots showing CD25 expression and CFSE dilution of WT T_{MEM} cells after 3 days of culture with the indicated dendritic cells. Percents displayed represent the portion of $CFSE^{lo}$ cells expression CD25. C) Summary data from (B) showing the proportion of $CFSE^{lo}$ cells, %CD25+, and CD25 gMFI on WT cells. D,E) Representative flow cytometry plots and summary data from CXCR3 KO T_{MEM} cells after 3 days of culture with the indicated dendritic cells. F) Representative histograms of CD25 expression on WT and CXCR3 KO T_{MEM} cells cultured with the indicated dendritic cells. G) Summary data of CD25 expression. Data were normalized to the WT T_{MEM} cells within each experiment. Data in (C) are combined from three independent experiments. Data in (E) and (G) are combined from two independent experiments. Statistical significance in (A) was determined using a paired t-test, while significance in (B-H) was determined using an unpaired t-test (*p<0.05, **p<0.01, ***p<0.001, ****p<0.0001).

Supplemental Figure 1

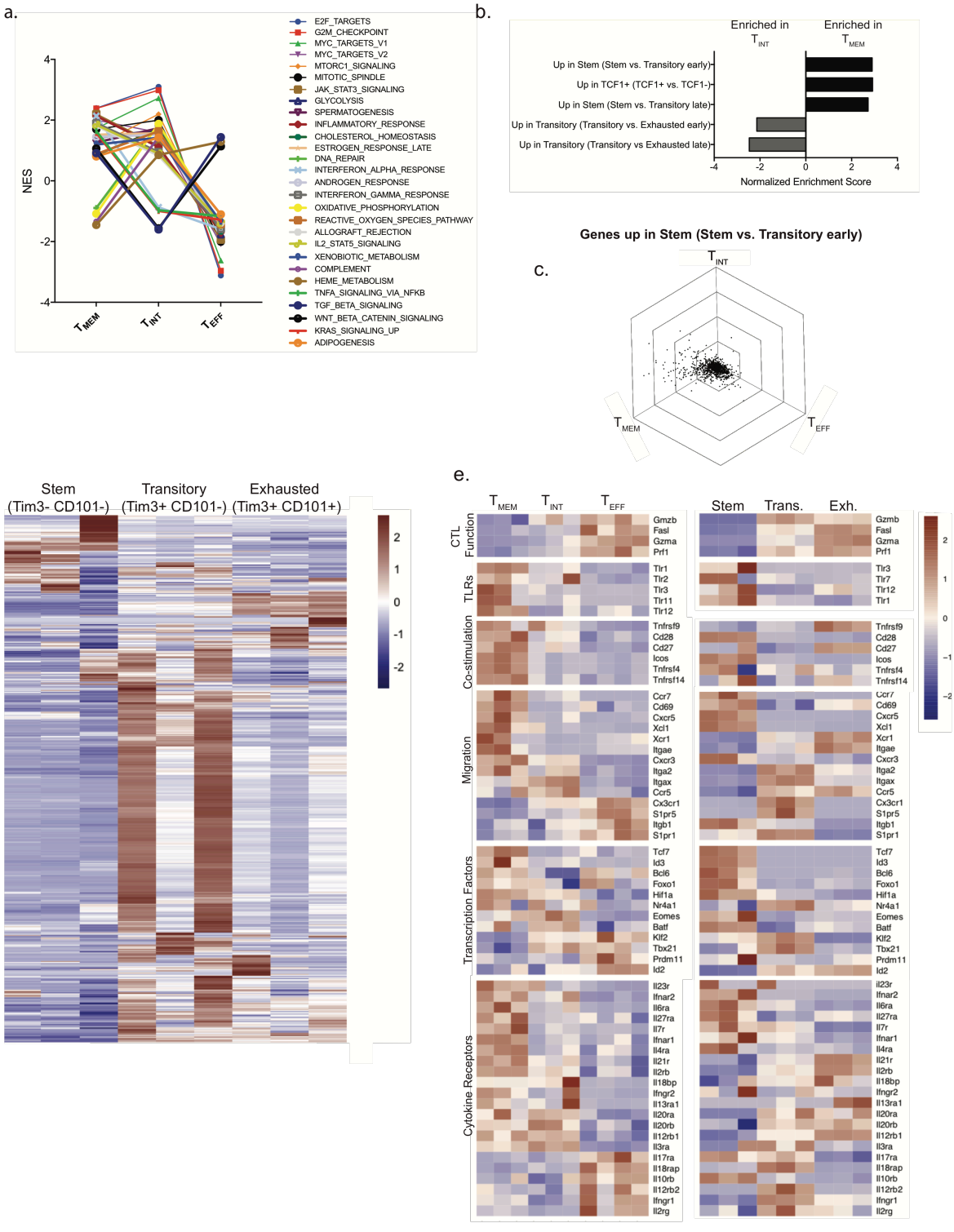

Supplemental Figure 1: RNAseq analyses of GRA6-specific subsets and CD8+ T cell populations from chronic LCMV infection A) Results of GSEA with Hallmark gene sets using one versus all comparisons (T_{MEM} vs. T_{INT} and T_{EFF}, T_{INT} vs. T_{MEM} and T_{EFF}, T_{MEM} vs. T_{EFF} and T_{INT}). Normalized enrichment scores for each T cell population are displayed for the 28 Hallmark gene sets that exhibited significant enrichment in at least one population (padj < 0.05). Data for selected categories of gene sets are shown in Figure 1D. B) GSEA was performed on the T_{MEM} vs. T_{INT} comparison using signatures generated from published RNA-seq datasets (Utzschneider *et al.*, 2016; Hudson *et al.*, 2019). A positive enrichment score indicates an enrichment of that signature in the T_{MEM} population, a negative score indicates an enrichment in the T_{INT} population. C) Triwise plot visualizing the enrichment for genes between T_{MEM}, T_{INT}, and T_{EFF}. The genes displayed belong to the Stem signature (Hudson *et al.*, 2019). D, E) Heatmaps displaying expression values from published RNAseq data from Stem, Transitory, and Exhausted cells (Hudson *et al.*, 2019). D) shows expression of genes specifically upregulated by T_{INT} cells. (cluster 7 from Figure 1c). E) shows the expression of selected genes for T_{MEM}, T_{INT}, T_{EFF} (current study) compared to Stem, Transitory, and Exhausted cells.

Supplemental Figure 2

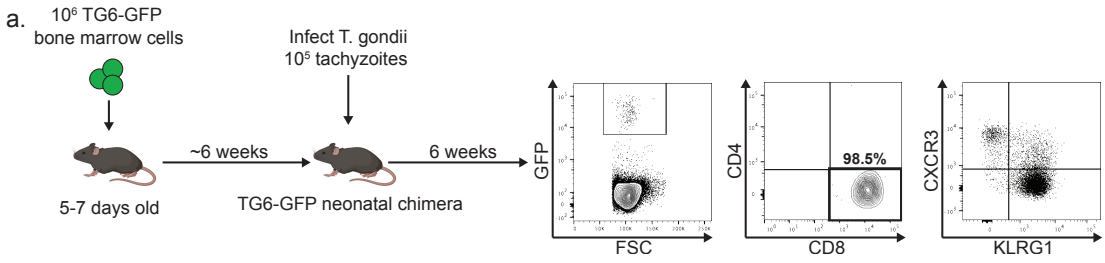

Supplemental Figure 2: Generation and validation of TG6-GFP neonatal bone marrow chimeras. A) Generation and validation of TG6-GFP chimeric mice. TG6-GFP bone marrow was injected into neonatal WT B6xB6.c F1 mice. Adult chimeric mice were infected with *T. gondii*. GFP+ cells expanded during infection and were made up of >90% CD8+ T cells. CD8+ GFP+ cells developed normal T_{MEM}, T_{INT}, and T_{EFF} populations after CXCR3 and KLRG1 staining.

Supplemental Figure 3

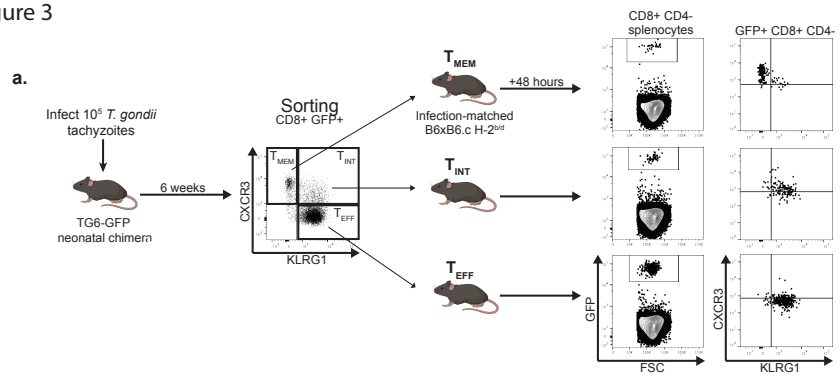

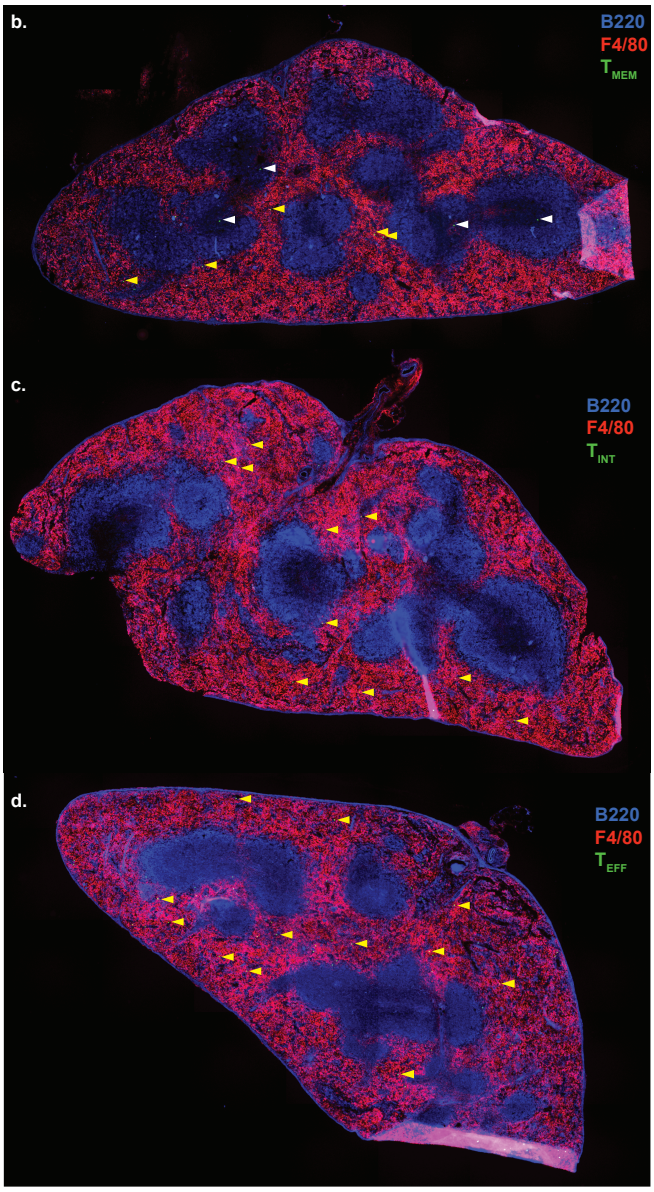

Supplemental Figure 3: TG6-GFP Adoptive transfer results
(Referenced in Fig. 2) A) TG6-GFP neonatal chimeric mice were infected with *T. gondii* for six weeks, then GFP+ T_{MEM}, T_{INT}, and T_{EFF} cells were sorted and adoptively transferred into separate infection-matched WT recipients for two days. Recipient spleens were analyzed by flow cytometry and confocal microscopy to determine the identity and location of GFP+ cells after adoptive transfer. B-D) Representative images from mice receiving T_{MEM} cells (B), T_{INT} cells (C), or T_{EFF} cells (D) are shown. B220 staining (blue) was used to highlight B cell follicles and F4/80 staining (red) was used to highlight the red pulp. Arrows highlight representative samples of scored cells, with white arrows indicating a white pulp-localized cell and yellow arrows indicating a red pulp-localized cell.

Supplemental Figure 4

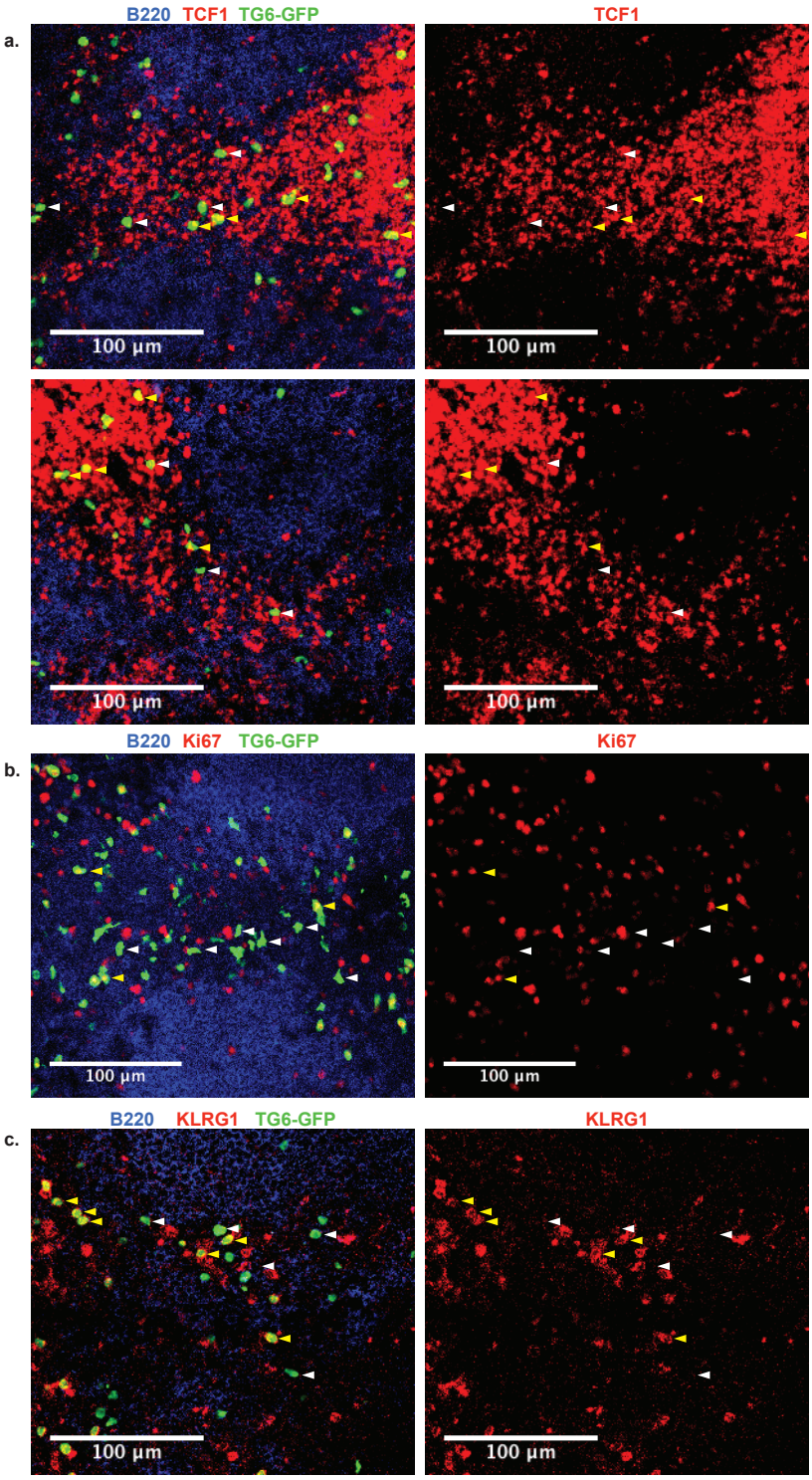

Supplemental Figure 4: Phenotypic analysis of cells within bridging channels. Spleens of TG6-GFP chimeric mice were imaged, and cells migrating along bridging channels were identified. TCF1 (A), Ki67 (B), and KLRG1 (C) expression was measured.

Supplemental Figure 5

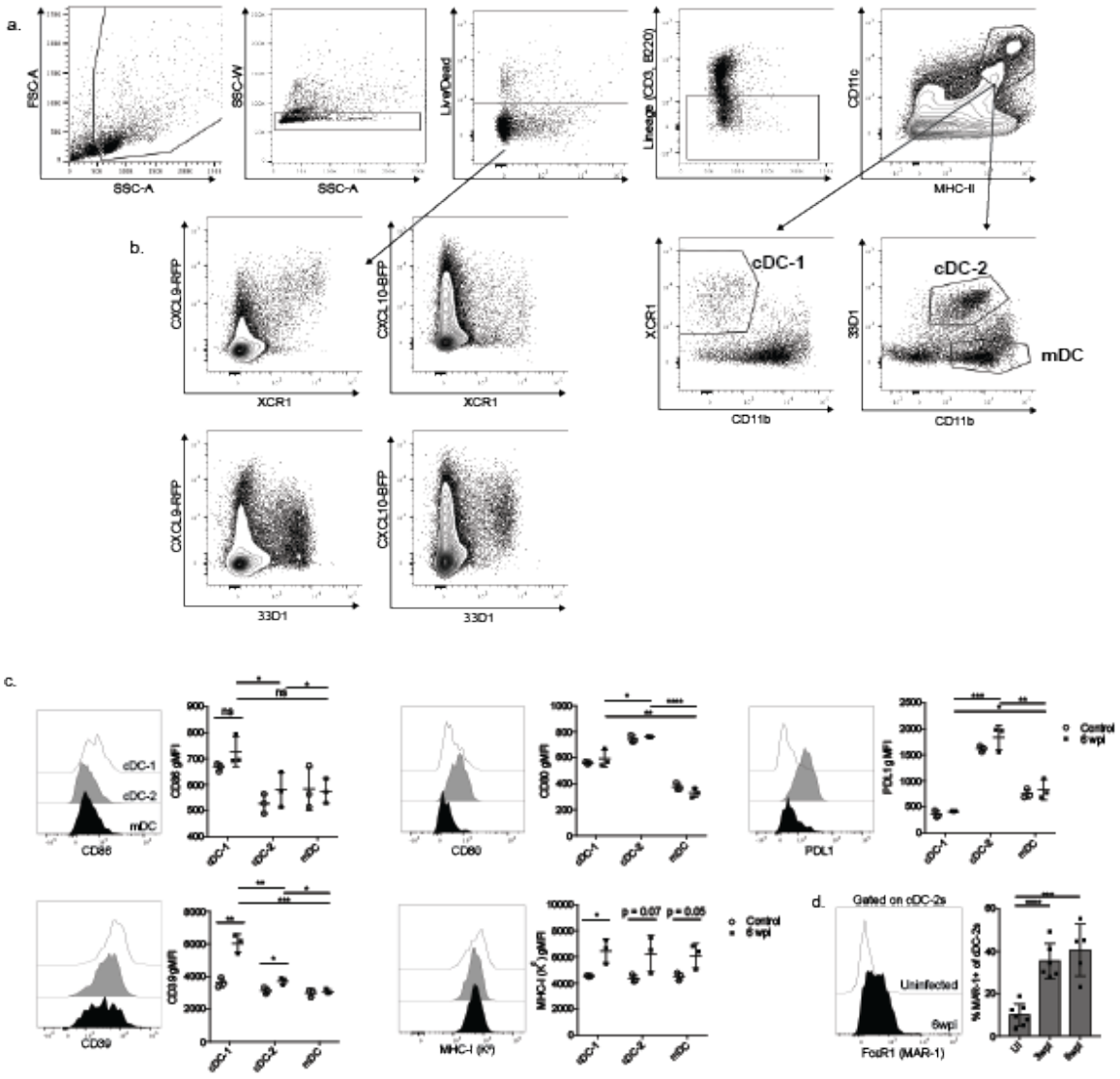

Supplemental Figure 5: Identification of dendritic cell subsets. A) Gating strategy used to identify cDC-1s (Lin- CD11c+ MHC-II+ XCR1+ CD11b-), cDC-2s (Lin- CD11c+ MHC-II+ 33D1+ CD11b+), and mDCs (Lin- CD11c+ MHC-II+ 33D1- CD11b+). B) Validation that XCR1 and 33D1 are effective markers of chemokine-producing cells. C) Flow cytometry data evaluating the expression of the indicated activating or inhibitory molecules on cDC-1s, cDC-2s, and mDCs before infection and during chronic infection. Representative histograms are taken from mice six weeks post-infection. D) Representative histograms and summary data of FcεR1 (MAR-1) staining on gated cDC-2s.

Supplemental Figure 6

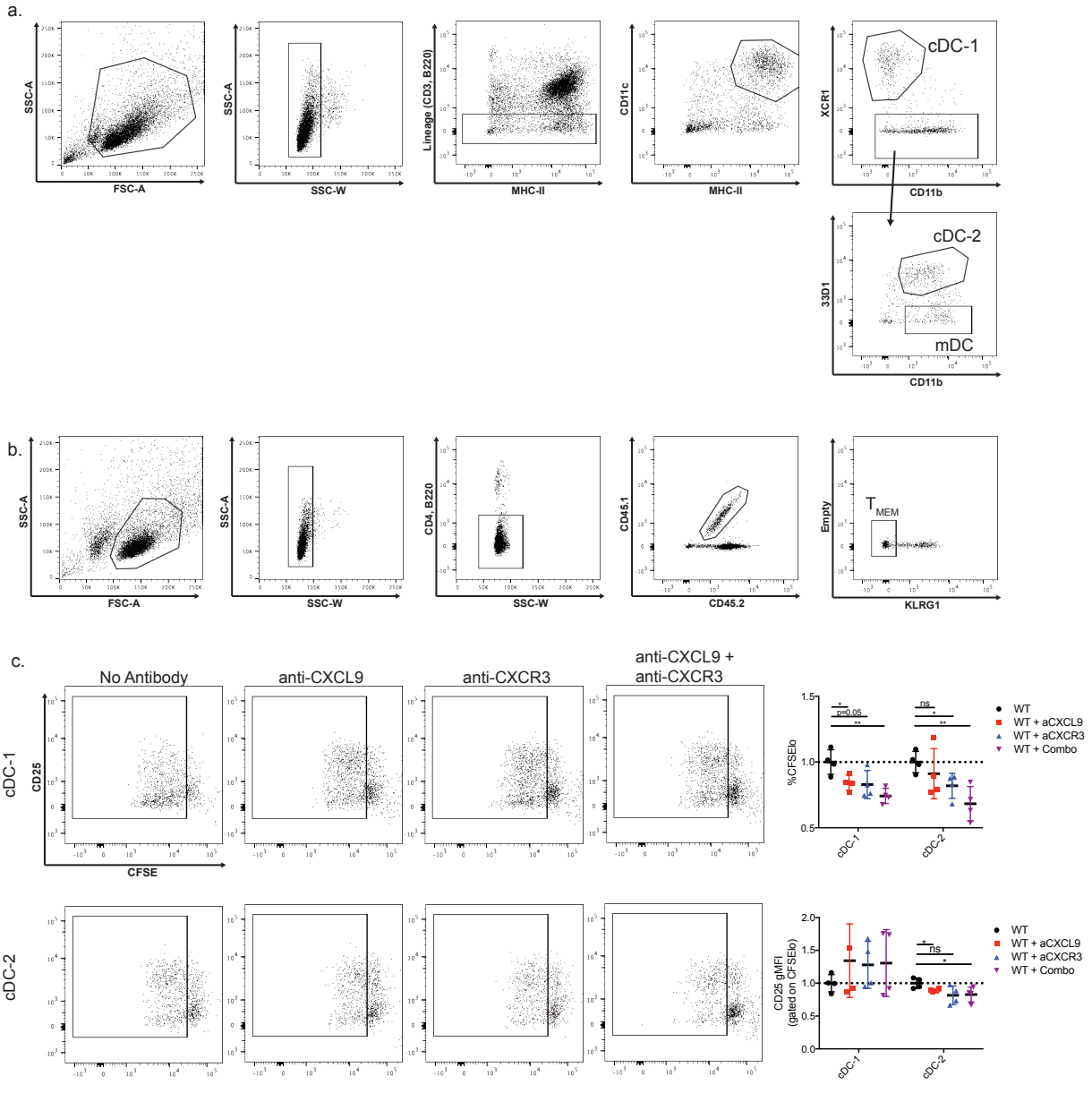

Supplemental Figure 6: Gating strategy and additional results from co-cultures of T_{MEM} cells and dendritic cell subsets. A) Gating strategy used to sort cDC-1, cDC-2, and mDC populations for co-culture. Example data shows splenocytes after density column enrichment for dendritic cells. B) Gating strategy used for sorting T_{MEM} cells (CD4- B220- CD45.1+/- CD45.2+/- KLRG1-). Example data shows splenocytes after CD8+ T cell negative isolation by magnetic column. C) WT T_{MEM} cells were cultured with either cDC-1s or cDC-2s for 3 days in the presence of the indicated antibodies. T_{MEM} proliferation and activation was measured by CFSE dilution and CD25 expression. Data are combined from two separate experiments and normalized to the No Antibody condition within each experiment.

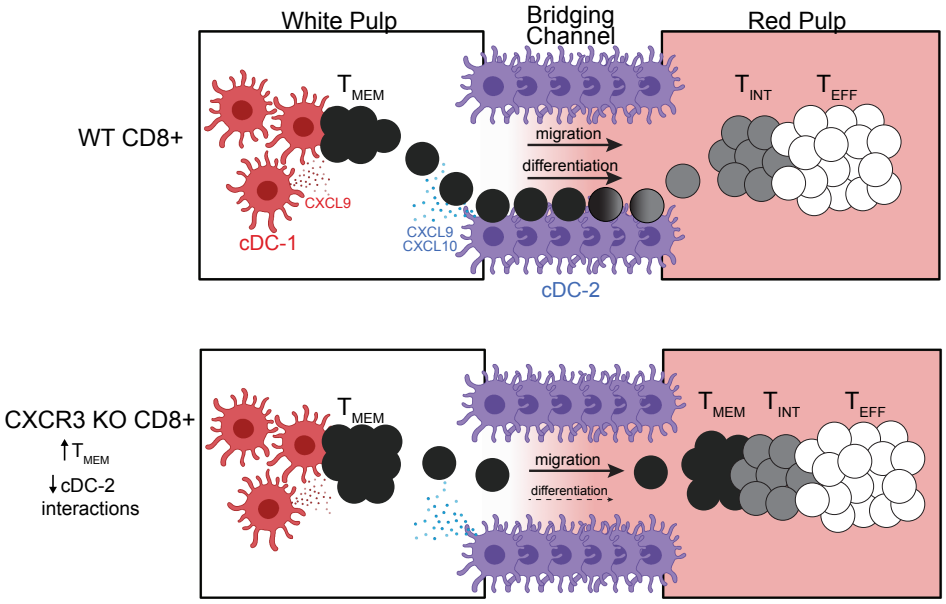

Supplemental Figure 7: Working model depicting the splenic environment during chronic *T. gondii* infection.

Chapter 3 - IFNγ neutralization promotes proliferative intermediate CD8+ T cells through the emergence of CXCL9/10+ antigen sources

Abstract

Mice chronically infected with the protozoan parasite *T. gondii* are able to effectively establish long-term control of the pathogen without achieving sterilizing immunity. While the parasite is primarily restricted to the brain during the chronic phase of infection, CD8+ T cells in the spleen experience continuous antigenic stimulation, resulting in ongoing proliferation and effector differentiation. Here, we investigated the role of IFNγ in regulating CD8+ T cell fate during chronic *T. gondii* infection. Neutralization of IFNγ during chronic infection led to dramatic changes in CD8+ T cell fate, promoting robust proliferation at the expense of terminal effector differentiation. These changes in CD8+ T cell fate were linked to increases in antigen presentation in the spleen which occurred in the absence of widespread parasite reactivation. The chemokine receptor CXCR3 was required for CD8+ T cells to respond to these increased antigenic signals. Finally, IFNγ neutralization resulted in the emergence of clusters of CD11c+ cells in the red pulp of the spleen that were robust producers of CXCR3 ligands and supported a proliferation rich-environment. These results highlight an ongoing role for IFNγ in mediating the clearance of *T. gondii* antigens during chronic infection and contribute to our understanding of the factors regulating CD8+ T cell fate.

3.1: Introduction

During infection, naive pathogen-specific CD8+ T cells rapidly expand and give rise to functionally heterogeneous populations of effector and memory T cells (Williams and Bevan, 2007). The fate determination of CD8+ T cells towards effector or memory differentiation is regulated by a combination of cell-intrinsic processes as well as environment signals, including the strength and frequency of T cell receptor signaling (signal 1), costimulatory signals (signal 2), and cytokines (signal 3). Many cytokines, inducing IL-12, type-I interferons, and IFNγ, can directly signal CD8+ T cells to influence their differentiation and proliferation (Curtsinger *et al.*, 1999, 2005; Badovinac, 2000; Tewari, Nakayama and Suresh, 2007). However, cytokines can also impact T cell fate by indirect mechanisms, including driving phenotypic changes in antigen presenting cells (APCs), promoting the expression of pro-inflammatory chemokines, or by mediating pathogen control (Schroder *et al.*, 2004).

Much of our understanding of CD8+ T cell differentiation comes from studies utilizing models of acute infection or vaccination. As a result, less is understood about the factors regulating CD8+ T cell fate during chronic infections. *Toxoplasma gondii* is a protozoan parasite that naturally establishes chronic infection in mice and humans. In mice, *T. gondii* infection results in an acute phase of infection characterized by widespread parasitemia. While adaptive immunity is able to establish control of the parasite in the majority of

tissues, *T. gondii* is able to form long-lived brain cysts that provide a reservoir of parasite replication during the chronic phase of infection. While C57BL/6J mice (H-2^b) eventually succumb to a progressing chronic infection (Bhadra *et al.*, 2011), mice harboring the MHC Class I molecule H-$2L^d$ control the chronic infection. As a result, H-2^d expressing mice exhibit little pathology and have a normal lifespan, in spite of the ongoing presence of brain cysts (Brown *et al.*, 1995; Chu *et al.*, 2016).

The ability of H-$2L^d$-expressing mice to control chronic *T. gondii* infection has been attributed to a highly protective CD8+ T cell response mounted against a peptide derived from the parasite protein GRA6 (Blanchard *et al.*, 2008). GRA6-specific CD8+ T cells retain high numbers in the spleen during chronic infection, and although the parasite is not detectable outside the brain, we have shown that GRA6-specific T cells experience continuous exposure to their antigen (Chu *et al.*, 2016). We have previously identified three functionally distinct populations in chronically infected mice that make up the GRA6-specific CD8+ T cell response (Chu *et al.*, 2016). CXCR3+ KLRG1- memory cells (T_{MEM}) are a relatively quiescent stem-like population. T_{MEM} cells give rise to highly proliferative CXCR3+ KLRG1+ intermediate (T_{INT}) cells that serve to amplify the response and feed into the population of terminally-differentiated CXCR3- KLRG1+ effector (T_{EFF}) cells that confer protection through the rapid cytokine production and efficient killing of target cells. A balance between self-renewal, proliferation, and effector differentiation in this system allows for the maintenance of all three T cell populations throughout chronic infection, and provides for continuous production of a large pool of armed T_{EFF} cells without depleting the stem-like T_{MEM} cells. While the function and lineage relationship between T_{MEM}, T_{INT}, and T_{EFF} cells has been determined, our understanding of the factors regulating the differentiation of these T cell subsets remains limited.

IFNγ is a critical cytokine that regulates an immense array of immunological processes, including both MHC-I and MHC-II antigen presentation (Chang, Cheong-Hee, Flavell, 1995; Lee *et al.*, 2013), production of the inflammatory chemokines CXCL9 and CXCL10 (Gil *et al.*, 2001), regulation of apoptosis (Xu *et al.*, 1998), and production of anti-microbial products such as nitric oxide (MacMicking, 2012). In addition, many studies have described a highly protective role for IFNγ during *T. gondii* infection (Suzuki *et al.*, 1988; Suzuki and Remington, 1990; Norose *et al.*, 2001). In particular, IFNγ can directly promote clearance of *T. gondii* through the induction of IFNγ-dependent GTPases that result in disruption of the parasitic vacuole (Martens *et al.*, 2005; Degrandi *et al.*, 2013). Through these many mechanisms, IFNγ has a highly important role in regulating the function and differentiation of CD8+ T cells during infection. Despite its well-described role in many immunological settings, how IFNγ regulates CD8+ T cell fate during chronic infection has not been addressed. Here, we investigate the impact of IFNγ on GRA6-specific CD8+ T cells in the spleen during chronic *T. gondii* infection. We observed that antibody neutralization of IFNγ caused a dramatic shift in T cell fate, resulting in a robust expansion of the T_{INT} population and a reduction in the T_{EFF} population. The ability of IFNγ to regulate CD8+ T cell differentiation was not due to direct IFNγR

signaling on the T cells, but was instead due to changes to the splenic environment. Mice treated with anti-IFNγ had increased antigen presentation in the spleen, and this antigen presentation appeared to come primarily from clusters of chemokine-producing dendritic cells in the red pulp of the spleen. These data indicate that IFNγ plays an ongoing role during chronic *T. gondii* infection in suppressing the parasite in the periphery and contribute to our understanding of the factors that impact the fate of CD8+ T cells during chronic infections.

3.2: Results

IFNγ neutralization results in a dramatic increase to the T_{INT} population and loss of T_{EFF} cells.

IFNγ has a critical role in mediating control of *T. gondii* infection and can impact the fate of CD8+ T cells early in infection (Shah *et al.*, 2015). To investigate how IFNγ impacts T_{MEM}, T_{INT}, and T_{EFF} CD8+ T cell populations during chronic *T. gondii* infection, we utilized antibody neutralization. Mice were infected with *T. gondii* and infection was allowed to progress to the late chronic stage (six weeks post-infection). Mice were then treated with an anti-IFNγ antibody or isotype control, and the differentiation of GRA6-specific CD8+ T cells in the spleen was determined using CXCR3 and KLRG1 staining **(Fig 1a)**. Compared to the isotype control, treatment with anti-IFNγ resulted in a dramatic increase in the proportion of CXCR3+ KLRG1+ T_{INT} cells and a simultaneous decrease in the proportion of terminally differentiated CXCR3- KLRG1+ T_{EFF} cells **(Fig 1b,c)**. These changes were evident by six days of neutralization and reached their maximum change by nine days of neutralization. The absolute numbers of T_{INT} cells also increased by six and nine days of neutralization, while the T_{EFF} population was reduced by six days but slightly recovered in numbers by nine days **(Fig 1d)**. Consistent with the increase in proliferative T_{INT} cells, we observed a dramatic increase in the proportion of GRA6 tetramer-positive cells that were dividing, as measured by Ki67 expression **(Fig 1e,f)**. Similar to the effects on T_{INT} cells, the increase in Ki67 expression was significantly different after 6 days of treatment and continued to increase after 9 days. While T_{INT} cells remained the most proliferative population, we observed increased Ki67 expression in all three subsets after IFNγ neutralization **(Fig 1g)**. Finally, we also examined the expression of Eomes, a transcription factor that is specifically upregulated at the T_{INT} stage (Chu *et al.*, 2016). Eomes expression among GRA6-specific cells increased after six and nine days of IFNγ neutralization, confirming the inflation of T_{INT} cells. We also examined the phenotype of GRA6-specific CD8+ T cells in the lymph node, where GRA6 antigen is also continuously presented during chronic infection but at a substantially lower level compared to the spleen (Chu *et al.*, 2016; Tsitsiklis *et al.*, 2020). GRA6-specific CD8+ T cells in the lymph node also experienced a slight increase in T_{INT} cells and proliferation, although the effects were less dramatic compared to the spleen **(Supp. Fig 1).** Together, these data show that neutralization of IFNγ during

chronic *T. gondii* infection results in a dramatic increase in the proliferative T_{INT} population in the spleen while causing a reduction in the T_{EFF} population.

We reasoned that loss of the T_{EFF} population may be due to a block in the differentiation of T_{INT} cells to T_{EFF}. Alternatively, IFNγ neutralization could impact the ability of GRA6-specific cells to migrate into tissues. To investigate this possibility, we examined the numbers of GRA6-specific CD8+ T cells found in the brain and liver after IFNγ neutralization. We observed no evidence of differences in cell numbers in either tissue, suggesting the ability of the cells to migrate into or reside within tissues was not impacted by IFNγ neutralization **(Supp. Fig 2).** One additional explanation for the loss of T_{EFF} cells is that they experience reduced survival after IFNγ neutralization. To determine how treatment impacted the survival of GRA6-specific cells, we utilized Annexin V staining to detect apoptotic cells (Van Engeland *et al.*, 1998). IFNγ neutralization did not have an impact on the Annexin V expression of either the total population of GRA6-specific cells or the T_{EFF} subset **(Supp. Fig 2)**. These data indicate that IFNγ neutralization does not result in increased apoptosis among the T_{EFF} population. Thus, the loss of T_{EFF} cells and increase to T_{INT} cells observed after IFNγ neutralization is likely due to a block in the differentiation of T_{INT} cells.

Direct IFNγ signaling on CD8+ T cells does not impact their fate during chronic infection

Direct cytokine signaling on CD8+ T cells can impact their differentiation and expansion during infection. Some reports have described a clear role for intrinsic IFNγ signaling in regulating CD8+ T cell fate (Whitmire, Tan and Whitton, 2005; Whitmire *et al.*, 2007), while others have observed no role for intrinsic signaling (Sercan *et al.*, 2006; Tewari, Nakayama and Suresh, 2007). To determine if direct IFNγ signaling impacts the fate of GRA6-specific T cells during chronic infection, we utilized a TCR transgenic mouse line specific for the GRA6 epitope, referred to as TG6. We adoptively transferred equal numbers of WT or IFNγR KO TG6 CD8+ T cells into a common recipient and examined the size and differentiation profile of both CD8+ populations throughout infection **(Fig 2a)**. WT and IFNγR KO TG6 CD8+ T cells in the spleen expanded similarly and retained similar total numbers of cells at both 3 and 6 weeks post-infection **(Fig 2b,c)**. In addition, the proportion of T_{MEM}, T_{INT}, and T_{EFF} cells showed no differences in the IFNγR KO population compared to WT at either 3 or 6 weeks in both the spleen and lymph nodes **(Fig 2d-g, Supp. Fig 3)**. To test if the effects of IFNγ-neutralization were dependent on direct T cell signaling, we treated the adoptive transfer recipients with anti-IFNγ for six days. Critically, the IFNγR KO TG6 cells responded to IFNγ neutralization in a similar manner as the WT cells. Both the WT and KO populations developed increased T_{INT} populations and had increased Ki67 expression following anti-IFNγ treatment **(Fig 2g,h).** These data indicate that cell-intrinsic IFNγ signaling does not impact CD8+ T cell expansion or differentiation during chronic *T. gondii* infection and suggests that IFNγ neutralization impacts CD8+ T cell fate by altering the splenic environment.

IFNγ neutralization results in increased antigen presentation in the spleen but does not cause the reactivation of infection

To better understand how IFNγ was impacting CD8+ T cell differentiation, we performed bulk RNA sequencing (RNA-seq). We sorted T_{MEM}, T_{INT}, and T_{EFF} cells from a population of adoptively transferred TG6 CD8+ T cells six weeks post-infection. The sorted cells were then processed for RNA-seq and the transcriptional profiles of each population was assessed. In addition, some mice were treated with anti-IFNγ, and the transcriptional profile of the cells after anti-IFNγ treatment was compared to the untreated populations. To understand the early effects of anti-IFNγ treatment that precede the changes in differentiation observed after 6 days **(Fig 1)**, we assessed the transcriptional changes after 4 days of treatment **(Fig 3a)**. T_{INT} cells showed the largest transcriptional changes after anti-IFNγ treatment, with T_{MEM} cells showing modest changes and T_{EFF} cells showing very little change **(Fig 3b,c)**, fitting with the pattern of susceptibility observed by flow cytometry **(Fig 1)**. T_{INT} cells from mice treated with anti-IFNγ showed increased expression of *Jun*, *Junb,* and *Fos*, components of the AP-1 transcription factor downstream of T cell receptor signaling **(Fig 3b,c)**. In addition, anti-IFNγ treatment resulted in increased T_{INT} expression of *Gbp2* and the eukaryotic translation initiation factor *Eif1a*. Interestingly, both *Gbp2* and a eukaryotic translation elongation factor *Eef1e1* are highly induced in CD4+ T cells after stimulation by DCs (Kotov *et al.*, 2019), suggesting T_{INT} cells were experiencing increased stimulation by DCs in the spleen. T_{INT} cells from anti-IFNγ treated mice also had increased expression of *Ly6a*, *Furin*, and *Nop58*, which have been associated with T cell activation and TCR stimulation (Tan *et al.*, 2017; DeLong *et al.*, 2018). Together, these results suggest that T_{INT} cells experience increased antigenic stimulation and activation after IFNγ neutralization. Many of the genes upregulated by T_{INT} after anti-IFNγ treatment were also upregulated by T_{MEM} cells but not T_{EFF} cells, including *Jun, Junb, Fos, Gbp2,* and *Furin* **(Fig 3c)**, suggesting T_{MEM} cells were also experiencing increased antigenic stimulation. Pathway analysis of the genes upregulated by T_{MEM} or T_{INT} cells after anti-IFNγ treatment showed an enrichment for several cytokine signaling pathways related to T cell activation, including TNF-alpha signaling via NF-kB and IL-2 signaling **(Fig 3d)**. Together, these data indicate that IFNγ neutralization primarily impacts T_{INT} and T_{MEM} cells, and promotes their activation through increased TCR stimulation.

While *T. gondii* is only directly detectable in the brain during chronic infection, we have previously observed that GRA6 antigen is robustly presented in the spleen throughout infection. To directly test if IFNγ neutralization impacted the presentation of GRA6 antigen in the spleen, we utilized an *in vivo* antigen presentation assay. Naive TG6 CD8+ T cells were adoptively transferred into the spleens of chronically infected mice, and the activation of the transferred cells was measured by expression of CD44 and dilution of the proliferation dye CFSE **(Fig 4a)**. Naive TG6 cells transferred into chronically infected mice upregulated CD44 and divided, demonstrating they were detecting GRA6 antigen *in vivo* and fitting with previous experiments **(Fig 4b)**. Interestingly, cells transferred into

mice treated with anti-IFNγ neutralizing antibodies had a significantly larger population of $CD44^{hi}$ $CFSE^{lo}$ cells compared to untreated mice, suggesting they were experiencing greater antigenic stimulation **(Fig 4b,c)**. In line with the cells receiving antigenic stimulation, TG6 cells transferred into chronically infected recipients had significantly elevated Nur77 expression, a measure downstream of TCR engagement **(Fig 4d,e)** (Moran *et al.*, 2011). Furthermore, TG6 cells transferred to recipients treated with anti-IFNγ had slightly higher Nur77 expression compared to untreated controls. Together these data indicate that IFNγ neutralization results in increased presentation of GRA6 antigen in the spleen.

IFNγ is critical for mediating control of *T. gondii* (Suzuki *et al.*, 1988; Suzuki and Remingtoni, 2020), and antibody neutralization of IFNγ can result in reactivation of the parasite in the brains of infected mice (Cabral *et al.*, 2016). To determine if IFNγ neutralization impacted control of the parasite, we measured the parasite burden directly in the brains of chronically infected mice treated with IFNγ neutralizing antibody or with isotype control. IFNγ neutralization did not result in an increase in parasite burden in the brain through day nine of treatment **(Fig 4f)**. Importantly, we did observe reactivation with the parasite after longer treatment with the neutralizing antibody (day 16 and 21). This suggests the impacts of IFNγ neutralization on CD8+ T cell fate that occur within the first nine days of treatment are due to increased GRA6 antigen presentation but are not due to the widespread reactivation of parasitic infection.

IFNγ neutralization alters the profile of CXCL9 and CXCL10 production in the spleen

IFNγ is known to promote the expression of the chemokines CXCL9 and CXCL10, which serve as the ligands for CXCR3. CXCR3 ligands can guide CD8+ T cells towards antigen presenting cells in the spleen during infection. Given the observation that IFNγ neutralization increased antigen presentation within the spleen, and given that CXCR3-expressing T_{MEM} and T_{INT} cells were most impacted, we considered that CXCR3 ligands may play an important role in mediating the effects of IFNγ neutralization. To investigate whether CXCR3 played a role, we examined the ability of CXCR3 KO TG6 CD8+ T cells to respond to the antibody treatment. In contrast to the response of WT and IFNγR KO TG6+ CD8+ T cells **(Fig 2)**, we observed no significant increase in proliferation among CXCR3 KO TG6 CD8+ T cells after six days of IFNγ neutralization **(Fig 5a)**. Importantly, the WT endogenous polyclonal CD8+ T cells in the same mice had increased Ki67 expression after anti-IFNγ treatment, indicating the treatment was effectively altering the splenic environment **(Fig 5b)**. Together, these data indicate that CXCR3 is critical for mediating the effects of IFNγ neutralization.

To further understand how CXCR3 ligands were impacted after IFNγ neutralization, we utilized REX3 mice, a dual reporter strain containing a CXCL9-RFP and CXCL10-BFP transgene (Groom *et al.*, 2012). Interestingly, REX3 mice treated with anti-IFNγ for six days had elevated chemokine expression **(Fig 5c)**. The frequency of CXCL9/10 +/+ and CXCL10+ cells was significantly increased

in the mice treated with anti-IFNγ, while the frequency of CXCL9+ cells was unchanged **(Fig 5d)**. CXCL9 and CXCL10 are induced by an array of inflammatory signals, suggesting that anti-IFNγ treatment promotes a pro-inflammatory environment in the spleen.

We had previously observed that CXCL9+ and CXCL9/10 +/+ splenocytes are primarily CD11c+ dendritic cells, while CXCL10+ splenocytes are primarily CD4+ T cells. To determine if anti-IFNγ treatment changed the identity of these populations, we stained splenocytes from REX3 mice with a variety of antibodies to delineate various myeloid and lymphoid cell types. The identity of CXCL9+ and CXCL9/10 +/+ splenocytes did not change after IFNγ neutralization and remained primarily CD11c+ cells **(Fig 5e)**. In contrast, the CXCL10+ population became more enriched for CD4+ T cells after IFNγ neutralization. We examined the expression of CXCL9/10 in these different populations and observed that both CD11c+ splenocytes and CD3+ CD4+ splenocytes had elevated CXCL10 production after anti-IFNγ treatment **(Fig 5f,g)**. In addition, the total proportion of CD11c+ and CD3+ CD4+ splenocytes increased **(Fig 5h)**. Together these results indicate that anti-IFNγ treatment results in increased chemokine production in the spleen due to an expansion of CXCL10-producing CD11c+ dendritic cells and CD4+ T cells.

IFNγ neutralization results in clusters of CXCL9+ CXCL10+ cells in the splenic red pulp

Given that anti-IFNγ treatment resulted in increased expression of CXCL9/10 in the spleen, we sought to understand where this increase in chemokine expression was localized. Using the REX3 mice, we examined the localization of CXCL9-RFP and CXCL10-BFP in the spleens of chronically infected with and without anti-IFNγ treatment. We observed the majority of CXCL9 and CXCL10 signal localized to the marginal zone and red pulp of the spleen **(Fig 6a)**, fitting with previous data. In agreement with the flow cytometry data, we observed that anti-IFNγ treatment resulted in slightly elevated CXCL9 production and substantially elevated CXCL10 production **(Fig 6a,b)**. Interestingly, this increased expression appeared to come from clusters of CXCL9/10-expressing cells that were mostly absent in the untreated mice. These CXCL9/10++ clusters were localized in the red pulp of the spleen, where we had also previously observed T_{INT} and T_{EFF} cells residing during chronic infection. Thus, T_{INT} cells may encounter CXCL9/10++ clusters in the red pulp and are poised to respond in a CXCR3-dependent manner.

To gain more information about the identity of the CXCL9/10 +/+ cells, we stained for CD11c and CD4, based on the flow cytometry data indicating these were two major producers of chemokines **(Fig 5e)**. The clusters of CXCL9/10++ cells that emerged after IFNγ neutralization were primarily CD11c+, suggesting they are likely the same populations of dendritic cells observed by flow cytometry **(Fig 6c)**. Despite their increased prevalence by flow cytometry, CXCL10+ CD4+ cells were rare in the images, perhaps due to lower fluorescence intensity observed by flow cytometry. However, the groups of CD11c+ CXCL9/10++ cells were surrounded by densely grouped CD4+ cells, suggesting that CXCL10+

CD4+ cells may be contributing to these inflammatory clusters as well. Finally, to determine if CXCL9/10 clusters were supporting a proliferative environment, we examined the expression of Ki67. CXCL9/10++ clusters were marked by local increases in Ki67+ cells compared to other regions of the red pulp where these clusters were absent **(Fig 5d,e)**. Together, these data suggest CXCL9/10++ clusters of dendritic cells and CD4+ T cells emerge after anti-IFNγ treatment and support a proliferative T_{INT} CD8+ T cell fate.

3.3: Discussion

IFNγ is a highly pleiotropic cytokine that plays a central role in regulating many aspects of the immune system. Here, we examined the role of IFNγ during mouse chronic infection with *Toxoplasma gondii* and the impact of IFNγ on CD8+ T cell fate. We observed that neutralization of IFNγ results in dramatic changes to T cell differentiation, promoting the expansion of highly proliferative T_{INT} cells at the expense of the terminally-differentiated T_{EFF} subset. We determined that these changes to T cell fate were due to increased antigenic stimulation in the spleen, and that this increase in antigen presentation was not due to a widespread reactivation of parasite infection. CXCR3 signaling was necessary for CD8+ T cells to respond to this increase in antigen, likely due to the fact that CXCL9/10-producing dendritic cells are the major antigen presenting cell types. Finally, we observed localized clusters of CD11c+ CXCL9+ CXCL10+ cells in the spleen that emerged after IFNγ neutralization and promoted local Ki67-rich environments.

Our results demonstrate that cell-intrinsic IFNγ signaling on CD8+ T cells plays no role in regulating their differentiation, expansion, or survival during *T. gondii* infection. WT and IFNγR KO TG6 cells transferred into a common recipient mouse produced nearly identical proportions of total cells and had equal proportions of T_{MEM}, T_{INT}, and T_{EFF} cells. While IFNγ is known to impact CD8+ T cell fate through a variety of mechanisms, whether cell-intrinsic IFNγ signaling plays a role in CD8+ T cell fate remains controversial. Some studies have indicated that direct IFNγ can promote CD8+ T cell memory (Whitmire, Tan and Whitton, 2005; Whitmire *et al.*, 2007), impair CD8+ T cell memory (Stoycheva *et al.*, 2015), or have no effect on CD8+ T cell fate (Puliaev *et al.*, 2004; Tewari, Nakayama and Suresh, 2007; Sercan *et al.*, 2010). Differences between these studies may be attributed to differences in experimental models and infections, including the amount of IFNγ produced and the use of TCR transgenic mice. Given the prevalence of IFNγ in *T. gondii* production, it seems unlikely that low IFNγ production explains the lack of a role for direct IFNγ signaling. In light of this, determining which factors induce CD8+ T cell susceptibility to IFNγ signaling is a critical open question.

We have previously shown that H-2^d-expressing mice are able to establish effective control of *T. gondii* during the chronic phase of infection without producing sterilizing immunity. Thus, chronic *T. gondii* infection in this setting is a well-regulated balance between the host and pathogen, allowing the parasite to persist in the brain indefinitely while providing continuous stimulation to the

immune response. Our results indicate that IFNγ plays a critical role in this balance. The emergence of CXCL9/10-producing antigen presenting cells in the IFNγ-neutralized mice suggests that IFNγ is continuously promoting the clearance of either GRA6 antigen or the parasite itself. In the normal setting, this rapid turnover allows small amounts of stimulation leading to a small and persistent T_{INT} population. However, depleting IFNγ tips the scales in the parasite's favor, and in turn allows greater stimulation to CD8+ T cells. Understanding the exact source of parasite antigen and the role IFNγ plays in mediating its clearance will be critical for future studies.

The clusters of CD11c+ CXCL9+ CXCL10+ cells that emerge after IFNγ neutralization provide interesting insight into the mechanisms of *T. gondii* antigen presentation and clearance in the spleen. We have previously observed that conventional type 2 dendritic cells (cDC-2s) and monocyte-derived dendritic cells (mDCs) are both capable of robustly producing both CXCL9 and CXCL10 together, while conventional type 1 dendritic cells (cDC-1s) show little capacity to produce CXCL10 but express CXCL9 constitutively. The increased prevalence of CXCL9/10 +/+ and CXCL9/10 -/+ CD11c+ cells indicates that cDC-2s and mDCs are likely connected to the increased antigen presentation and T_{INT} fate. We have also previously observed that mDCs and especially cDC-2s are capable of promoting T_{INT} differentiation after stimulating T_{MEM} cells *in vitro*. The increased production of CXCL9 and CXCL10 in the spleen together with the corresponding surge of T_{INT} cells further support this role and highlight how CD8+ T cell fate is highly dependent on activation with distinct lineages of dendritic cells. We have previously determined that cDC-2s are localized specifically within the bridging channel and marginal zone of the spleen during chronic *T. gondii* infection, making it likely that mDCs are the primary population responsible for the red pulp-localized clusters that emerge after IFNγ neutralization. The CXCL9/10+ clusters observed herein have clear parallels to granulomas observed during *Salmonella enterica* infection, where CXCL9/10-producing granulomas allow T cell stimulation while also mediating IFNγ-dependent control of the pathogen (Goldberg 2018). The similarities between these two infection settings suggest this may be a common mechanism of pathogen control in the spleen that also allows continuous stimulation of the adaptive immune system.

Our results also highlight the critical role of CXCR3 in promoting the activation of CD8+ T cells and their interaction with ligand-producing dendritic cells. Our previous work described the critical role of CXCR3 in regulating GRA6-specific CD8+ T cell fate in the steady state of chronic infection through promoting interactions with cDC-2s and converting T_{MEM} cells into T_{INT} cells as they enter the red pulp. The results of IFNγ neutralization indicate that CXCR3 can also promote the activation and proliferation of T_{INT} cells after they have entered the red pulp through additional interactions with APCs in that compartment. CXCR3 was necessary for TG6 cells to respond to the increased antigen presentation observed after IFNγ neutralization, implying CXCR3 is necessary for the T_{INT} cells to migrate to antigen-presenting CXCL9/10+ clusters. Together these results support a two-step model of T_{INT} fate: 1) CXCR3 promotes the conversion of T_{MEM} into T_{INT} through interactions with cDC-2s in the

bridging channels and 2) CXCR3 promotes the proliferation and activation of T_{INT} cells in the red pulp through interactions with CXCL9/10+ clusters in the red pulp.

3.4: Materials and Methods

Mice and Infections

C57BL/6, B6c (B6.C-*H2d*/bByJ), IFNγR KO, and CXCR3 KO B6 mice were originally purchased from The Jackson Laboratory. TG6 transgenic mice were generated in our lab as previously described (Chu *et al.*, 2016). REX3 transgenic mice were received from the lab of Andrew Luster. All mice were bred in the UC Berkeley animal facility and were used with the approval of the Animal Care and Use Committee (ACUC) of the University of California. All experiments were performed on B6xB6c H-$2^{b/d}$ F1 mice. For all infections, mice received 10^5 tachyzoites of the type II Prugniuad-tomato-OVA strain i.p. as previously described (Chu *et al.*, 2016).

Spleen tissue cryosectioning

Spleens from infected mice were removed and cut in half laterally. Spleens were fixed in 4% paraformaldehyde at room temperature in the dark for six hours, washed twice with PBS, then dehydrated in 10% sucrose, 20% sucrose, and 30% sucrose for at least 6 hours each at 4°C. Spleens were imbedded in OCT (Fisher) cut side-down and frozen in a slurry of dry ice and ethanol, then stored at -80°C until sectioning. Spleens were cut into 12-micron sections on a cryostat microtome (Leica Biosystems) and stored at -80°C until used for immunofluorescence.

Immunofluorescence

Spleen sections were thawed at room temperature in the dark until dry. Sections were rehydrated with PBS for 10 minutes, fixed with 4% paraformaldehyde for 3 minutes, and permeabilized in 0.5% Triton-X for 15 minutes. Samples were blocked with CAS-Block (ThermoFisher) at 4C for 1 hour, then stained with antibodies for 1 hour at 4°C before imaging. Samples were stained with antibodies against B220 (clone RA3-6B2), F4/80 (BM8), Ki67 (SolA15), CD11c (N418), and CD4 (GK1.5). Samples were imaged using a LSM 880 NLO AxioExaminer (Zeiss). CXCL9-RFP and CXCL10-BFP fluorescence were measured using ImageJ. Density of Ki67+ spots was measured using Imaris software (Bitplane Scientific Software).

Flow Cytometry

Spleens were dissociated in FACS buffer (0.5% BSA in PBS) to generate single-cell suspensions. Splenocytes were passed through a 70um filter and then RBC lysed using ACK lysis buffer (0.15M NH4CL, 1mM KHC3, 0.1mM Na2EDTA) for 5 minutes at room temperature. Samples were stained with Ghost Dye Violet 510 (Tonbo) for 20 minutes at 4°C, then stained with the following antibodies: CD4 (GK1.5), B220 (RA3-6B2), CD8 (YTS156.7.7), CXCR3 (CXCR3-173), KLRG1 (2F1/KLRG1), Ki67 (B56), CD44 (1M7), CD3 (145-2C11), CD11c (N418), MHC-II

(M5/114.15.2), CD11b (M1/70), CD45.1 (A20), CD45.2 (104), NK1.1 (PK136), Ly6G (1A8), and Eomes (Dan11mag). In some experiments, cells were labeled with CFSE proliferation dye (ThermoFisher) following the manufacturer's protocol. For intracellular staining, samples were fixed and permeabilized using the eBioscience FoxP3 staining kit (ThermoFisher). Samples were processed using an LSR Fortessa Analyzer (BD) and analyzed using FlowJo software.

Adoptive Transfers

For adoptive transfer of naïve CD8+ T cells prior to infection, spleens were isolated from donor mice and single-cell suspensions were generated. CD8+ T cells were isolated by negative enrichment using a magnetic column (Miltenyi Biotec.) according to manufacturer's instruction. $5x10^4$ naïve CD8+ T cells were transferred into recipient mice intravenously (i.v.) and recipient mice were infected 24 hours later. In experiments where two naïve CD8+ T cell populations were transferred, $2.5x10^4$ of each population was injected. For *in vivo* antigen presentation assays, 10^6 naïve CFSE-labeled TG6 CD8+ T cells were injected into infected recipient mice intravenously after being isolated as described above.

IFNγ neutralization

IFNγ neutralizing antibody (clone XMG1, BioXcell) was diluted in sterile PBS and injected i.p. into infected mice at a dosage of 200ug/mouse. In some experiments, rat IgG1 (BioXcell) was used as an isotype control and was injected at the same concentration. Mice were injected every three days.

RNA Sequencing

Splenocytes were isolated from mice infected with *T. gondii* for 6 weeks. TG6 CD8+ T_{MEM}, T_{INT}, and T_{EFF} cells were sorted using a BD FACSAria Fusion by CD44+ CD45.1+ and CXCR3xKLRG1 staining. RNA was harvested using a Quick-RNA Microprep Kit from Zymo Research (Cat. No. R1050) according to manufacturer's instructions. RNA integrity was confirmed via Bioanalyzer and Qbit. RNA was sent to BGI Genomics for library generation and RNA sequencing on an Illumina HiSeq2500/4000 to a depth of 20 million reads.

RNA-seq analysis

Sequencing reads were processed with Trimmomatic (Bolger, Lohse and Usadel, 2014) to remove adapter sequences and trim low-quality bases. Reads were aligned to the mm10 genome using Bowtie2 (Langmead and Salzberg, 2012) and transcripts were quantified using RSEM (Li and Dewey, 2011). PCA was performed on RNA-seq data following normalization by VST with DESeq2 (Love, Huber and Anders, 2014). Differential expression testing was performed using DESeq2, which produced adjusted p-values corrected by the Benjamini-Hochberg procedure. In each test, genes with an adjusted p-value < 0.05 and $|\log_2$ fold change$|$ > 1 were considered differentially expressed. Gene set enrichment analysis (GSEA) was performed for each DESeq2 comparison using FGSEA (Korotkevich *et al.*, 2016) with gene sets downloaded from MigDB (Liberzon *et al.*, 2011).

3.5: References

Badovinac, V. P. (2000) 'Regulation of Antigen-Specific CD8+ T Cell Homeostasis by Perforin and Interferon-gamma', *Science*, 290(5495), pp. 1354–1357. doi: 10.1126/science.290.5495.1354.

Bhadra, R. *et al.* (2011) 'Control of Toxoplasma reactivation by rescue of dysfunctional CD8 + T-cell response via PD-1-PDL-1 blockade', *Proceedings of the National Academy of Sciences of the United States of America*, 108(22), pp. 9196–9201. doi: 10.1073/pnas.1015298108.

Blanchard, N. *et al.* (2008) 'Immunodominant, protective response to the parasite Toxoplasma gondii requires antigen processing in the endoplasmic reticulum.', *Nature immunology*, 9(8), pp. 937–44. doi: 10.1038/ni.1629.

Bolger, A. M., Lohse, M. and Usadel, B. (2014) 'Trimmomatic: A flexible trimmer for Illumina sequence data', *Bioinformatics*, 30(15), pp. 2114–2120. doi: 10.1093/bioinformatics/btu170.

Brown, C. R. *et al.* (1995) 'Definitive identification of a gene that confers resistance against Toxoplasma cyst burden and encephalitis.', *Immunology*, 85(3), pp. 419–28. Available at: http://www.ncbi.nlm.nih.gov/pubmed/7558130%0Ahttp://www.pubmedcentral.nih.gov/articlerender.fcgi?artid=PMC1383915.

Chang, Cheong-Hee, Flavell, R. A. (1995) 'Class II Transactivator Regulates the Expression of Multiple Genes Involved in Antigen Presentation', *Journal of Experimental Medicine*, 181(February), pp. 765–767.

Chen, E. Y. *et al.* (2013) 'Enrichr: Interactive and collaborative HTML5 gene list enrichment analysis tool', *BMC Bioinformatics*, 14. doi: 10.1186/1471-2105-14-128.

Chu, H. H. *et al.* (2016) 'Continuous Effector CD8+ T Cell Production in a Controlled Persistent Infection Is Sustained by a Proliferative Intermediate Population', *Immunity*, pp. 159–171. doi: 10.1016/j.immuni.2016.06.013.

Curtsinger, J. M. *et al.* (1999) 'Inflammatory cytokines provide a third signal for activation of naive CD4+ and CD8+ T cells.', *Journal of immunology (Baltimore, Md.: 1950)*, 162(6), pp. 3256–62. Available at: http://www.ncbi.nlm.nih.gov/pubmed/10092777.

Curtsinger, J. M. *et al.* (2005) 'Cutting Edge: Type I IFNs Provide a Third Signal to CD8 T Cells to Stimulate Clonal Expansion and Differentiation', *The Journal of Immunology*, 174(8), pp. 4465–4469. doi: 10.4049/jimmunol.174.8.4465.

Degrandi, D. *et al.* (2013) 'Murine Guanylate Binding Protein 2 (mGBP2) controls Toxoplasma gondii replication', *Proceedings of the National Academy of Sciences of the United States of America*, 110(1), pp. 294–299. doi: 10.1073/pnas.1205635110.

Van Engeland, M. *et al.* (1998) 'Annexin V-affinity assay: A review on an apoptosis detection system based on phosphatidylserine exposure', *Cytometry*, 31(1), pp. 1–9. doi: 10.1002/(SICI)1097-0320(19980101)31:1<1::AID-CYTO1>3.0.CO;2-R.

Gil, M. P. *et al.* (2001) 'Biologic consequences of Stat1-independent IFN signaling', *Proceedings of the National Academy of Sciences of the United States of America*, 98(12), pp. 6680–6685. doi: 10.1073/pnas.111163898.

Groom, J. R. *et al.* (2012) 'CXCR3 Chemokine Receptor-Ligand Interactions in the Lymph Node Optimize CD4+ T Helper 1 Cell Differentiation', *Immunity*. Elsevier Inc., 37(6), pp. 1091–1103. doi: 10.1016/j.immuni.2012.08.016.

Korotkevich, G. *et al.* (2016) 'Fast gene set enrichment analysis', pp. 1–29. doi: 10.1101/060012.

Langmead, B. and Salzberg, S. L. (2012) 'Fast gapped-read alignment with Bowtie 2', *Nature Methods*, 9(4), pp. 357–359. doi: 10.1038/nmeth.1923.

Lee, J. C. *et al.* (2013) 'Cellular responses to interferon gamma', 13(1978), pp. 618–634.

Li, B. and Dewey, C. N. (2011) 'RSEM: accurate transcript quantification from RNA-Seq data with or without a reference genome', *Bioinformatics*, pp. 21–40. doi: 10.1186/1471-2105-12-323.

Liberzon, A. *et al.* (2011) 'Molecular signatures database (MSigDB) 3.0', *Bioinformatics*, 27(12), pp. 1739–1740. doi: 10.1093/bioinformatics/btr260.

Love, M. I., Huber, W. and Anders, S. (2014) 'Moderated estimation of fold change and dispersion for RNA-seq data with DESeq2', *Genome Biology*, 15(12), pp. 1–21. doi: 10.1186/s13059-014-0550-8.

MacMicking, J. D. (2012) 'Interferon-inducible effector mechanisms in cell-autonomous immunity', *Nature Reviews Immunology*. Nature Publishing Group, 12(5), pp. 367–382. doi: 10.1038/nri3210.

Martens, S. *et al.* (2005) 'Disruption of Toxoplasma gondii parasitophorous vacuoles by the mouse p47-resistance GTPases', *PLoS Pathogens*, 1(3), pp. 0187–0201. doi: 10.1371/journal.ppat.0010024.

Moran, A. E. *et al.* (2011) 'T cell receptor signal strength in Treg and iNKT cell development demonstrated by a novel fluorescent reporter mouse', *Journal of Experimental Medicine*, 208(6), pp. 1279–1289. doi: 10.1084/jem.20110308.

Norose, K. *et al.* (2001) 'Organ infectivity of Toxoplasma gondii in interferon-γ knockout mice', *Journal of Parasitology*, 87(2), pp. 447–452. doi: 10.1645/0022-3395(2001)087[0447:oiotgi]2.0.co;2.

Puliaev, R. *et al.* (2004) 'Differential requirement for IFN-gamma in CTL maturation in acute murine graft-versus-host disease.', *Journal of immunology (Baltimore, Md. : 1950)*, 173, pp. 910–919. doi: 10.4049/jimmunol.173.2.910.

Schroder, K. *et al.* (2004) 'Interferon-gamma: an overview of signals, mechanisms and functions.', *Journal of leukocyte biology*, 75(2), pp. 163–89. doi: 10.1189/jlb.0603252.

Sercan, O. *et al.* (2010) 'IFN- Receptor Signaling Regulates Memory CD8+ T Cell Differentiation', *The Journal of Immunology*, 184(6), pp. 2855–2862. doi: 10.4049/jimmunol.0902708.
Sercan, Ö. *et al.* (2006) 'Cutting Edge: Innate Immune Cells Contribute to the IFN- γ -Dependent Regulation of Antigen-Specific CD8 + T Cell Homeostasis', *Journal of immunology (Baltimore, Md. : 1950)*, 176, pp. 735–739. doi: 10.4049/jimmunol.176.2.735.

Shah, S. *et al.* (2015) 'An extrafollicular pathway for the generation of effector CD8+T cells driven by the proinflammatory cytokine, IL-12', *eLife*, 4(AUGUST2015), pp. 1–21. doi: 10.7554/eLife.09017.

Stoycheva, D. *et al.* (2015) 'IFN-γ Regulates CD8 $^{+}$ Memory T Cell Differentiation and Survival in Response to Weak, but Not Strong, TCR Signals', *The Journal of Immunology*, 194(2), pp. 553–559. doi: 10.4049/jimmunol.1402058.

Suzuki, Y. *et al.* (1988) 'Interferon-γ: The major mediator of resistance against Toxoplasma gondii', *Science*, 240(4851), pp. 516–518. doi: 10.1126/science.3128869.

Suzuki, Y. and Remington, J. S. (1990) 'The effect of anti-IFN-gamma antibody on the protective effect of Lyt-2+ immune T cells against toxoplasmosis in mice.', *Journal of immunology (Baltimore, Md. : 1950)*, 144(5), pp. 1954–6. Available at: http://www.ncbi.nlm.nih.gov/pubmed/2106557.

Tewari, K., Nakayama, Y. and Suresh, M. (2007) 'Role of Direct Effects of IFN- on T Cells in the Regulation of CD8 T Cell Homeostasis', *The Journal of Immunology*, 179(4), pp. 2115–2125. doi: 10.4049/jimmunol.179.4.2115.

Tsitsiklis, A. *et al.* (2020) 'An Unusual MHC Molecule Generates Protective CD8+ T Cell Responses to Chronic Infection', *Frontiers in Immunology*, 11(July), pp. 1–13. doi: 10.3389/fimmu.2020.01464.

Whitmire, J. K. *et al.* (2007) 'Direct Interferon- Signaling Dramatically Enhances CD4+ and CD8+ T Cell Memory', *The Journal of Immunology*, 179(2), pp. 1190–1197. doi: 10.4049/jimmunol.179.2.1190.

Whitmire, J. K., Tan, J. T. and Whitton, J. L. (2005) 'Interferon-γ acts directly on CD8 $^{+}$ T cells to increase their abundance during virus infection', *The Journal of Experimental Medicine*, 201(7), pp. 1053–1059. doi: 10.1084/jem.20041463.

Williams, M. A. and Bevan, M. J. (2007) 'Effector and memory CTL differentiation', *Annual Review of Immunology*, 25, pp. 171–192. doi: 10.1146/annurev.immunol.25.022106.141548.

Xu, X. *et al.* (1998) 'IFN-γ induces cell growth inhibition by fas-mediated apoptosis: Requirement of STAT1 protein for up-regulation of Fas and FasL expression', *Cancer Research*, 58(13), pp. 2832–2837.

Figure 1

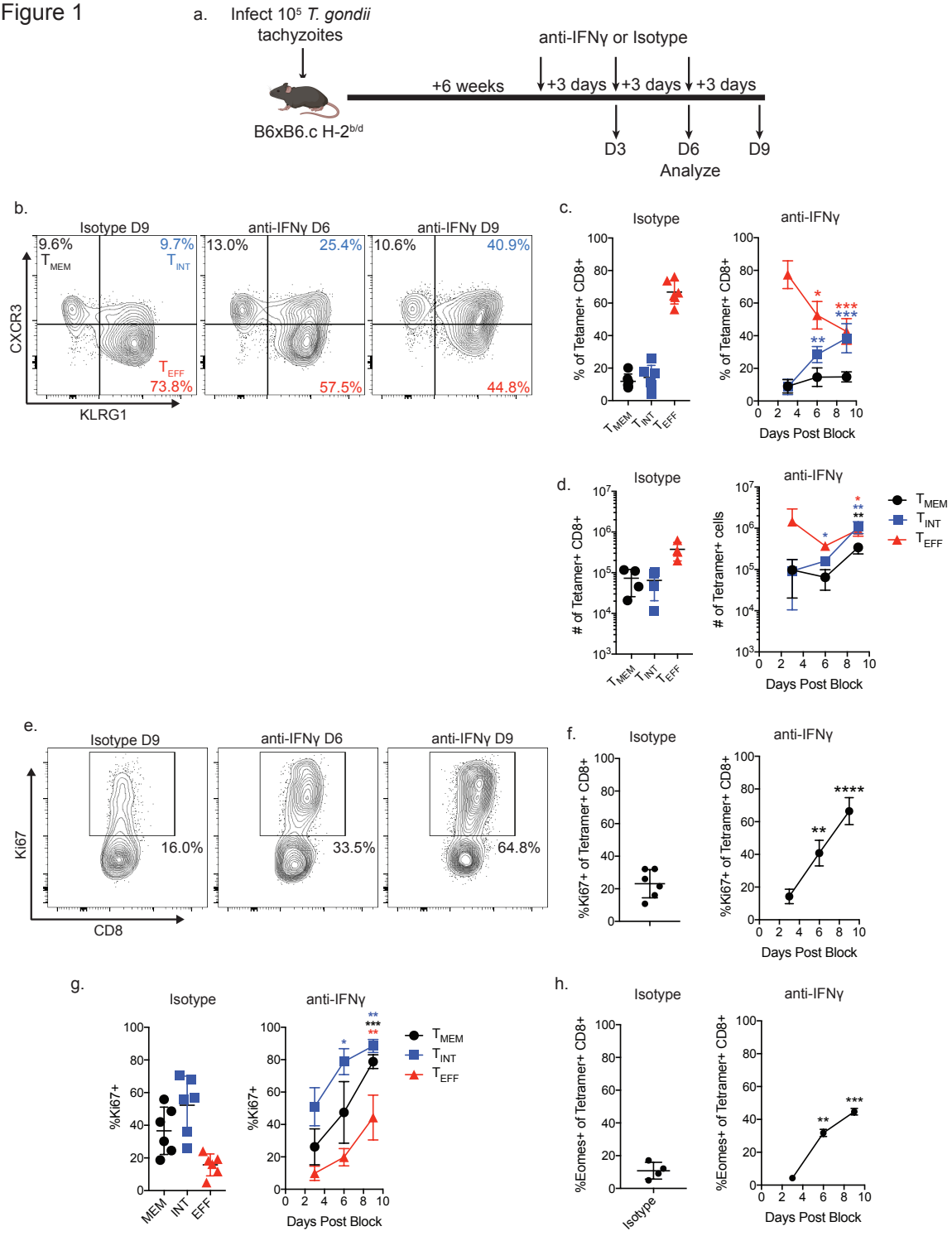
a.
Infect 10⁵ T. gondii tachyzoites
B6xB6.c H-2b/d
+6 weeks
anti-IFNγ or Isotype
+3 days
+3 days
+3 days
D3
D6
D9
Analyze
b.
Isotype D9
anti-IFNγ D6
anti-IFNγ D9
9.6%
T MEM
9.7%
T INT
T EFF
73.8%
13.0%
25.4%
57.5%
10.6%
40.9%
44.8%
CXCR3
KLRG1
c.
Isotype
anti-IFNγ
% of Tetamer+ CD8+
% of Tetamer+ CD8+
T MEM
T INT
T EFF
Days Post Block
d.
Isotype
anti-IFNγ
# of Tetamer+ CD8+
# of Tetramer+ cells
T MEM
T INT
T EFF
Days Post Block
e.
Isotype D9
anti-IFNγ D6
anti-IFNγ D9
16.0%
33.5%
64.8%
Ki67
CD8
f.
Isotype
anti-IFNγ
%Ki67+ of Tetramer+ CD8+
%Ki67+ of Tetramer+ CD8+
Days Post Block
g.
Isotype
anti-IFNγ
%Ki67+
%Ki67+
MEM
INT
EFF
T MEM
T INT
T EFF
Days Post Block
h.
Isotype
anti-IFNγ
%Eomes+ of Tetramer+ CD8+
%Eomes+ of Tetramer+ CD8+
Isotype
Days Post Block

Figure 1: IFNγ neutralization results in a dramatic increase to the T_{INT} population and loss of T_{EFF} cells. a) Experimental outline. B6xB6.c H-$2^{b/d}$ F1 mice were infected with *T. gondii*, and 6 weeks post-infection mice were treated with anti-IFNγ neutralizing antibody or isotype control every three days. Mice were sacrificed after 3, 6, and 9 days of treatment and splenocytes were analyzed by flow cytometry. b) Representative flow cytometry plots of gated GRA6 tetramer+ CD8+ T cells taken from mice given with the indicated antibody treatment. Plots show the proportion of T_{MEM}, T_{INT}, and T_{EFF} cells using CXCR3 and KLRG1 staining. c,d) Summary data showing the proportion (c) and absolute numbers (d) of GRA6-specific T_{MEM}, T_{INT}, and T_{EFF} cells after IFNγ neutralization or treatment with the isotype control antibody. e) Representative flow cytometry plots of gated GRA6 tetramer+ CD8+ T cells taken from mice given the indicated antibody treatment. Plots show Ki67 staining and the percent of Ki67+ cells. f) Summary data of Ki67 expression on the total GRA6 tetramer+ CD8+ T cell population after treatment with the anti-IFNγ or isotype control. g) Summary data of Ki67 expression on GRA6-specific T_{MEM}, T_{INT}, or T_{EFF} cells. h) Summary data of Eomes expression on the total GRA6 tetramer+ CD8+ T cell population after the indicated treatment. Statistical significance was determined using a t-test comparing to the isotype control data (*$p<0.05$, **$p<0.01$, ***$p<0.001$, ****$p<0.0001$).

Figure 2

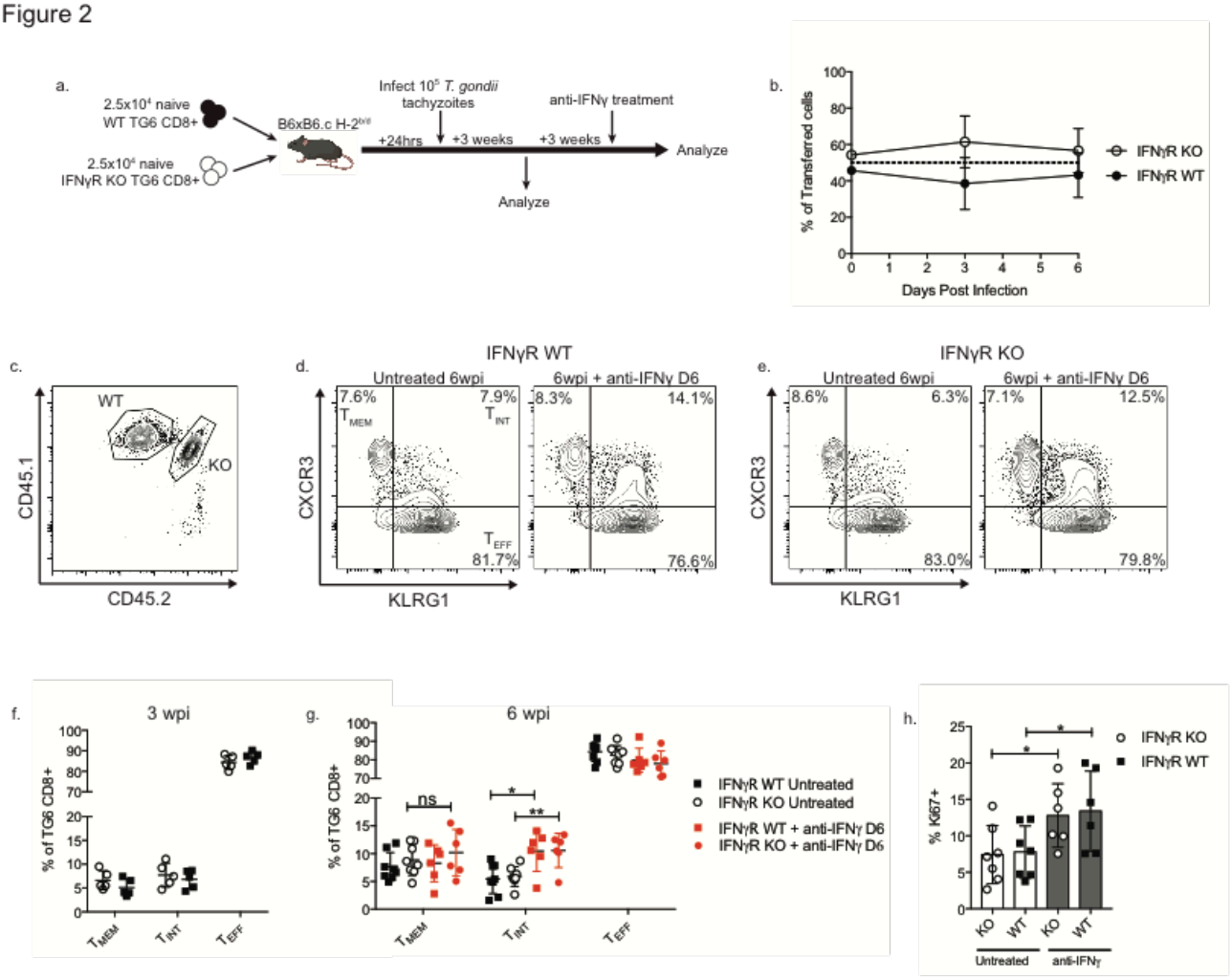
a.
2.5x10⁴ naive WT TG6 CD8+
2.5x10⁴ naive IFNγR KO TG6 CD8+
B6xB6.c H-2bxd
Infect 10⁵ T. gondii tachyzoites
+24hrs
+3 weeks
anti-IFNγ treatment
+3 weeks
Analyze
Analyze
b.
% of Transferred cells
Days Post Infection
IFNγR KO
IFNγR WT
c.
WT
KO
CD45.1
CD45.2
d.
IFNγR WT
Untreated 6wpi
6wpi + anti-IFNγ D6
7.6%
T MEM
7.9%
T INT
8.3%
14.1%
T EFF
81.7%
76.6%
CXCR3
KLRG1
e.
IFNγR KO
Untreated 6wpi
6wpi + anti-IFNγ D6
8.6%
6.3%
7.1%
12.5%
83.0%
79.8%
CXCR3
KLRG1
f.
3 wpi
% of TG6 CD8+
T MEM
T INT
T EFF
g.
6 wpi
% of TG6 CD8+
ns
*
**
IFNγR WT Untreated
IFNγR KO Untreated
IFNγR WT + anti-IFNγ D6
IFNγR KO + anti-IFNγ D6
h.
% Ki67+
*
*
IFNγR KO
IFNγR WT
KO
WT
KO
WT
Untreated
anti-IFNγ

Figure 2: Direct IFNγ signaling on CD8+ T cells does not impact their fate during chronic infection. a) Experimental outline. B6xB6.c H-$2^{b/d}$ F1 mice were given equal numbers of naive WT and IFNγR KO TG6 CD8+ T cells. Mice were then infected and the proportion and differentiation profile of the WT and IFNγR KO cells was measured at three weeks and six weeks post-infection. At six weeks post-infection, some mice received anti-IFNγ treatment for six days. b) The proportion of transferred cells belonging to the WT and KO populations was measured before adoptive transfer and at three and six weeks post-infection. c) Representative flow plot of gated GRA6 tetramer+ CD8+ T cells showing the transferred WT and KO TG6 cells after six weeks of infection using CD45.1 and CD45.2 staining. d,e) Representative flow plots showing CXCR3 and KLRG1 staining on the gated WT TG6 cells (d) or KO TG6 cells (e) at six weeks post-infection with no treatment or anti-IFNγ treatment for six days. f) Summary data showing the proportion T_{MEM}, T_{INT}, and T_{EFF} cells in the WT and IFNγR KO TG6 CD8+ T cells at three weeks post-infection. g) Summary data of the proportion of T_{MEM}, T_{INT}, and T_{EFF} cells at six weeks post-infection and after the indicated antibody treatment. h) Summary data of Ki67 expression in the indicated population. Statistical significance was determined using a t-test (*$p<0.05$, **$p<0.01$, ***$p<0.001$, ****$p<0.0001$).

Figure 3

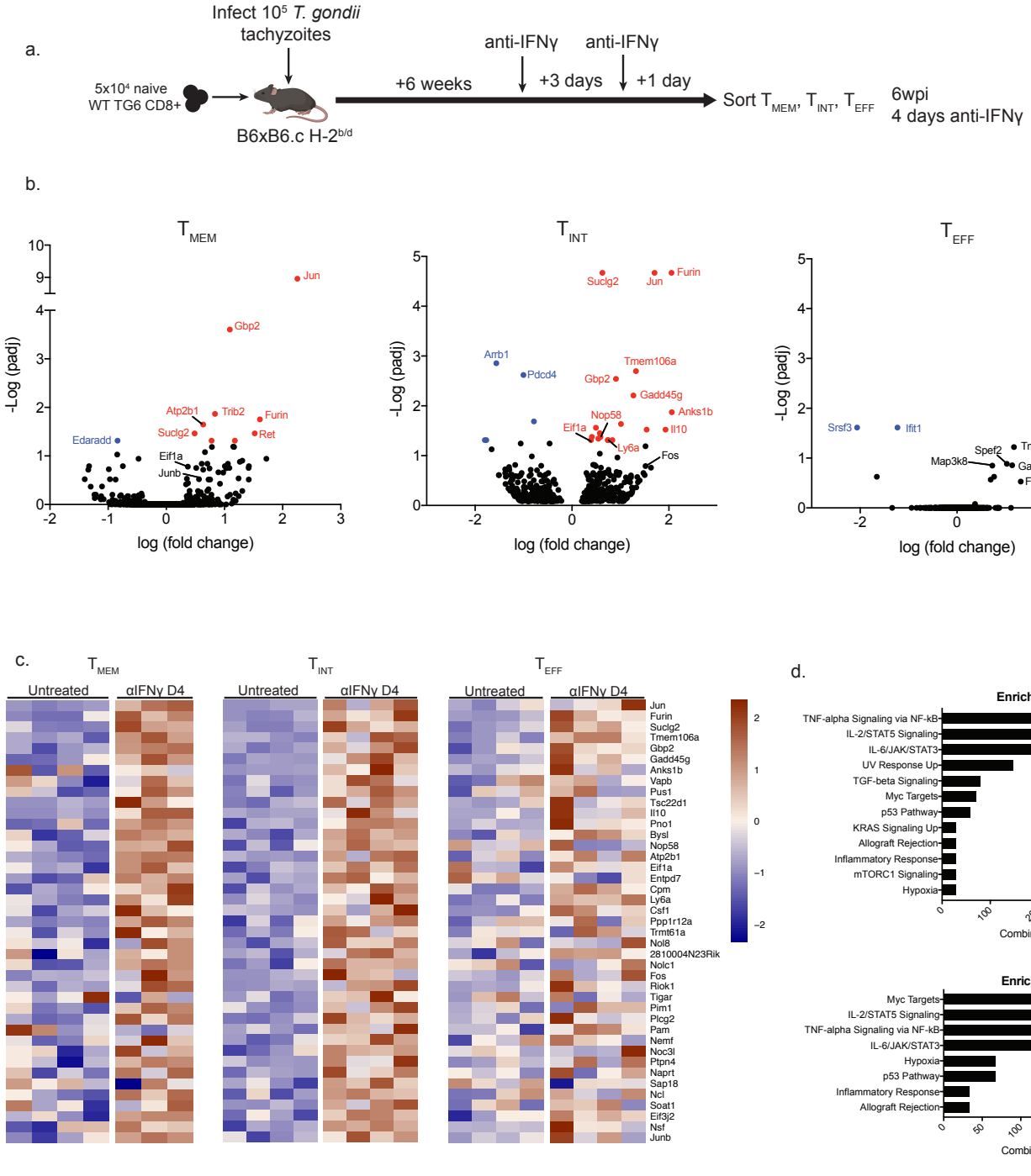
a.
Infect 10^5 T. gondii tachyzoites
5x10^4 naive WT TG6 CD8+
B6xB6.c H-2^b/d
+6 weeks
anti-IFNγ
+3 days
anti-IFNγ
+1 day
Sort T_MEM, T_INT, T_EFF
6wpi
4 days anti-IFNγ
b.
T_MEM
T_INT
T_EFF
-Log (padj)
log (fold change)
Jun
Gbp2
Atp2b1
Trib2
Furin
Suclg2
Ret
Edaradd
Eif1a
Junb
Arrb1
Pdcd4
Suclg2
Jun
Furin
Tmem106a
Gbp2
Gadd45g
Anks1b
Nop58
Eif1a
Il10
Ly6a
Fos
Srsf3
Ifit1
Spef2
Tmem106a
Map3k8
Gadd45g
Furin
c.
T_MEM
T_INT
T_EFF
Untreated
αIFNγ D4
Jun
Furin
Suclg2
Tmem106a
Gbp2
Gadd45g
Anks1b
Vapb
Pus1
Tsc22d1
Il10
Pno1
Bysl
Nop58
Atp2b1
Eif1a
Entpd7
Cpm
Ly6a
Csf1
Ppp1r12a
Trmt61a
Nol8
2810004N23Rik
Nolc1
Fos
Riok1
Tigar
Pim1
Plcg2
Pam
Nemf
Noc3l
Ptpn4
Naprt
Sap18
Ncl
Soat1
Eif3j2
Nsf
Junb
d.
Enriched in T_MEM
TNF-alpha Signaling via NF-kB
IL-2/STAT5 Signaling
IL-6/JAK/STAT3
UV Response Up
TGF-beta Signaling
Myc Targets
p53 Pathway
KRAS Signaling Up
Allograft Rejection
Inflammatory Response
mTORC1 Signaling
Hypoxia
Combined Score
Enriched in T_INT
Myc Targets
IL-2/STAT5 Signaling
TNF-alpha Signaling via NF-kB
IL-6/JAK/STAT3
Hypoxia
p53 Pathway
Inflammatory Response
Allograft Rejection
Combined Score

Figure 3: anti-IFNγ treatment drives transcriptional changes in T_{MEM} and T_{INT} cells reflecting increased antigen exposure. a) Experimental outline. Mice received naive WT TG6 CD8+ T cells and were infected with *T. gondii*. Six weeks post-infection, half the mice were treated with anti-IFNγ. Four days after anti-IFNγ treatment, T_{MEM}, T_{INT}, and T_{EFF} cells were sorted from the TG6 populations from untreated mice or those treated with anti-IFNγ. b) Volcano plots showing the top 500 differentially expressed genes in the T_{MEM}, T_{INT}, and T_{EFF} cells after anti-IFNγ treatment. A positive log fold change indicates an enrichment in the cells after anti-IFNγ treatment. Red colored points indicate genes that were significantly upregulated in the anti-IFNγ condition (padj<0.05), blue indicates genes that were significantly upregulated in the untreated condition. c) Heatmaps displaying the expression of indicated genes in the T_{MEM}, T_{INT}, and T_{EFF} populations sorted from untreated mice or mice treated with anti-IFNγ for four days. The genes displayed are the genes with the largest fold change in the T_{INT} anti-IFNγ compared to T_{INT} untreated. Gene expression values are scaled within each population. d) The top 50 genes upregulated after anti-IFNγ treatment in T_{MEM} or T_{INT} cells were analyzed to determine the enrichment of pathways using Enrichr (Chen *et al.*, 2013). The plots display Combined Scores indicating an enrichment in each pathway, and all pathways displayed had a padj < 0.05.

Figure 4

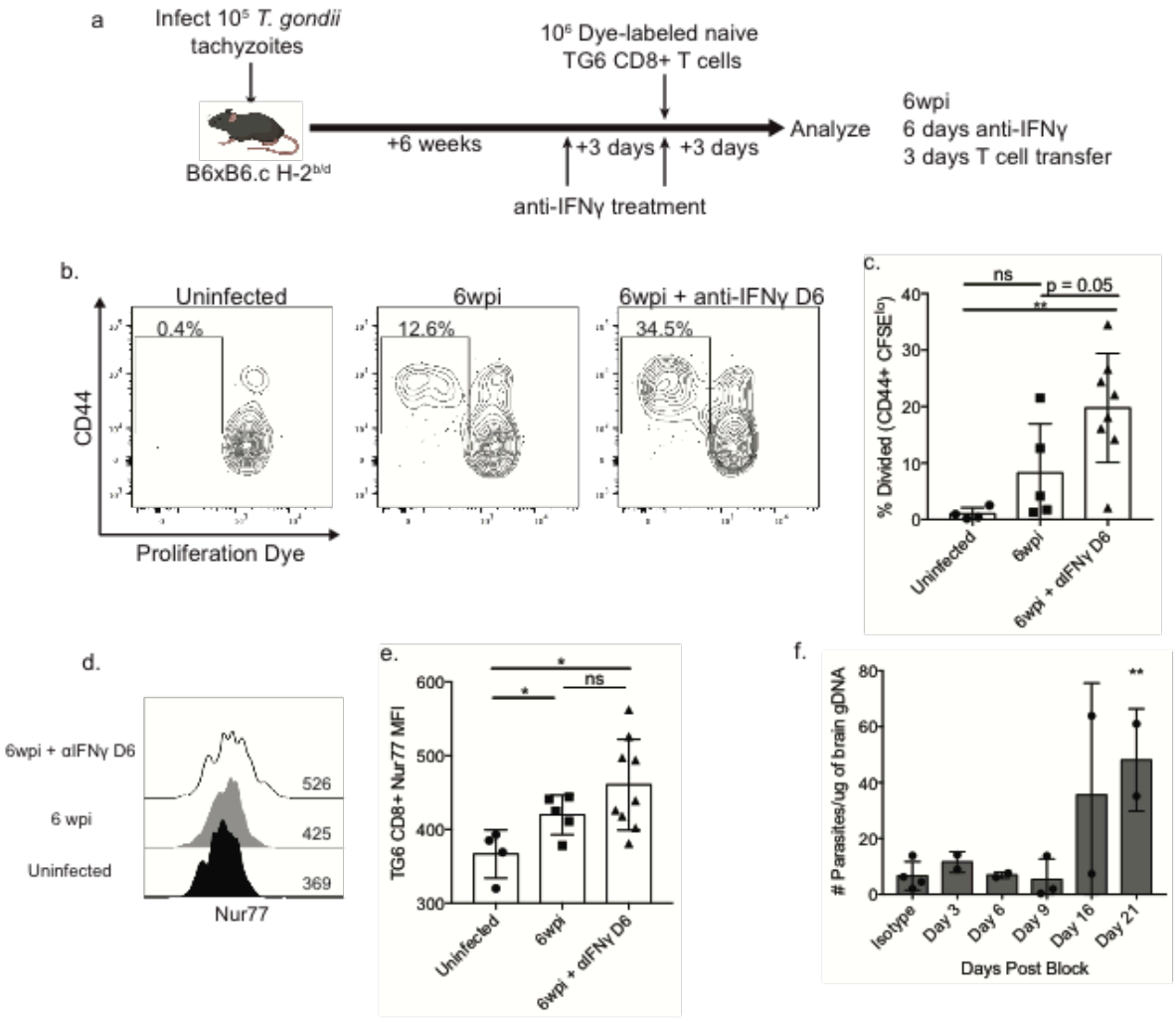
a
Infect 10⁵ T. gondii tachyzoites
B6xB6.c H-2b/d
10⁶ Dye-labeled naive TG6 CD8+ T cells
+6 weeks
+3 days
+3 days
Analyze
anti-IFNγ treatment
6wpi
6 days anti-IFNγ
3 days T cell transfer
b.
Uninfected
6wpi
6wpi + anti-IFNγ D6
0.4%
12.6%
34.5%
CD44
Proliferation Dye
c.
ns
p = 0.05
**
% Divided (CD44+ CFSElo)
Uninfected
6wpi
6wpi + αIFNγ D6
d.
6wpi + αIFNγ D6
6 wpi
Uninfected
526
425
369
Nur77
e.
*
*
ns
TG6 CD8+ Nur77 MFI
Uninfected
6wpi
6wpi + αIFNγ D6
f.
**
Parasites/ug of brain gDNA
Isotype
Day 3
Day 6
Day 9
Day 16
Day 21
Days Post Block

Figure 4: IFNγ neutralization results in increased antigen presentation in the spleen but does not cause the reactivation of systemic infection. a) Experimental outline of *in vivo* antigen presentation assay. Mice infected for six weeks were either left untreated or treated with anti-IFNγ, and all mice received dye-labeled naive TG6 CD8+ T cells. The activation of the transferred cells was measured three days later. b) Representative flow plots gated on the transferred TG6 CD8+ T cells showing CD44 expression and proliferation dye dilution. c) Summary data showing the proportion of CD44+ dye-diluted cells after adoptive transfer into the indicated recipient mouse. d) Representative flow cytometry histogram of Nur77 staining, gated on transferred TG6 CD8+ T cells. e) Summary data of Nur77 expression by transferred TG6 cells in the indicated recipient mice. f) Mice chronically infected with *T. gondii* were treated with anti-IFNγ or isotype control. The brains of these mice were then harvested and parasite burden was measured using qPCR. Statistical significance was determined using a t-test (*p<0.05, **p<0.01, ***p<0.001, ****p<0.0001).

Figure 5

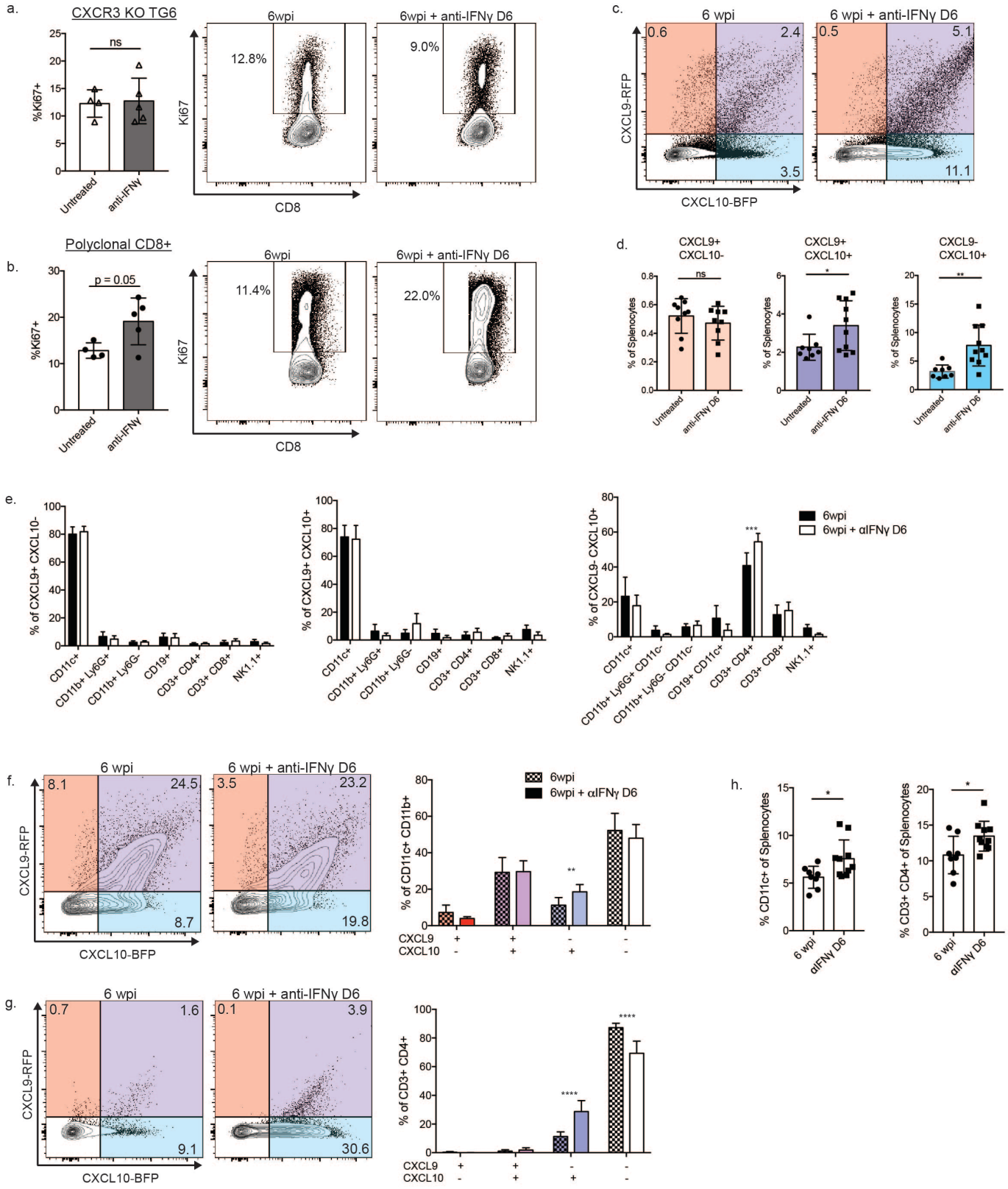
a.
CXCR3 KO TG6
ns
%Ki67+
Untreated
anti-IFNγ
6wpi
6wpi + anti-IFNγ D6
12.8%
9.0%
Ki67
CD8
b.
Polyclonal CD8+
p = 0.05
11.4%
22.0%
c.
6 wpi
6 wpi + anti-IFNγ D6
0.6
2.4
3.5
0.5
5.1
11.1
CXCL9-RFP
CXCL10-BFP
d.
CXCL9+ CXCL10-
CXCL9+ CXCL10+
CXCL9- CXCL10+
% of Splenocytes
e.
% of CXCL9+ CXCL10-
% of CXCL9+ CXCL10+
% of CXCL9- CXCL10+
6wpi
6wpi + αIFNγ D6
CD11c+
CD11b+ Ly6G+
CD11b+ Ly6G-
CD19+
CD3+ CD4+
CD3+ CD8+
NK1.1+
CD11b+ Ly6G+ CD11c-
CD11b+ Ly6G- CD11c-
CD19+ CD11c+
f.
6 wpi
6 wpi + anti-IFNγ D6
8.1
24.5
8.7
3.5
23.2
19.8
% of CD11c+ CD11b+
CXCL9
CXCL10
g.
0.7
1.6
9.1
0.1
3.9
30.6
% of CD3+ CD4+
h.
% CD11c+ of Splenocytes
% CD3+ CD4+ of Splenocytes
6 wpi
αIFNγ D6

Figure 5: IFNγ neutralization increases CXCL9 and CXCL10 production a,b) Representative flow cytometry plots and summary data of Ki67 expression gated on CXCR3 KO TG6 CD8+ T cells (a) or polyclonal CD8+ T cells (b) after six weeks of infection. c) Representative flow cytometry plots showing CXCL9-RFP and CXCL10-BFP expression in REX3 splenocytes after six weeks of infection and after IFNγ neutralization. d) Summary data of CXCL9 and CXCL10 expression six weeks post-infection in mice left untreated or treated with anti-IFNγ for six days. e) Summary data showing expression of the indicated marker on splenocytes producing the indicated chemokines after six weeks of infection. f,g) Flow cytometry plots and summary data showing chemokine expression gated on CD11c+ splenocytes (f) or CD3+ CD4+ splenocytes (g). h) Summary data showing the proportion of splenocytes staining positive for CD11c or CD3+ and CD4+. Statistical significance was determined using a t-test (*$p<0.05$, **$p<0.01$, ***$p<0.001$, ****$p<0.0001$).

Figure 6

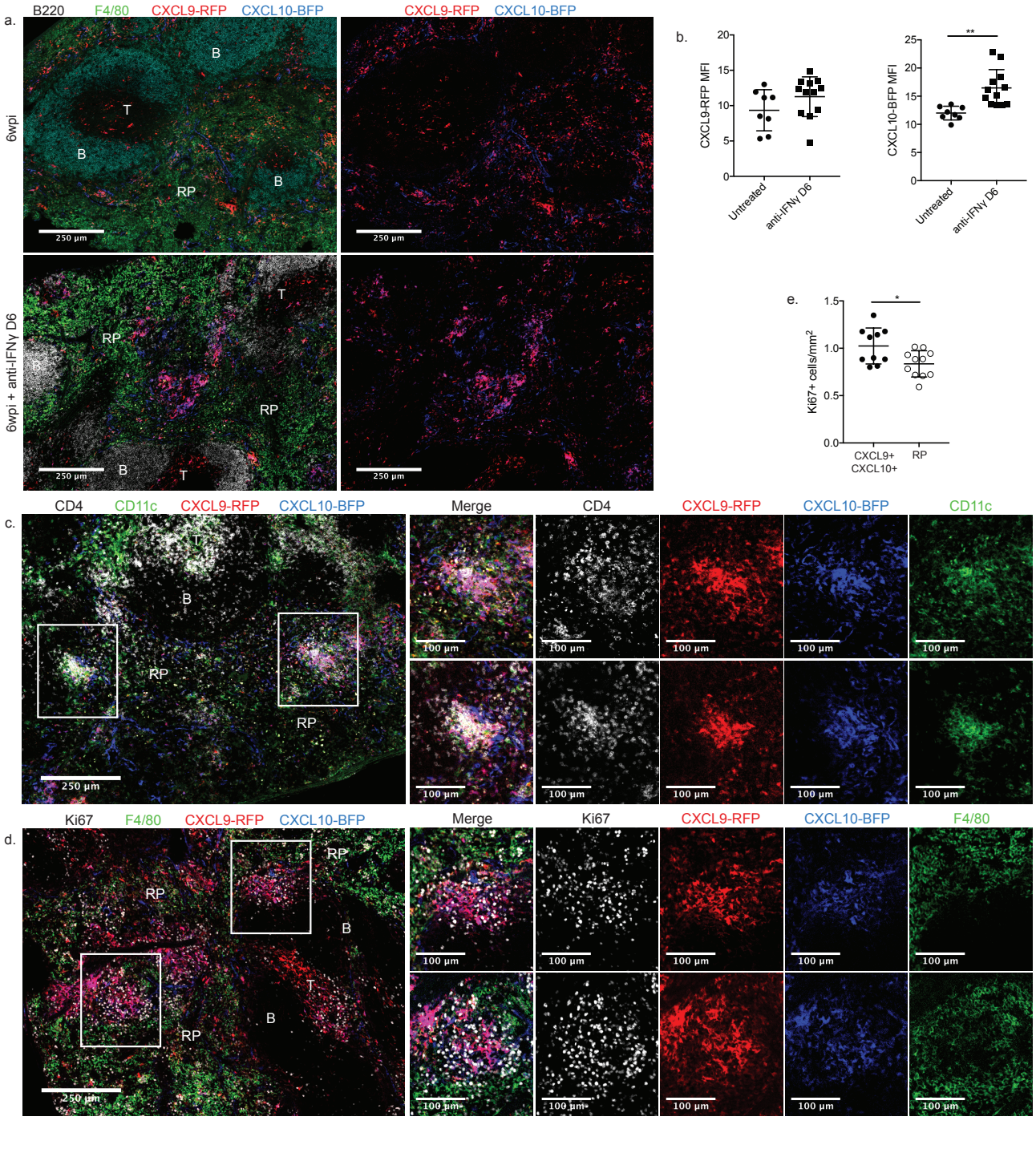
a.
B220
F4/80
CXCL9-RFP
CXCL10-BFP
6wpi
6wpi + anti-IFNγ D6
B
T
RP
250 μm
b.
CXCL9-RFP MFI
CXCL10-BFP MFI
Untreated
anti-IFNγ D6
**
e.
Ki67+ cells/mm2
CXCL9+ CXCL10+
RP
*
c.
CD4
CD11c
Merge
100 μm
d.
Ki67

Figure 6: IFNγ neutralization results in clusters of CXCL9+ CXCL10+ cells in the splenic red pulp. a) REX3xB6.c H-2b/d F1 mice were infected for six weeks and given the indicated antibody treatment. Images depict splenic sections stained with B220 (gray) and F4/80 (green) to identify the B cell zones (B) and red pulp (RP), respectively. Additionally, CXCL9-RFP (red) and CXCL10-BFP (blue) fluorescence were measured. b) Summary data showing the mean fluorescence intensity of CXCL9-RFP and CXCL10-BFP in images taken of chronically infected mice either left untreated or treated with anti-IFNγ for six days. c) The spleens of REX3xB6.c mice treated with anti-IFNγ for six days were imaged. Sections were stained with CD4 (gray) and CD11c (green) to identify CD4+ T cells and dendritic cells. CD4 staining was used to identify the T cell zone (T) and other labeled splenic structures were identified using background autofluorescence. d) The spleens of REX3xB6.c mice treated with anti-IFNγ for six days were stained with F4/80 (green) to identify the red pulp (RP) and Ki67 (gray) to identify proliferating cells. e) The density of Ki67+ spots was measured in regions of intense CXCL9/10 signal (as depicted in (d)) or in areas of the red pulp with low chemokine expression. Statistical significance was determined using a t-test (*$p<0.05$, **$p<0.01$, ***$p<0.001$, ****$p<0.0001$).

Supplemental Figure 1

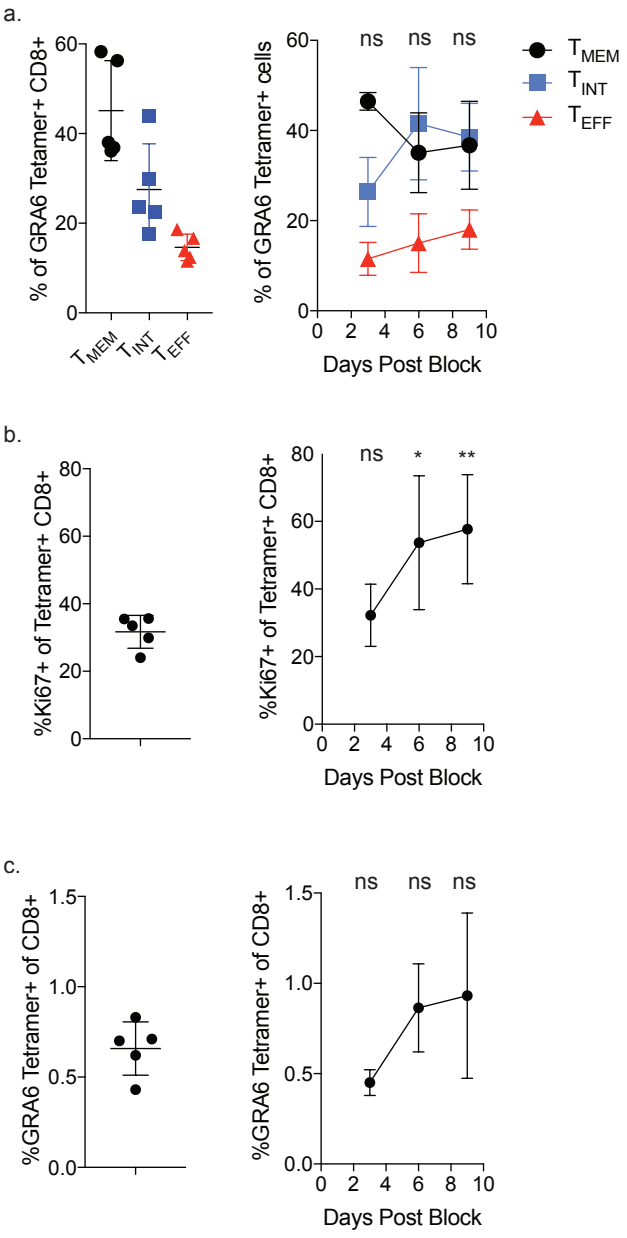

Supplemental Figure 1: Effects of anti-IFNγ treatment on CD8+ T cells in the lymph node. Mice were infected with *T. gondii*, and six weeks post-infection mice were treated with anti-IFNγ neutralizing antibodies or an isotype control. The phenotype of GRA6-specific CD8+ T cells in the lymph node was analyzed. a) The proportion of T_{MEM}, T_{INT}, and T_{EFF} cells among GRA6 tetramer-positive CD8+ T cells after the indicated number of days of anti-IFNγ treatment. b) The total percentage of tetramer+ CD8+ T cells after anti-IFNγ treatment is shown. c) The proportion of total tetramer+ cells that stained positive for Ki67. Statistical significance was determined using a t-test comparing to the isotype control data (*p<0.05, **p<0.01, ***p<0.001, ****p<0.0001).

Supplemental Figure 2

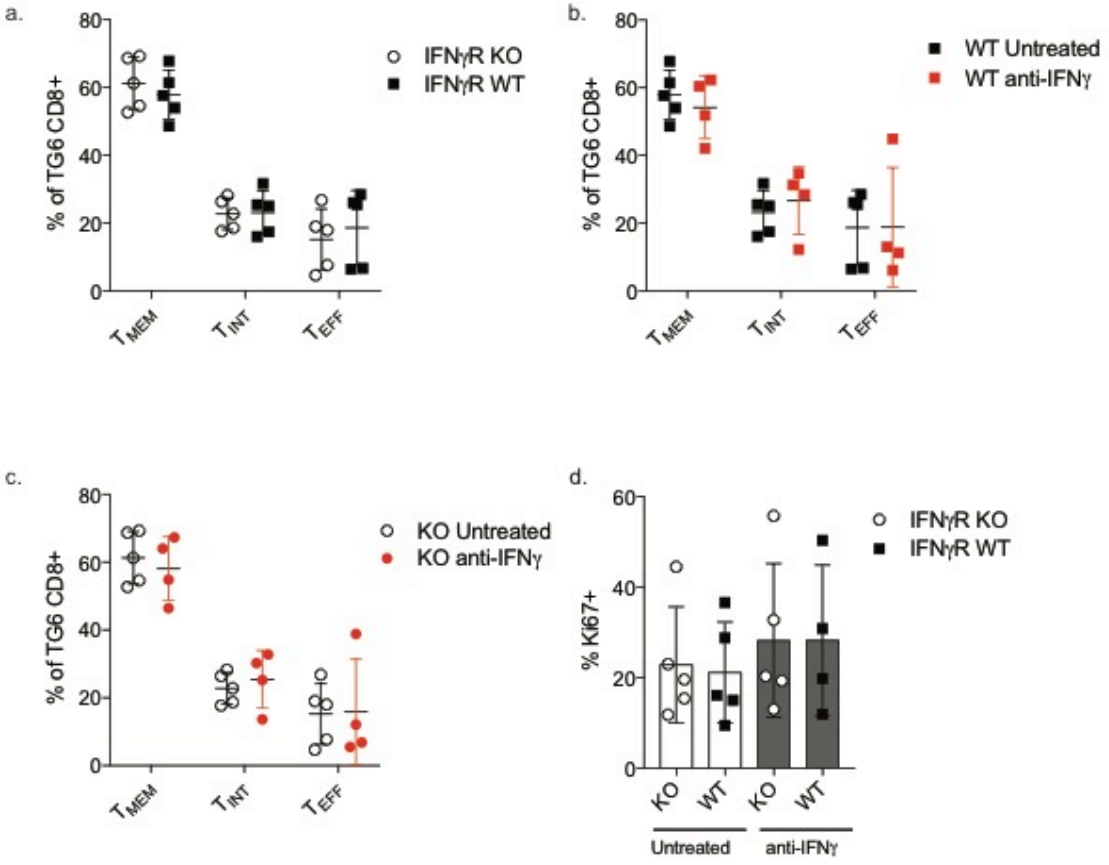

Supplemental Figure 2: IFNγ neutralization does impact the ability of CD8+ T cells to reside in tissues or their survival. a-b) Mice were infected with *T. gondii* for six weeks and half were treated with anti-IFNγ for six days. The brains (a) and liver (b) were harvested, and the numbers of CD8+ T cells, numbers of GRA6 tetramer+ CD8+ T cells, and percentage of GRA6 tetramer+ CD8+ T cells was measured. c) Representative flow cytometry histograms of GRA6 tetramer+ cells from chronically infected mice stained with Annexin V. e-f) Summary data showing the proportion of the indicated population that stained positively with Annexin V (e) or the geometric mean fluorescence intensity (gMFI) of Annexin V staining (f). Statistical significance was determined using a t-test (*$p<0.05$, **$p<0.01$, ***$p<0.001$, ****$p<0.0001$).

Supplemental Figure 3

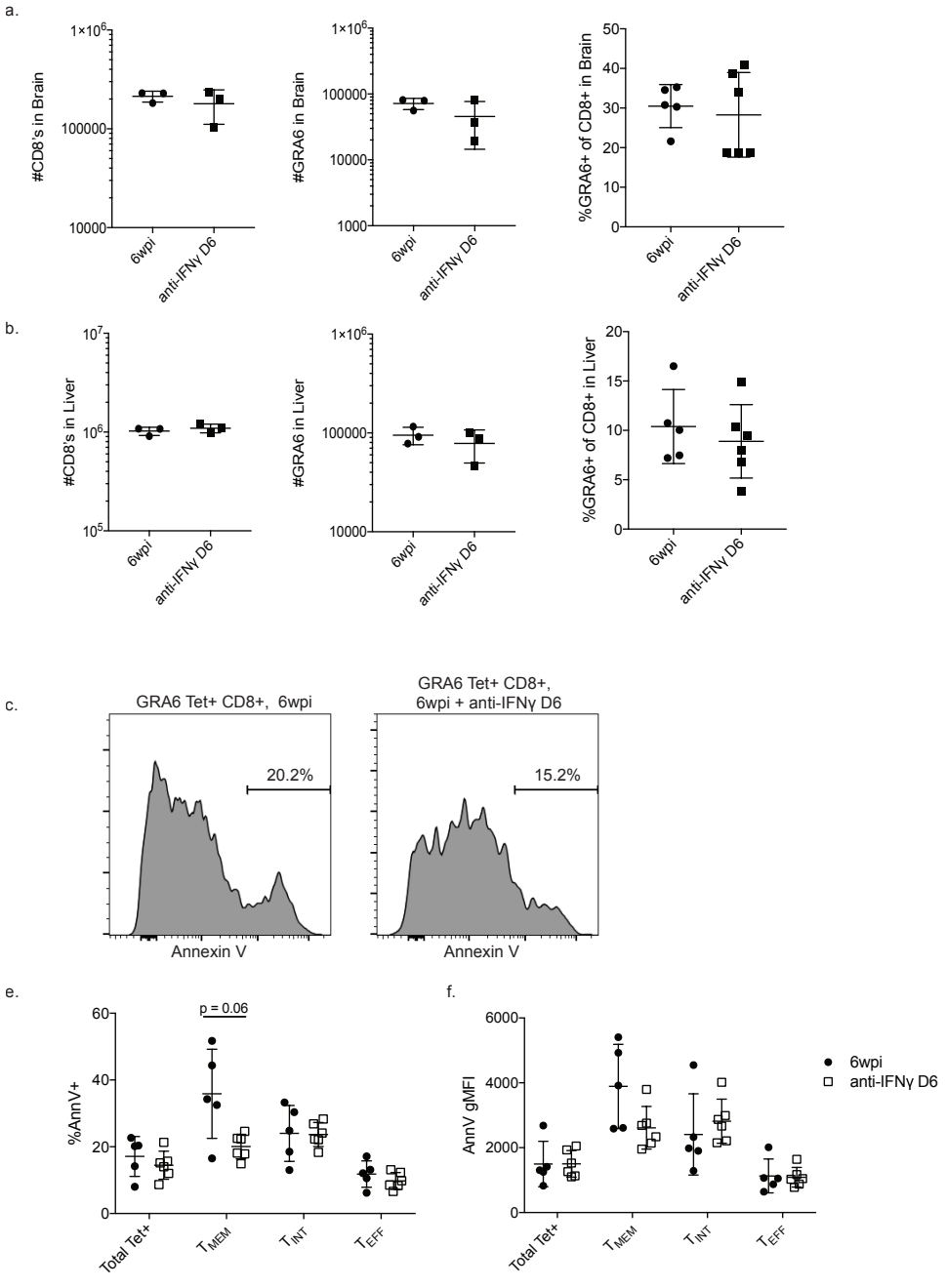

Supplemental Figure 3: Phenotype of IFNγR KO CD8+ T cells in the lymph node. (Related to Figure 2). Mice received equal numbers of naïve WT and IFNγR KO CD8+ T cells 24 hours prior to infection, and the two populations were examined at six weeks post infection. a-c) Phenotype of WT and KO CD8+ T cells after six weeks of infection and after the indicated treatment. d) The proportion of transferred WT and KO cells that were Ki67+ was measured after six weeks of infection and the indicated treatment. Statistical significance was determined using a t-test (*p<0.05, **p<0.01, ***p<0.001, ****p<0.0001).